Gamma-Ray Bursts and their Environments

Andrew J. Levan

Supervisor:
Martin Barstow

Thesis submitted for the degree of
Doctor of Philosophy
at the University of Leicester.

X-ray & Observational Astronomy Group
Department of Physics and Astronomy
University of Leicester

November 1, 2005

UMI Number: U488073

All rights reserved

INFORMATION TO ALL USERS
The quality of this reproduction is dependent upon the quality of the copy submitted.

In the unlikely event that the author did not send a complete manuscript
and there are missing pages, these will be noted. Also, if material had to be removed,
a note will indicate the deletion.

UMI®
Dissertation Publishing

UMI U488073
Published by ProQuest LLC 2013. Copyright in the Dissertation held by the Author.
Microform Edition © ProQuest LLC.
All rights reserved. This work is protected against
unauthorized copying under Title 17, United States Code.

ProQuest®

ProQuest LLC
789 East Eisenhower Parkway
P.O. Box 1346
Ann Arbor, MI 48106-1346

© Andrew Levan 2005

This thesis is copyright material and no quotation from it may be published without proper acknowledgement.

Declaration

I hearby declare that no part of this thesis has been previously submitted to this, or any other, University as part of the requirement for a higher degree. The work described herein was conducted by the undersigned, except for contributions from collegues as acknowledged in the preface or main text.

Andrew Levan

July 2005

Gamma-Ray Bursts and their Environments

Andrew J. Levan

ABSTRACT

Gamma-ray Bursts (GRBs) are the most energetic explosive events known in the universe and manifest themselves as a brief flash of high energy (X-ray and γ-ray) photons lasting for a few seconds. Subsequent to the prompt γ-ray flash, longer lasting afterglow emission is seen at X-ray, optical and radio wavelengths. These afterglows have allowed the precise positioning of GRBs on the sky, redshift measurements and the identification of host galaxies. They have also demonstrated that GRBs with durations of > 2s are relativistically beamed jetted outflows associated with the collapse of massive stars in a type Ic supernova.

In this thesis I present observations of several GRB afterglows and a large survey of GRB host galaxies. The goal of the research is to better understand the connection between GRBs, stellar collapse and star formation. The work presented here demonstrates that GRBs are a diverse population, showing that the supernovae associated with GRBs can span an order of magnitude in absolute luminosity, and are sometimes invisible, even in deep searches.

This work has also located the first good example of a GRB which is heavily optically extinguished due to the presence of dust in its host galaxy, demonstrating that dust extinction can account for a fraction of the "dark bursts", which are invisible at optical wavelengths.

Finally, the connection of GRBs to star formation at large is addressed via a comparison of the properties of the host galaxies of GRBs and core collapse supernovae. I show that GRBs are much more concentrated on their host galaxy light than supernovae and, furthermore, have host galaxies significantly smaller and less luminous than those of SN. Jointly these results indicate that GRBs may originate in low metallicity environments, and come from the most massive stars. This result may have important consequences for the use of GRBs as probes of high redshift star formation.

Additional Publications

In addition to the work presented in this thesis the following publications have also resulted from work in which I have participated during the course of my PhD studies. Only work to which I have contributed significantly (normally represented by a first author publication) is presented in this thesis.

1. **" The locations of cosmic explosions"**
   A.S. Fruchter, **A.J. Levan**, L. Strolger, P.M. Vreeswijk, S.E. Thorsett, D. Bersier, I. Burud, J.M. Castro Ceron, C. Conselice, T. Dahlen, H.C. Ferguson, J.P.U. Fynbo, P.M. Garnavich, R.A. Gibbons, J. Gorosabel, T.R. Gull, J. Hjorth, S.T. Holland, C. Kouveliotou, Z. Levay, M. Livio, P.E. Nugent, L. Petro, E. Pian, J.E. Rhoads, A.G. Riess, K.C. Sahu, A. Smette, N.R. Tanvir, R.A.M.J. Wijers, S.E. Woosley
   Nature, submitted

2. **"The millimetric properties of GRB host galaxies"**
   R.S. Priddey, N.R. Tanvir, **A.J. Levan**, R.A.M.J. Wijers, A. Fruchter, C. Kouveliotou, I. Smith
   MNRAS, submitted

3. **"A mean redshift of 2.8 for Swift gamma-ray bursts"**
   P. Jakobsson, **A. Levan**, J.P.U Fynbo, R. Priddey, J. Hjorth, N. Tanvir, D. Watson, B.L. Jensen, J. Sollerman, P. Natarajan, J. Gorosabel, J.M. Castro Ceron, K. Pedersen, T. Pursimo, A.S. Arnadottir, A.J. Castro-Tirado, C.J. Davis, H. Deeg, D.A. Fiuza, S. Mykolaitis, S.G. Sousa
   A&A, submitted astro-ph/0509888

4. **"Discovery and identification of the very high redshift afterglow of GRB 050904"**
   J.B. Haislip, M.C. Nysewander, D.E. Reichart, **A. Levan**, N. Tanvir, S.B. Cenko, D.B. Fox, P.A. Price, A.J. Castro-Tirado, J. Gorosabel, C.R.Evans, E. Figuerdo, C. MacLeod, J. Kirschbrown, M. Jelenik, S. Guizy, A de Ugarte Postigo, E.S. Cypriano, A. LaCluyze, J. Graham, R. Priddey, R. Chapman, J. Rhoads, A.S. Fruchter, D.Q. Lamb, C. Kouveliotou, R.A.M.J. Wijers, B.P. Schmidt, A.M. Soderberg, S.R. Kulkarni, F.A. Harrison, D.S. Moon, A. Gal-Yam, M.M. Kasliwal, R. Hudec, S. Vitek, P. Kubanek, J.A. Crain, A.C. Foster, M.B. Bayliss, J.C. Clemens, J.W. Bartleme, R. Canterna, D.H. Hartmann, A.A. Henden, S. Klose, H-S. Park, G.G. Williams, E. Rol, P. O'Brien, D. Bersier, F. Prado, S. Pizarro, D. Maturana, P. Ugarte, A. Alvarez, A.J.M.

Fernadez, M.J. Jarvis, M. Moles, E. Alfaro, N.D. Kumar, C.Mack, N. Gehrels, S. Barthelmy, D.N. Burrows,

Nature, in press, astro-ph/0509660

5. **"Swift observations of the X-ray bright GRB 050315"**

   S. Vaughan, M.R. Goad, A. Beardmore, P.T. O'Brien, J. P. Osborne, K.L. Page, S.D. Barthelmy, D.N. Burrows, S. Campana, J.K. Cannizzo, M. Capaldi, G. Chincarini, J.R. Cummings, G. Cusumano, P. Giommi, O. Godet, J.E. Hill, S. Kobyashi, P. Kumar, V. La Parola, **A. Levan**, V. Mangano, P. Meszaros, A. Moretti, D. Morris, J.A. Nousek, C. Pagani, D.M. Palmer, J.L. Racusin, P. Romano, G. Tagliaferri, B. Zhang, N. Gehrels

   ApJ, in press, astro-ph/0510677

6. **"a log N(HI) of 22.5 DLA in a dark gamma-ray burst: the environment of GRB 050401"**

   D. Watson, J.P.U. Fynbo, C. Ledoux, P. Vreeswijk, J. Hjorth, K. Aoki, T. Augusteijn, A. Beardmore, D. Bersier, J.M. Castro-Ceron, P. D'Avanzo, D. Diaz-Fraile, P. Hirst, P. Jakobsson, B.L. Jensen, N. Kawai, G. Kosugi, **A. Levan**, J. Masegosa, J. Naranen, K.L. Page, K. Perderson, A. Pozanenko, J.N. Reeves, V. Rumyantsevv, T. Shahbaz, D. Sharapov, A. Smette, J. Sollerman, R.L.C. Starling, N. Tanvir. K. Torstensson, K. Wiersema

   ApJ, submitted, astro-ph/0510368

7. '**"Gas and dust properties in the afterglow spectrum of GRB 050730"**

   R.L.C. Starling, P.M. Vreeswijk, S.L. Ellison, E. Rol, K. Wiersema, **A. Levan**, N.R. Tanvir, R.A.M.J. Wijers, C. Tadhunter, J.R. Zaurin, R. Gonzalez Delgado, C. Kouveliotou

   A&A 2005, 442, 21

8. **"The soft X-ray blast in the apparently sub-luminous GRB 031203"**

   D. Watson, S.A. Vaughan, R. Willingale, J. Hjorth, S. Foley, J.P.U. Fynbo, P. Jakobsson, **A. Levan**, P.T. O'Brien, J.P. Osborne, K. Pederson, J.N. Reeves, J.A. Tedds, M.G. Watson

   ApJ, in press, astro-ph/0509477

9. **"Some short duration γ-ray bursts originate in the low redshift universe"**

   N.R. Tanvir, R. Chapman, **A.J. Levan**, R. Priddey

   Nature, in press

10. **"A near-IR spectrum of the DO white dwarf RE J0503-285"**

P.D. Dobbie, M.R. Burleigh, **A.J. Levan**, M.A. Barstow, R. Napiwotski, I. Hubeny
A&A, 2005, 439, 1159

11. **"GRB 050223: A faint Gamma-Ray Burst discovered by *Swift*"**
K.L. Page, E. Rol, **A.J. Levan**, B. Zhang, J.P. Osborne, P.T. O'Brien, A. P. Beardmore, D.N. Burrows, S. Campana, G. Chincharini, J.R. Cummings, G. Cusumano, N. Gehrels, P. Giommi, M.R. Goad, O. Godet, V. Mangano, G. Tagliaferri, A.A. Wells
MNRAS, 2005, 363, 76

12. **"Constraints on short gamma-ray burst models with optical limits of GRB 050509b"**
J. Hjorth, J. Sollerman, J. Gorosabel, J. Granot, S. Klose, C. Kouveliotou, J. Melinder, E. Ramirez-Ruiz, R. Starling, B. Thomsen, M. I. Andersen, J. P. U. Fynbo, B. L. Jensen, P. M. Vreeswijk, J. M. Castro Cerón, P. Jakobsson, **A. Levan**, K. Pedersen, J. E. Rhoads, N. R. Tanvir, D. Watson, R. A. M. J. Wijers
ApJL, 2005, 630, 117

13. **"The first localization of a short gamma-ray burst by Swift"**
N. Gehrels, C.L. Sarazin, P.T. O' Brien, B. Zhang, L. Barbier, S.D. Barthemly, A. Blustin, D.N. Burrows, J. Cannizzo, J.R. Cummings, M. Goad, S.T. Holland, C.P. Hurkett, J.A. Kennea, **A. Levan**, C.B. Markwardt, K.O. Mason, P. Meszaros, M. Page, D.M. Palmer, E. Rol, T. Sakamoto, R. Willingale, L. Angelini, A. Beardmore, P.T. Boyd, A. Breeveld, S. Campana, M.M. Chester, G. Chincarini, L.R. Cominsky, G. Cusumano, M. de Pasquale, E.E. Fenimore, P. Giommi, C. Gronwall, D. Grupe, J.E. Hill, D. Hinshaw, J. Hjorth, D. Hullinger, K.C. Hurley, S. Klose, S. Kobayashi, C. Kouveliotou, H.A. Krimm, V. Mangano, F.E. Marshall, K. McGowan, A. Moretti, R.F. Moshotzky, K. Nakazawa, J.P Norris, J.A. Nousek, J.P. Osborne, K. Page, A.M. Parson, S. Patel, M. Perri, T. Poole, P. Romano, P.W.A. Roming, S. Rosen, G. Sato, P. Schady, A.P. Smale, J. Sollerman, R. Starling, M. Still, M. Suzuki, G. Tagliaferri, T. Takashashi, M. Tashiro, J. Tueller, A.A. Wells, N.E. White, R.A.M.J. Wijers
Nature, 2005, 437, 851

14. **"Gamma-Ray Burst Selected High Redshift Galaxies: Tracing the Starbursting Population to $z \sim 3$"**
C. J. Conselice, P. M. Vreeswijk, A. S. Fruchter, **A. Levan**, C. Kouveliotou, J. Fynbo, J. Gorosabel, N. R. Tanvir, and S. E. Thorsett

ApJ, 2005, 633, 29

15. **"Infrared and Optical Observations of GRB 030115 and its Extremely Red Host Galaxy: Implications for Dark Bursts"**

    Andrew Levan, Andrew Fruchter, James Rhoads, Bahram Mobasher, Nial Tanvir, Javier Gorosabel, Evert Rol, Chryssa Kouveliotou, Ian Dell'Antonio, Michael Merrill, Eddie Bergeron, Jose Maria Castro Ceron, Nicola Masetti, Paul Vreeswijk, Angelo Antonelli, David Bersier, Alberto Castro-Tirado, Johan Fynbo, Peter Garnavich, Stephen Holland, Jens Hjorth, Peter Nugent, Elena Pian, Alain Smette, Bjarne Thomsen, Stephen Thorsett, Ralph Wijers

    ApJ, submitted

16. **"Late-epoch optical and near-infrared observations of GRB 000911 and its host galaxy**

    N. Masetti, E. Palazzi, E. Pian, L. Hunt, J.P.U Fynbo, J. Gorosabel, S. Klose, S. Benetti, R. Falomo, A. Zeh, L. Amati, M.I. Andersen, A.J. Castro-Tirado, J.M. Castro Ceron, J. Danziger, F. Frontera, A.S. Fruchter, J. Greiner, J. Hjorth, B.L. Jensen, L. Kaper, C. Kouveliotou, **A. Levan**, A. Magazzu, P. Moller, L. Nicastro, H. Pederson, N.R. Tanvir, P.M. Vreeswijk, R.A.M.J. Wijers, E.P.J. van den Heuvel.

    A&A, 2005, 438, 841

17. **" A possible bright blue SN in the afterglow of GRB 020305"**

    J. Gorosabel, J.P.U. Fynbo, A. Fruchter, **A. Levan**, J. Hjorth, P. Nugent, A.J. Castro-Tirado, J.M. Castro Ceron, J. Rhoads, D. Bersier, I. Burud

    A&A, 437,411, 2005

18. **" On the afterglow and host galaxy of GRB 021004: A comprehensive study with the Hubble Space Telescope"**

    J.P.U Fynbo, J. Gorosabel, A. Smette, A. Fruchter, J. Hjorth, K. Pederson, **A. Levan**, I. Burud, K. Sahu, P.M. Vreeswijk, E. Bergeron, C. Kouveliotou, N. Tanvir, S. E. Thorsett R.A.M.J. Wijers, J.M. Castro Ceron, A. Castro-Tirado, P. Garnavich, S.T. Holland, P. Jakobsson, P. Moller, P. Nugent, E. Pian, B. Thomsen, D. Watson, S. Woosley.

    ApJ, in press

19. **" A deep search with HST for late time supernova signatures in the hosts of XRF 011030 and XRF 020427"**

    Andrew Levan, Sandeep Patel, Chryssa Kouveliotou, Andrew Fruchter, James Rhoads, Ev-

ert Rol, Jens Hjorth, Ralph Wijers, Johan Fynbo, Enrico Ramirez-Ruiz, Alberto Castro-Tirado, Elena Pian, Stephen Holland, Stephen Thorsettt, Jose Maria Castro Ceron, Nial Tanvir
ApJ, 2005, 622, 977

20. **"A near-IR spectroscopic search for very low mass companions to notable DA white dwarfs"**
P.D. Dobbie, M.R. Burleigh, **A.J. Levan**, M.A. Barstow, R. Napiwotski, J.B. Holberg, I. Hubeny, S.B. Howell
MNRAS, 2005, 357, 1049

21. **"The Ultimate Outcome of BH-NS mergers"**
Melvyn B. Davies, **Andrew J. Levan**, Andrew R. King
MNRAS, 2005, 356, 54

22. **" GRB 020410: A GRB afterglow discovered by its supernova light"**
Andrew Levan, Peter Nugent, Andrew Fruchter, Ingunn Burud, David Branch, Alberto Castro-Tirado, Javier Gorosabel, Jose Maria Castro Ceron, Stephen Thorsett, Chryssa Kouveliotou, Sergey Golentskii, Johan Fynbo, Peter Garnavich, Stephen Holland, Jens Hjorth, Palle Moller, Elena Pian, Nial Tanvir, Mihail Ulanov, Ralph Wijers, Stan Woosley
ApJ, 2005, 624, 880

23. **"Discovery of the faint Near-IR afterglow of GRB 030528"**
A. Rau, J. Greiner, S. Klose, M. Salvato, J.M. Castro Ceron, D.H., Hartmann, A. Fruchter, **A. Levan**, N.R. Tanvir, J. Gorosabel, J. Hjorth, A. Zeh, A Kupcu Yoldas, J. Beaulieu, J. Donatawicz, C. Vinter, A.J. Castro-Tirado, J.P.U. Fynbo, D.A. Kann, C. Kouveliotou, N. Masetti, P. Moller, E. Palazzi, E. Pian, J. Rhoads, R.A.M.J. Wijers, E.P.J. van den Heuvel.
A&A, 2004, 427, 815

24. **"The line-of-sight towards GRB 030429 at $z = 2.66$: Probing the matter at stellar, galactic and intergalactic scales"**
P. Jakobbson, J. Hjorth, J.P.U. Fynbo, M. Weidinger, J. Gorosabel, C. Ledoux, D. Watson, G. Bjornsson, E. Gudmundsson, R.A.M.J. Wijers, K. Pederson, J. Soller man, P. Moller, A.A. Henden, B.L. Jensen, A. Gilmore, P. Kilmartin, **A. Levan**, J.M. Castro Ceron, A.J. Castro-Tirado, N. Masetti, P. Vreeswijk, and N. Tanvir
A&A, 2004, 427, 785

25. **"On the Afterglow of the X-Ray Flash of July 23 2003: Photometric evidence for an off-axis**

Gamma-Ray Burst with an associated Supernova?"

J. P. U. Fynbo, J. Sollerman, J. Hjorth, F. Grundahl, J. Gorosabel, M. Weidinger, P. Moller, B. L. Jensen, P. M. Vreeswijk, C. Fransson, E. Ramirez-Ruiz, P. Jakobsson, S. F. Jorgensen, C. Vinter, M. I. Andersen, J. M. Castro Ceron, A. J. Castro-Tirado, A. S. Fruchter, J. Greiner, C. Kouveliotou, **A. Levan**, S. Klose, N. Masetti, H. Pedersen, E. Palazzi, E. Pian, J. Rhoads, E. Rol, T. Sekiguchi, N. R. Tanvir, P. Tristram, A. de Ugarte Postigo, R. A. M. J. Wijers, E. van den Heuvel

ApJ, 2004, 609, 962

26. **"Chandra Observations of the X-ray Environs of SN 1998bw/GRB 980425"**

C. Kouveliotou, S.E. Woosley, S.K. Patel, **A. Levan**, R. Blandford, E. Ramirez-Ruiz, R.A.M.J. Wijers, M.C. Weisskopf, A. Tennant, E. Pian, P. Giommi

ApJ, 2004, 608, 872

27. **"A very low luminosity X-ray flash: XMM-Newton observations of GRB 031203"**

D. Watson, J. Hjorth, **A. Levan**, P. Jakobsson, P.T. O'Brien, J. P. Osborne, K. Pederson, J.N. Reeves, J.A. Tedds, S. Vaughan, M. J. Ward, R. Willingale

ApJL, 2004, 605, 101

28. **"The host of GRB 030323 at z = 3.372: a very high column density DLA system with a low metallicity"** P.M. Vreeswijk, S.L. Ellison, C. Ledoux, R.A.M.J. Wijers, J.P.U. Fynbo, P. Moller, A. Henden, J. Hjorth, G. Masi, E. Rol, N. Tanvir, **A. Levan** , J.M. Castro Ceron, J. Gorosabel, A.J. Castro-Tirado, A.S. Fruchter, C. Kouveliot ou, I. Burud, J. Rhoads, N. Masetti, E. Palazzi, E. Pian, H. Pederson, L. Kaper, A. Gilmore, P. Kilmartin, J. V. Buckle, M.S. Seigar, D.H. Hartmann, K. Lindsay, E.P.J van den Heuvel

A&A, 2004, 419, 927.

29. **" The X-ray, optical and radio evolution of the GRB 030329 afterglow and the associated SN2003dh"**

R. Willingale, J. Osborne, P. O'Brien, M.J. Ward, **A. Levan**, K. Page MNRAS, 2004, 349, 31

30. **"The discovery of an evolving dust scattered X-ray halo around GRB 031203' '**

S. Vaughan, R. Willingale, P.T. O'Brien, J.P. Osborne, J.N. Reeves, **A.J. Levan**, M.G. Watson, J.A. Tedds, D. Watson, M. Santos-Lleo, P.M. Rodr iguez Pascual, N. Schartel

Astrophysical Journal Letters, 2004, 603, L5

31. **"A comparison of white dwarf temperatures and gravities from FUSE Lyman line and ground based Balmer line observations"**
M.A. Barstow, S.A. Good, M.R. Burleigh, I. Hubeny, J.B. Holbery, **A. Levan**
MNRAS, 2003, 344, 562

32. **"Optical photometry of GRB 021004: The first month"**
Stephen T. Holland, Michael Weidinger, Johan P.U. Fynbo, Javier Grosabel, Jens Hjorth, Kristian Pederson, Micahel I. Anderson, Thomas Augusteujn, Jose M. Castro Ceron, Alberto Castro-Tirado, Haakon Dahle, M.P. Egholm, Pall Jakobsson, Brain Jensen, **Andrew Levan**, Javier Mendez, Pa lle Moller, Holder Pederson, Tapio Pursimo, Pilar Ruiz-Lapeunte and Bjarne Thoms en.
Astronomical Journal, 125, 2291-2298, May 2003

33. **"Optical and near-infrared observations of the GRB 020405 afterglow"**
N. Masetti, E. Palazzi, E. Pian, A. Simoncelli, K.L. Hunt, E. Maiorano, **A. Levan**, L. Christensen, E. Rol, S. Savaglio, R. Falomo, A.J . Castro-Tirado, J. Hjorth, A. Delsanti, M. Pannella, V. Mohan, S.B. Pandey, R. Sagar, L. Amati, I. Burud, J.M. Castro-Ceron, F. Frontera, A.S. Fruchter, J.P.U. Fynbo, J. Gorosabel, L. Kaper, S. Klose, C. Kouveliotou, L. Nicastro, H. Peders on, J. Rhoads, I. Salamanca, N. Tanvir, P.M. Vreeswijk, R.A.M.J Wijers, E.P.J v an den Heuval.
Astronomy & Astrophysics, 404, 465, 2003

34. **"The Afterglow of GRB 0111211 and its Host Galaxy"**
P. Jakobsson, J. Hjorth, J. Fynbo, J. Grosabel, K. Pederson, I. Burud, **A. Levan**, A. Fruchter, J. Rhoads, T.Grav, M.W. Hansen, R. Michelsen, M.I. Anderson, B.L. Jensen, H. Pederson, B. Thomsen, M. Weidinger, S.G. Bhargavi, R. Cowsik and S.B. Pandey.
Astronomy and Astrophysics, 2003, 408, 941

35. **"A comparison of white dwarf temperatures and gravities from Lyman and Balmer line studies"**
M.A. Barstow, J.B. Holberg, I. Hubeny, S.A. Good, **A.J. Levan** and F. Meru
Monthly Notices of the Royal Astronomical Society, 328, 211, 2001

Further to these works results many results have been rapidly disseminated to the community via GCN circulars, these circulars are numbers:

2005:3028,3031,3051,3176,3372,3374,3378,3521,3613,3618,3620,3632, 3685, 3710, 3927,3940, 4053

2004:2684,2682,2655,2638,2636,2602,2544,2513

2003:2490,2489,2263,2243,2242,2240,2185,2006,1866,1844,1818

2002:1781,1767,1761,1758,1756,1696,1688,1684,1597,1585,1557,1536,1518,1517,1512,1474 1453,1440

Preface

GRB astronomy is a rapidly evolving and observationally demanding field. The study of GRBs necessitates the near simultaneous use of a large number of observatories with wide geographical and wavelength coverage. This is best achieved by working in large collaborations spanning available national facilities and providing experience at many wavelengths from γ-ray to radio. The work presented in this thesis has been performed over the period September 2002-July 2005, while working within two of these large collaborations (as well as smaller groups working on the UK national telescopes). These are the Gamma-Ray Afterglow Collaboration at ESO (GRACE) and the GRB Optical Studies with HST Collaboration (GOSH).

The work which is presented in this thesis is largely my own. However it has been improved by the comments and insight of many members of the collaborations in which I work. In addition to this there are a number of specific data points which others have contributed, these are described below.

In chapter 3 the *Konus-Wind* data were provided by Sergei Golenetskii. Photometry of the afterglow was compared to expectations of supernovae template spectra which were produced by Peter Nugent.

The analysis of the Chandra observations of XRF 011030 and 020427 was performed by Sandy Patel, while the extrapolation of the X-ray data into the optical regime was done by Evert Rol.

Initial processing of the NICMOS observations of GRB 030115 was performed by Eddie Bergeron and the images of GRB 030115 obtained at the Nordic Optical Telescope were provided by Johan Fynbo. Template spectra and priors for use in BPZ were provided by Bahram Mobasher, as were the photometry catalogues for GOODS and the Ultra-Deep Field.

Astrometry and early data reduction for several of the host galaxies presented in Chapter 7 (mainly those observered prior to 2001) was undertaken by Paul Vreeswijk and Andy Fruchter. The supernovae presented in chapter 7 were initially discovered and typed by the GOODS collaboration (in particular by Lou Strolger). The reduced images used for the analysis were provided by GOODS. All subsequent analysis was performed by myself.

Additionally, all of the ground based optical observations obtained for this thesis have been conducted as Target of Opportunity observations triggered by myself or other members of the collaborations of which I am member. The observers who performed these observations have also played an important role in the scientific results presented in this thesis, often at the expense of their own programmes.

Acknowledgements

Well, where to start. I guess with those people who have contributed to this thesis directly. I would like to thank Andy Fruchter, who apart from introducing me to the science of Gamma-Ray Bursts as a summer student way back in 2001, has been a constant source of knowledge and encouragement through the completion of this work. Also many thanks to Martin Barstow for allowing me the freedom to pursue my work on GRBs, much to the neglect of white dwarf studies! I have been very lucky to have many others who have been there to offer help and advice along the road and have kept me motivated and interested throughout. I am extremely appreciative for the help I have received from Nial Tanvir, Melvyn Davies, Chryssa Kouveliotou, Evert Rol, James Rhoads, Paul O'Brien, Jens Hjorth, Ralph Wijers and many others. The large supporting network provided by GRACE and GOSH has been a constant help in providing both an endless supply of data and a great wealth of experience. It has been a pleasure to work with the many wonderful people in each of these collaborations.

I have been greatly priviledged over the last three years to occupy a lively and cheerful office, with office mates who have not only provided interesting scientific discussion, but have also provided me with much needed relief in stressful times (such as approaching proposal deadlines). Thanks to Leigh, Pam, Mark, Becks and Cheryl for this, and a special thanks to Ann-Marie for always being there to listen, understand, and help when it was needed.

My friends have alas not seen as much of me as I would have liked, especially over the past few months. None-the-less they have been invaluable to me throughout. Without your support and friendship the road over the past three years would have been much harder to travel. In particular I would like to thank David, for enabling my escapism; Stuart for a long, friendly competition which drove us through school and University. Thanks to Jeff for his early encouragement as I became interested in physics and to Carly for her continuing support. Finally to Sam, for her long friendship and ability to always make me smile.

I am forever indebted to my family, for their fantastic support in every way throughout my education and for encouraging me to pursue my dreams from the earliest of ages. The unconditional support that I have had from you all has meant more to me than I can explain, and I am forever grateful.

CONTENTS

1 Introduction **2**

1.1 A Brief History of Gamma-Ray Bursts 2

1.2 Theory of GRB production 7

1.2.1 Prompt Emission 7

1.2.2 The central engine 10

1.2.3 Afterglow Models 14

1.2.4 Optical Light Curves 14

1.3 Host Galaxies 17

1.4 GRBs as Probes of Environments 19

1.4.1 GRBs as probes of stellar physics 19

1.4.2 GRBs as probes of galactic and intergalactic structure 20

1.4.3 GRBs as cosmological probes 20

1.5 This thesis 22

2 Methods and Observational Strategies **24**

2.1 Locating GRBs 24

2.1.1 Detecting GRBs 25

2.1.2 BeppoSAX 25

2.1.3 HETE-2 26

2.2 Distributing Information: The GCN Network 26

2.3 The need for speed 28

2.4 The role of Optical and IR observations 28

2.5 *HST* observations and this thesis 29

2.6 Drizzle 31

2.7 GRB vital properties 33

3 GRB 020410 and its supernova **36**

3.1 Introduction 36

3.2 Observations 37

3.2.1 Photometry and Light Curve 39

3.2.2 Host Galaxy 46

3.3 Supernova lightcurve fitting 47

3.4 Comparison with other GRBs 55

3.5 Conclusions 56

4 A supernova search in two XRF hosts **58**

4.1 Introduction 58

4.2 Observations 60

4.3 *HST* Observations 63

4.3.1 Astrometric Alignment 64

4.3.2 Lack of residual optical emission at 40 days after the burst trigger 65

4.4 Discussion 69

4.5 Conclusions 75

5 GRB 030115 and its host galaxy **77**

5.1 Introduction 77

5.2 Observations 80

5.2.1 Infrared observations 81

5.2.2 Optical Observations of the GRB 030115 afterglow 82

5.2.3 *HST* observations of the GRB 030115 host galaxy 84

5.2.4 Photometry and Light Curve 85

5.3 The Host Galaxy – Photometric Redshift 86

5.4 Comparison of host properties 90

5.4.1 Host Galaxy Star Formation Rate and Extinction 92

5.5 A possible cluster at $z \sim 2.5$ 93

5.5.1 The number of density of EROs about GRB 030115 99

5.6 Energetics 100

5.7 The origin of the optical faintness of GRB 030115 101

5.7.1 Extinction 101

5.7.2 A dark burst caught? 102

5.8 Conclusions 102

6 Cosmic Explosions and their Host Galaxies **106**

6.1 Gamma-Ray Bursts and Star Formation 106

6.2 The sample 107

6.3 Supernova host galaxies 109

6.3.1 The GOODS Survey 109

6.4 Locations on host galaxies 111

6.5 Comparative properties of host galaxies 115

6.6 Why are GRBs and SNe different 117

6.7 Conclusions 123

7 Conclusions and Future Prospects **124**

7.1 The current status of GRB astronomy 124

7.2 Gamma-Ray Bursts, X-ray Flashes and Supernovae 125

7.3 Dusty GRBs 127

7.4 How do GRBs relate to massive star formation? 130

7.5 The Future 131

7.5.1 Swift 131

7.5.2 How does the GRB rate relate to metallicity? 132

7.5.3 What is the nature of the GRB host galaxies? 132

7.5.4 What is the GRB rate with redshift? 133

7.5.5 What is the true GRB energy release and are they standard candles? 134

7.5.6 What is the precise nature of the stars which produce GRBs? 134

7.5.7 What are the short duration GRBs? 136

7.6 Epilogue: Lighting up the Universe with GRBs 139

LIST OF FIGURES

1.1 2 classes of GRB 4

1.2 The sky distribution of BATSE GRBs 5

1.3 The temporal evolution of the spectrum of GRB 030329, showing the appearance of SN 2003dh 8

1.4 The lightcurve of a BATSE GRB 10

1.5 Spectra of GRBs and XRFs 11

1.6 The density structure of a rapidly rotating massive star shortly after core collapse . . . 13

1.7 A typical synchrotron spectrum of a GRB afterglow 15

1.8 The optical lightcuve of GRB 990510 17

1.9 The spectrum of the GRB 030323 afterglow and a *HST* image of its host galaxy 21

2.1 The GCN Network 27

2.2 A schematic reconstruction of the drizzle process 30

2.3 The "great eye chart in the sky", as seen through various *HST* optics 32

3.1 The lightcurve of GRB 020410 as seen by Konus-Wind 40

3.2 The optical light curve of GRB 020410 41

3.3 *HST*/STIS images of the afterglow and host galaxy of GRB 020410, taken at 4 epochs . 45

3.4 The lightcurves of normal supernovae Ia as a function redshift 48

3.5 The colour evolution of supernovae IIL over a range of redshifts 49

3.6 The lightcurve of an SN IIL at $z = 0.2$ 50

3.7 A fit to the afterglow of GRB 020410 using a high velocity SN Ic template 51

3.8 Colour and peak magnitude constraints on the redshift of GRB 020410 52

3.9 The contour range of redshifts for GRB 020410 53

4.1 The host galaxies of XRF 011030 and 020427 62

4.2 Extrapolation of the X-ray afterglows of XRF 011030 and 020427 to the optical band, compared to the optical limits 66

4.3 Limits on a SN in the XRF 011030 field 70

4.4 Limits on a SN in the XRF 020427 field 71

5.1 The discovery images of GRB 030115 82

5.2 The nIR light curve of GRB 030115 86

5.3 The spectral energy distribution of the GRB 030115 afterglow and host galaxy 87

5.4 The host galaxy of GRB 030115 as seen by *HST* 88

5.5 The best fitting spectral energy distribution for the host galaxy of GRB 030115 91

5.6 The (R-K) colours of GRB host galaxies as a function of redshift 95

5.7 Histogram of photometric redshifts for galaxies in the 030115 field, compared to photometric redshifts in the GOODS field 96

5.8 A histogram of the colours of possible members of the rich cluster in the GRB 030115 field 97

5.9 The colour magnitude distribution for galaxies in the GRB 030115 field 98

5.10 Normalised afterglow magnitudes compared to host galaxy colours for GRB hosts . . . 103

5.11 Comparative colours of GRB afterglows and host galaxies 104

6.1 A mosaic of the host galaxies of GRBs 110

6.2 A mosaic of the host galaxies of core collapse supernovae 112

6.3 The Locations of Explosions in Relation to Host Light 114

6.4 Absolute magnitude and size distributions for hosts of GRBs and SN 116

7.1 The luminosity function of XRF supernovae 128

7.2 Comparative redshifts and colours for GRB host galaxies and bright submm emitters . 129

7.3 The location of GRB 050509b in the BATSE catalogue 138

LIST OF TABLES

3.1 Optical photometry of the GRB 020410 afterglow 42

4.1 Properties of the X-ray afterglows of XRF 011030 and 020427 60

4.2 Photometry of the host galaxies of XRF 011030 and 020427 63

5.1 Optical and near Infrared observations of the GRB 030115 afterglow 83

5.2 *HST* photometry of the host galaxy of GRB 030115 84

5.3 Secondary IR standards in the GRB 030115 field 85

5.4 The colours and magnitudes of host galaxies and afterglows of a sample of GRB host galaxies 94

6.1 Fundamental properties of GRB host galaxies observed by HST 119

6.2 Fundamental properties of GRB host galaxies observed by HST (continued) 120

6.3 Fundamental properties of GRB host galaxies observed by HST (continued) 121

6.4 Properties of the host galaxies of core collapse supernovae 122

Part I :
Introduction and Techniques

Chapter 1

Introduction

1.1 A Brief History of Gamma-Ray Bursts

Gamma-Ray Bursts (GRBs) were discovered serendipitously by the US launched VELA satellites in the mid 1960s. These satellites were originally launched to monitor the 1964 Nuclear Test Ban Treaty between the US and the Soviet Union, however their enduring legacy will be the discovery of the rapid flashes of γ-rays, the brightest objects in the γ-ray sky, whose origin has been a mystery for much of the past 40 years. Throughout this time our ignorance was fueled largely by the inability of γ-ray observations to provide accurate celestial positions. The degree size error boxes provided by most GRB monitoring satellites largely precluded observations at longer wavelengths and therefore the ability to precisely locate GRBs on the sky and determine their location within the universe. As such, their distance scale remained largely uncertain, and was unable to constrain the plethora of models for GRB production. This gave rise to the "great debate" in the early 1990s between protagonists who believed in a galactic origin and those who believed that GRBs were located at cosmological distances.

It took nearly a quarter of a century from the first discovery for significant progress to be made towards GRB origins. The first major revolution occurred with the launch of the Compton Gamma-Ray Observatory (CGRO) in 1991. CGRO carried the Burst Alert Transient Experiment (BATSE). This consisted of a 8 γ-ray detectors placed at each corner of the satellite, these could record both the temporal and spectral properties of the GRBs and, via the relative γ-ray fluxes recorded at different detectors, could

also provide crude (few degree) positions on the sky. While its positional accuracy was not greatly enhanced from previous satellites BATSE's sensitivity lead to the discovery of a total of 2704 bursts over its 9 year lifetime. The analysis of these bursts lead to crucial insights into the nature of GRBs. The most important of these were:

- BATSE confirmed indications from earlier observations that the time distribution of GRBs was bimodal, split into bursts which are short < 2s with a hard spectrum and those with durations $>$ 2s and a softer spectrum (Kouveliotou et al. 1993, also Figure 1.1).
- The distribution of GRBs on the sky is isotropic, implying no correlation with the galactic plane or other nearby structures (see Figure 1.2). While not ruling out GRBs which lay within specific distance scales (e.g. in the halo, or within the scale height of the galactic disk) this result was generally taken as evidence of cosmological origin (Briggs et al. 1996).

These discoveries prompted further interest in locating the signatures of GRBs at wavelengths other than the γ-ray, leading to the development of a progenitor independent model for longer wavelength emission from GRBs, known as the fireball model (Mészáros & Rees 1992; Paczynski & Rhoads 1993). This model describes the generic evolution of a relativistic fireball caused by the deposition of a large energy within a small volume (conditions implied by the likely large distance scale and observed rapid variability). In this model the GRB itself is caused by internal shocks within the expanding outflow, while the interaction with the interstellar medium can lead to an observable afterglow at X-ray, optical and radio wavelengths.

Through the course of the 1990s various attempts were made to locate afterglows. These were largely concentrated on the follow-up of bursts which were detected by an array of satellites called the Interplanetary Network (IPN). The large separations between these satellites made it possible to obtain relatively small error boxes which could be searched at longer wavelengths. However the alerts were typically slow, and the predicted afterglows therefore faint. Despite the substantial efforts which were invested in this follow-up programme no afterglow identifications were forthcoming.

The afterglow era was instead heralded by the launch of the Italian-Dutch X-ray astronomy satellite *BeppoSAX*. *BeppoSAX* contained both narrow field X-ray Instruments (NFIs) and two wide field cameras, each capable of viewing a large (20×20 degree) region of sky at a given time. As such the wide

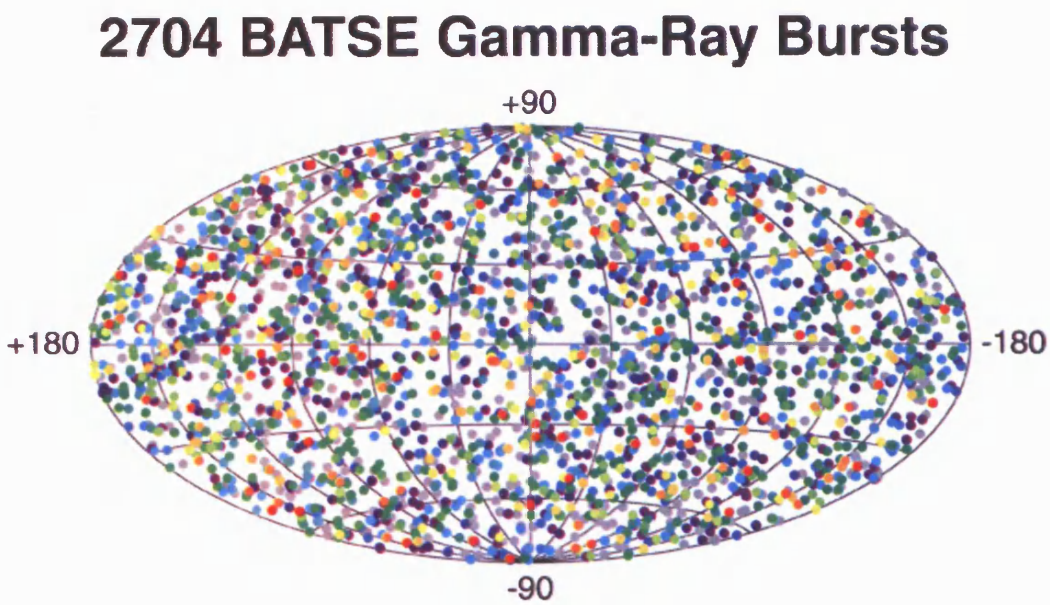

Figure 1.2: The sky distribution of GRBs observed by BATSE. This is consistent with being isotropic, and inconsistent with any correlation within the galactic plane

field cameras could capture GRBs and provide locations sufficiently accurate for follow-up with the NFIs. NFI positions were in turn accurate enough to allow follow-up at longer wavelengths (e.g. in the optical or radio passbands)*.

The breakthrough came with the burst of 28th February 1997 (GRB 970228; the convention for naming GRBs is GRB (year)(month)(day)). *BeppoSAX* detected this burst and pointed the NFI in $\sim$ 8 hours. A second observation obtained 4 days later revealed that a bright source within the position reported by the WFC had faded, this was the first discovered X-ray afterglow to a GRB (Costa et al. 1997). Observations of GRB 970228 were also pursued at optical wavelengths. Images obtained at the William Herschel Telescope only a few hours after burst revealed the presence of a fading point source when compared with images taken at the Issac Newton Telescope (INT) 7 nights later (van Paradijs et al. 1997). The precise position afforded by optical observations allowed for long time-base, multiwavelength observations for the first time, thereby enabling improved strategies for GRB searches to be implemented.

*Even without NFI positions WFC positions were sufficiently accurate enough to be observed from ground based facilities which had large field of views.

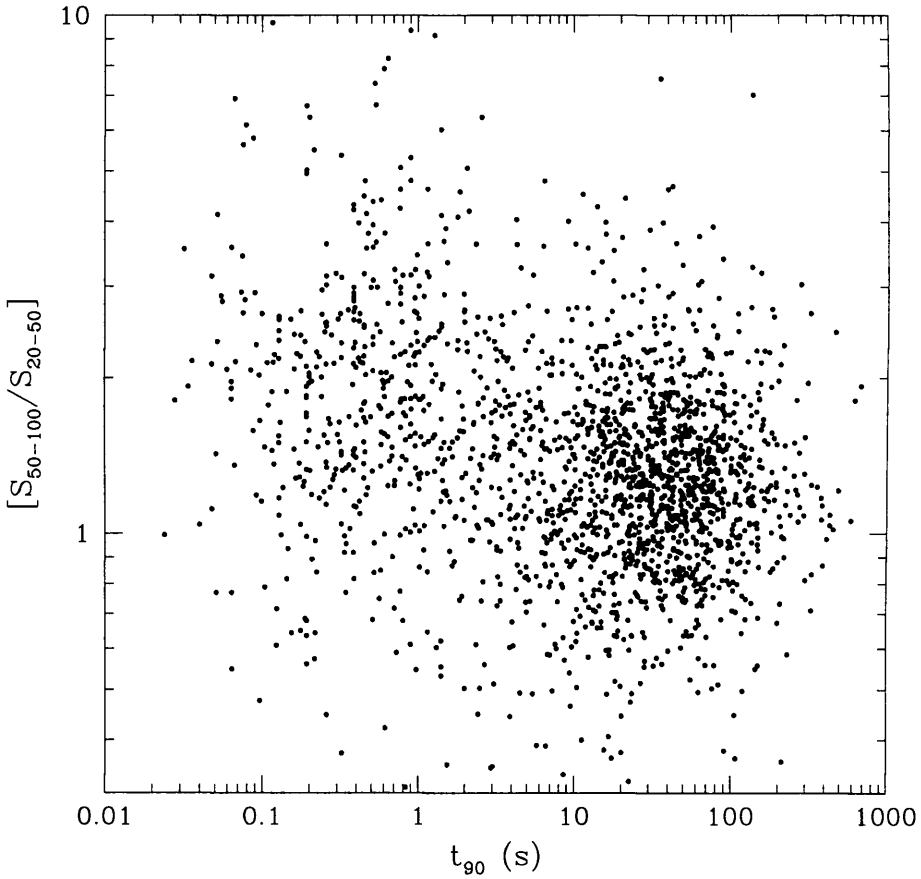

Figure 1.1: Durations and hardness ratios for GRBs detected by BATSE. The x-axis represents the duration over which 90% of the fluence of the burst arrived. The y-axis is the ratio of flux in the 25-50 and 50-100 keV bands. As can be seen the bursts split into two broad classes, long bursts with a fairly soft spectrum and short bursts with a harder spectrum. To date all optical afterglows have been located only for the long bursts.

Although GRB 970228 provided the first afterglow localisation, and a vital observational characterisation of the GRB phenomenon, it did not answer (at least at first) the most important question; where in the Universe do GRBs originate? Despite the "fuzzy" nature of the medium about the burst which was revealed by observations after the afterglow had faded it wasn't clear whether this was a local nebula or distant host galaxy, since a redshift measurement was not available. The distance to GRBs was finally resolved by spectroscopic observations of the afterglow of GRB 970508 which showed absorption lines at $z = 0.835$, finally proving that GRBs are of cosmological origin (Metzger et al. 1997).

BeppoSAX continued to localise GRBs throughout the late 1990s delivering approximately 10 bursts per year, allowing greater insight into the nature and diversity of GRBs. A further major breakthrough occurred with the burst GRB 980425. Optical observations of its error box failed to locate the fading afterglow but instead found a bright supernova, located at $z = 0.0085$ or 35 Mpc, a factor of 200 closer than the median GRB distance, and with an energy 10^5 times lower than typical GRBs (Galama et al. 1998). The supernova, named SN 1998bw was very unusual, belonging to the SN Ic class of supernovae, containing no hydrogen or helium in their spectra. The spectrum also showed exceptionally high velocities, higher than seen in any supernova before. The probability of a chance alignment of SN 1998bw with GRB 980425 was very small ($< 1 \times 10^{-5}$), and provided the first strong evidence for a connection between GRBs and SNe (see e.g. Zeh et al. 2004 and chapters 3 & 4 of this thesis).

The localisation of this low redshift supernova prompted searches for supernovae signatures in the lightcurves of higher redshift bursts. Supernovae light curves are powered by the Nickel production and its subsequent decay to Cobalt and Iron. They reach a peak days to weeks after core collapse with typical absolute magnitudes of $-16 < M_V < -19$. In contrast GRB afterglows are at their most luminous at early times (often $> 10,000$ times as luminous as the peak of a supernova) and fall rapidly. Therefore a supernova underlying a GRB would be seen to slow, or even reverse the decline of the afterglow itself. Additionally the (roughly) blackbody colours of the SN would begin to dominate over the power-law of the afterglow emission. This was first seen in the burst GRB 980326 (Bloom et al. 1999)[†] but such photometric bumps have since been seen in the afterglows of many GRBs.

However a number of other possible sources of bumps in GRB light curves have been proposed, includ-

[†]Note that although this GRB occurred before GRB 980425, late time images were not obtained for over a year, demonstrating that a plateau in the lightcurve, initially thought to be an underlying host galaxy, was in fact a contribution from a SN

ing inhomogeneities in the ISM about the progenitor, structure in the GRB outflow or the "refreshing" of the shockwave via the injection of energy after the burst. It was therefore clear that confirming the supernova connection would require the unambiguous observation of a supernova in a cosmological GRB. This evidence came from GRB 030329 at $z = 0.17$, the closest GRB since GRB 980425. Extensive observing campaigns on this burst with 8-10m class telescopes showed a clear supernova spectrum superimposed on the afterglow (see Figure 1.3), finally securing the relation between long duration GRBs and supernovae (Hjorth et al. 2003a; Stanek et al. 2003).

As GRBs are related to massive stars they have several others uses. Specifically they can be used to pinpoint the location of massive star formation in the early universe. The GRB rate as a function of redshift may be used as a proxy for the universal star formation rate and their galaxy type fraction is a means of constraining galaxies which contribute to star formation at any given cosmic epoch. Ultimately they may enable the detection of the location of the first, population III stars which are expected to produce bright GRBs due to their zero metallicity. The impact of metallicity on the production of GRBs will be discussed in more detail in chapter 6 of this thesis.

1.2 Theory of GRB production

1.2.1 Prompt Emission

The temporal structure of GRBs is highly diverse, varying from smooth to highly complex variability (Figure 1.4), they have a broad range of durations from 0.01 to 1000 seconds which is bimodal with peaks at ~ 1 and 30s. The lightcurves themselves show significant substructure and they can exhibit a multi-peaked structure with rapid variability. The most rapid millisecond variations in the temporal structure can be used to place limits on the physical size of the emitting region via light travel time arguments (the physical size of the region (R) is simply given by $c\delta t$ where the timescale of the rapid variations is δt), implying that the region is compact, and only a few kilometers across. This can be combined with the observed flux to place a limit on the photon density at the source of the GRB. These fluxes can be very large, up to 10^{-4} ergs s^{-1} cm^{-2}, which in turn indicates that the photon density at the source is very high for any GRB at cosmological distances. At this density photon-photon scattering leading to pair production should bar the production of very high energy photons (i.e. for photons with

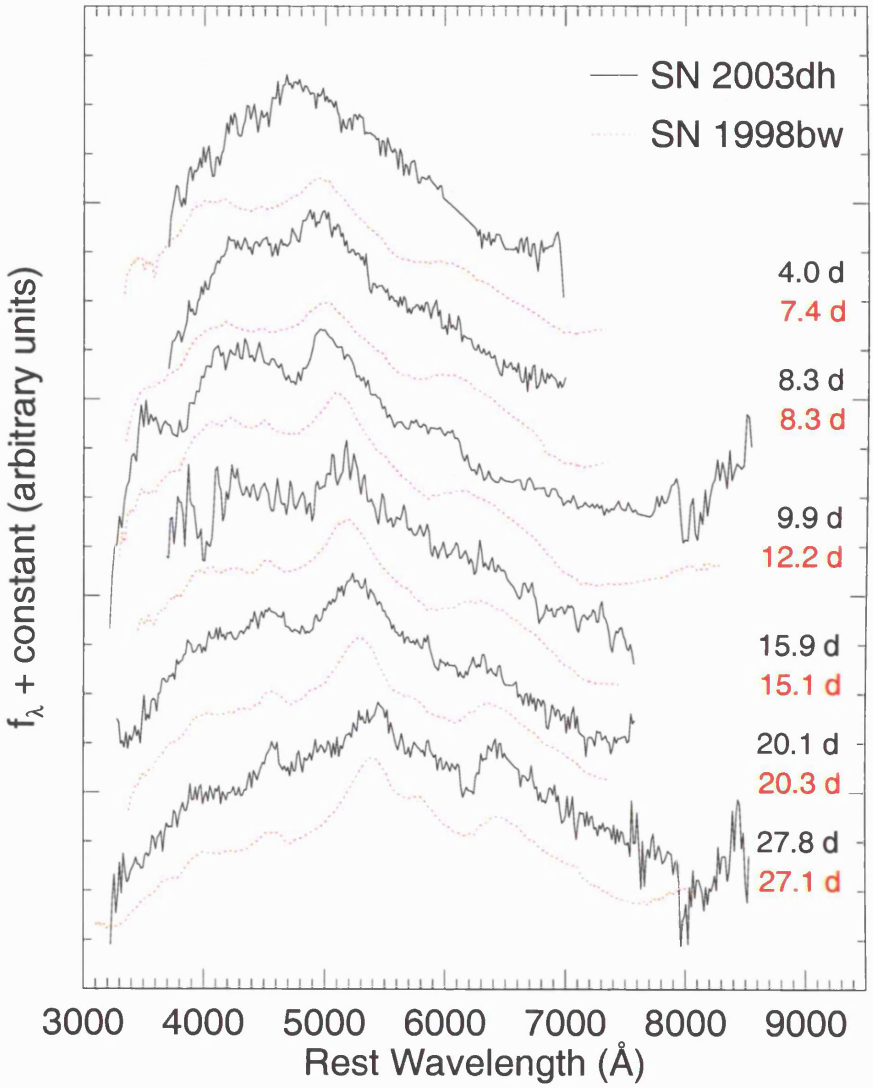

Figure 1.3: From Hjorth et al. 2003a: The time resolved spectrum of the GRB 030329 afterglow (at $z = 0.17$), compared with the spectrum of SN 1998bw taken at similar times. This burst, more than any other to date allowed for a conclusive confirmation of at least some long-GRBs with highly energetic core collapse SNe.

$E > 0.511$ MeV the reaction $\gamma + \gamma => e^+ + e^-$ should occur, blocking the emission of any very high energy photons). The solution to this problem is that the source must be expanding ultrarelativistically, with a bulk Lorentz factor (Γ) of 100 or more (corresponding to 99.995 % of the speed of light). In this case the energy of the photons is modified by $E_{obs} = \Gamma E_{true}$, (where E_{true} is the energy of the photons in their rest frame) so that the rest frame energies of the photons are dramatically reduced compared to the observed energies and are not sufficient for pair production. This can be expressed by the so called "compactness parameter" (Cavallo & Rees 1978; van Paradijs, Kouveliotou & Wijers, 2001).

$$C = \frac{L\sigma_T}{m_p c^3 R} \approx \frac{F_\gamma d^2 \sigma_T}{m_p c^4 \delta t} \sim 10^{12} F_{\gamma-4} d^2_{Gpc}/(\delta t)_{ms} \tag{1.1}$$

Where m_p and σ_T are the mass of a proton and the Thompson cross section, d is the luminosity distance to the GRB and $F_{\gamma-4}$ the peak flux of the GRB in units of 10^{-4} ergs s^{-1} cm^{-2}. C is essentially a measure of the optical depth of the fireball, thus in the non-relativistic case $C > 1$ would imply the fireball is optically thick. In this case pair production would block the production of γ-rays and the observed spectrum would be thermal. Therefore the presence of a non-thermal spectrum (see below) and of high energy emission directly implies that GRBs are ultrarelativistic explosions.

GRB spectra are more uniform than their temporal properties and are best fit by a non-thermal synchrotron spectrum with a two component power-law having a break energy (E_0) between the two components which lies in the range 100-1000 keV (Band et al. 1993). A range of behaviours for the prompt spectra of GRBs are shown in Figure 1.5. The peak of the νF_ν spectrum (E_p) can be seen to lie across a wide range of energies and indeed its location has been used to further sub-divide the GRBs into X-ray rich GRBs and X-ray flashes (XRFs) which are both characterised by increasingly softer spectra and lower peak energies. The most extreme population, the XRFs, actually emit the majority of their energy in the X-ray rather than γ-ray bands and were only discovered when GRBs began to be detected in softer bands by the *BeppoSAX* WFCs and HETE-2. The XRFs account for approximately 1/3 of the total burst population but were unseen by the higher energy detectors on BATSE. The origin of XRFs has been of great interest recently and is discussed in more detail in chapter 4.

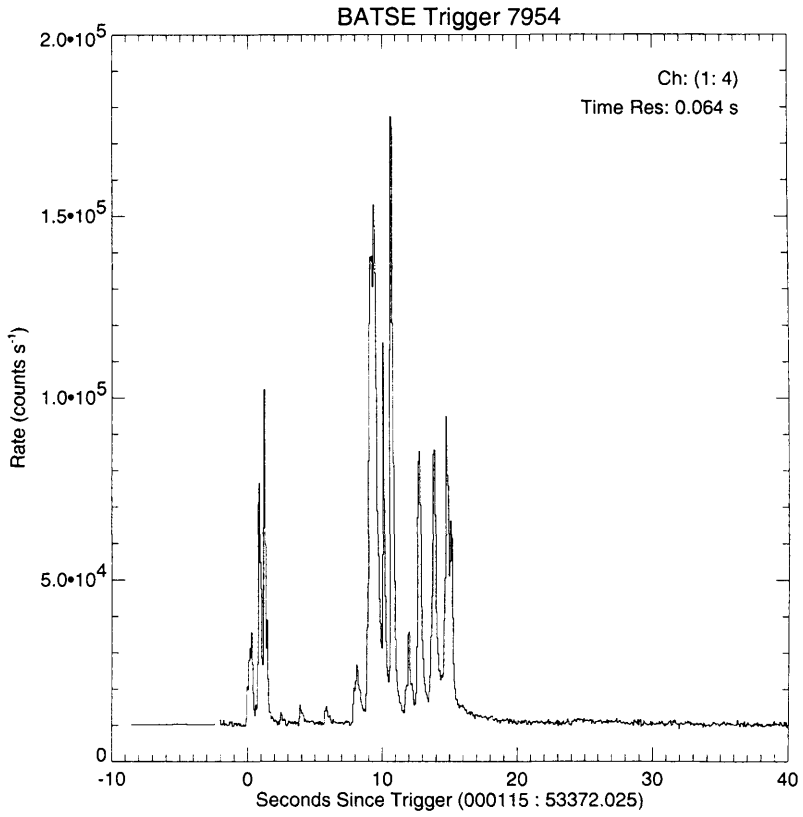

Figure 1.4: The lightcurve of a GRB observed with BATSE, showing several peaks. GRB lightcurves exhibit a wide range of behaviour including structure such as that seen here and smooth lightcurves lasting from a fraction of a second up to ten minutes or more.

1.2.2 The central engine

The discovery that GRBs lie at cosmological distances led to the realisation that their energy releases were very large, if the emission is assumed to be isotropic then the inferred energy can be as high as 10^{54} ergs, although it is likely that this emission is strongly beamed, reducing the true energy release to only 10^{51} ergs. However, this energy budget is still very large, and there are relatively few known mechanisms which can plausibly create such energy, these necessarily require the study of extreme astrophysical phenomena including ultrarelativistic outflows and the formation of black holes.

The most popular model for the production of a GRB is the collapse of a torus surrounding a black hole (see e.g. Fryer, Woosley & Hartmann 1999). This black hole accretion disk (BHAD) system can originate from a variety of different mechanisms the most popular of which are the collapse of a

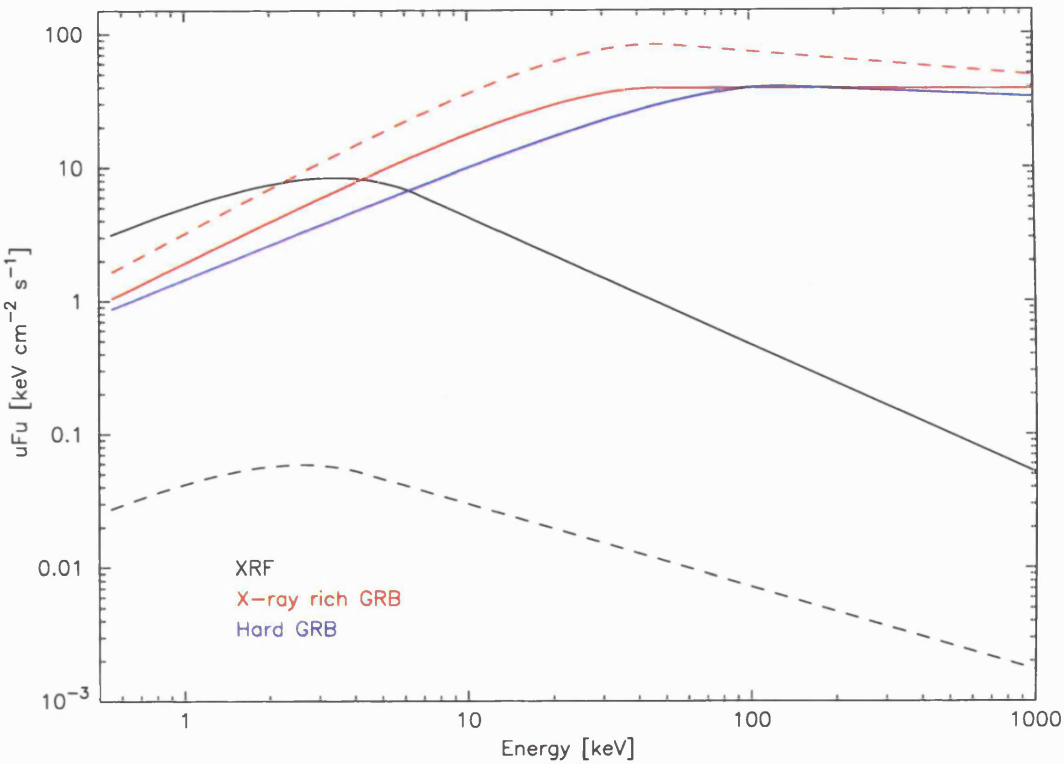

Figure 1.5: The variety of spectral properties exhibited by GRBs. Typical hard spectrum GRBs are shown in blue (GRB 030328), X-ray rich bursts are shown in red (GRB 010613, solid line and GRB 021211, dashed) and X-ray Flashes are shown in black (XRF 010213, solid line and XRF 020903, dashed).

rapidly rotating massive star or the merger of a tight binary containing two compact objects (neutron stars or black holes). Long duration GRBs are most likely caused by the former mechanism, although the latter remain of interest as candidate progenitors of the short duration bursts, which to date have no convincing optical counterparts.

Supernova Progenitors

Although it is now clear that long duration bursts are caused by stellar core collapse, the supernovae in which they are formed are by no means ordinary. The most likely model for the production of GRBs in core collapse is the collapsar model, first suggested by Woosley (1993). In this model the BHAD forms at the centre of a rapidly rotating massive star, which, at the time of collapse is a naked Helium core (a Wolf-Rayet star). Upon collapse a black hole is formed in the centre of the star, however due to the

rapid rotation the outer envelope of the star possesses too much angular momentum to directly collapse onto the newly formed black hole and instead falls in and forms a torus. The subsequent collapse of this torus creates opposing jets along the rotational axis of the star. These jets are launched as highly relativistic outflows and pierce the remaining envelope of the star on a timescale of a few seconds. A GRB is then observed by any observer whose line of sight is down the jet-axis. An isotropic supernova is also launched at the same time as radioactive elements are produced during collapse. As the hydrogen envelope of the progenitor star has been lost it will be observed as a type Ib/c supernova, while the torus at its centre may act as an engine, producing a very high velocity explosion. The structure of a collapsar based on a numerical simulation is shown in Figure 1.6.

As a GRB is only seen by an observer whose line of sight is directly down the jet-axis this implies that the true rate of GRBs is much higher than is observed. Indeed current estimates that the beaming angle θ_j illuminates only 1% of the sky imply that the true GRB rate is $1/\theta_j \sim 100$ times larger than observed.

Compact Binary Progenitors

Another channel for the production of BHAD systems is that of a the merger of a binary consisting of compact objects. These are formed when a binary system containing two massive stars survives the supernova creating each neutron star (NS) or black hole (BH) and leaves the system only a few solar radii apart. These binaries gradually lose orbital energy and angular momentum due to the effects of gravitational radiation and systems which began life sufficiently close together will merge within a Hubble time. In the case of NS-NS binaries this merger pushes the remnant over the maximum mass at which neutron degeneracy pressure can support the star and a BH is formed (Eichler et al. 1989). The orbital angular momentum of the merging system creates the torus about black hole and the evolution from this point is comparable to that in the collapsar model. For NS-BH systems the BH has formed prior to the merger, however the NS shreds upon contact with the BH and therefore creates the torus to power the GRB[‡].

[‡]These compact binary systems will, in addition to creating GRBs also create strong gravitational wave signals, the observation of which is a key goal of current gravitational wave detectors such as LIGO

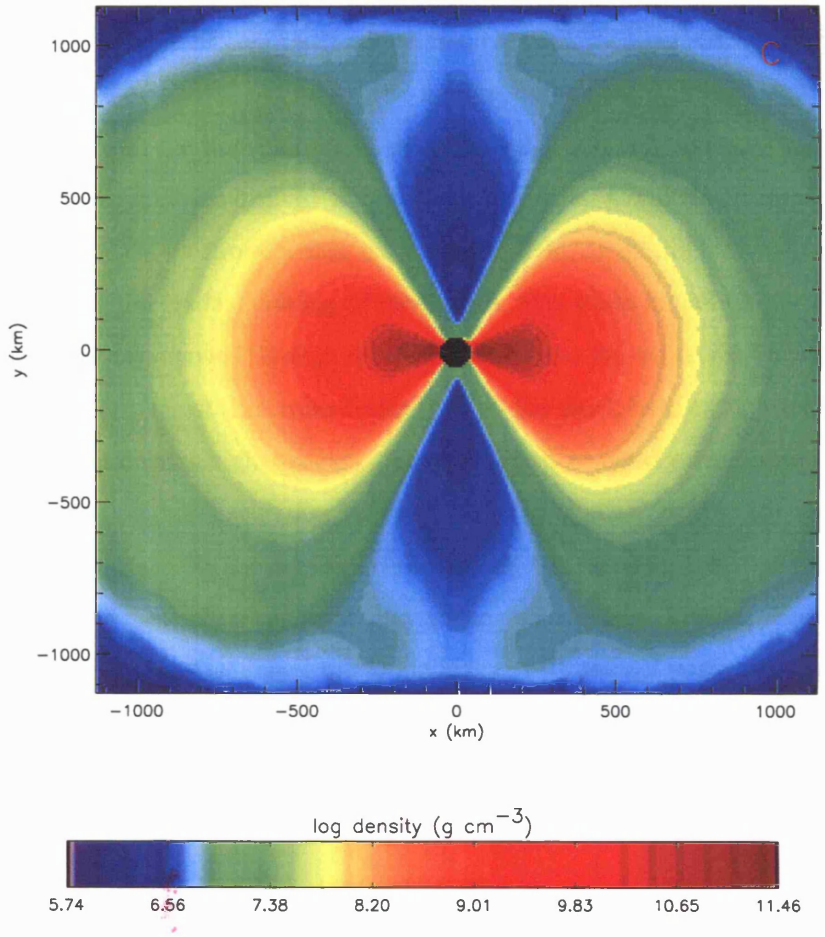

Figure 1.6: The density structure of a rapidly rotating massive star shortly after core collapse, taken from smoothed particle hydrodynamics simulations performed by MacFadyen, Woosley & Heger (2001). A massive dense disk forms around a nascent black hole, this is the disk which powers the subsequent GRB, when ultrarelativistic jets are launched through the low density polar regions.

1.2.3 Afterglow Models

Under the fireball model the afterglow is the result of external shocks between the expanding explosion and the interstellar/circumstellar medium about the progenitor. This interaction accelerates the electrons in the shock and gives them a power-law range of energy $N(\gamma_e) \propto \gamma_e^{-p}$, the spectrum of which is adequately described by a set of connected powerlaws, each representing a different physical process. The three key frequencies needed to characterise a given fireball are i) the self absorption frequency ν_a, this is associated with the transition between an optically thin and optically thick fireball, and is generally found at radio wavelengths. ii) The peak frequency (ν_m), which corresponds to the peak of the power spectrum of the electrons within the magnetic field, as the fireball evolves this frequency decreases representing the gradual cooling of the fireball, thus while initially in the mid-IR it has, on a timescale of several days moved through the sub-mm and into the radio. iii) The cooling break (ν_c) is the final frequency of interest. Electrons cooling within the shock have a characteristic cooling time which is based on their energy, higher energy electrons cool more rapidly than lower energies and thus the position of this cooling break with time reflects the energy of electrons which have had time to cool since the initiation of the shock. The cooling break is commonly found to lie between the X-ray and optical bands, although in principle it can lie at much longer wavelengths. The overall spectral behaviour of the fireball depends on the location of the cooling break with respect to the peak frequency and differentiates the "fast" and "slow" cooling regimes. The power-law indices which reflect each component of the synchrotron spectrum are different in each of these cases and are shown schematically in figure 1.7.

Since the discoveries of afterglows this model has been confirmed by many observations (e.g. Panaitescu & Kumar 2001; Yost et al. 2003; Willingale et al. 2004). Various additions have been made to account for jets (Rhoads 1999; Berger et al. 2003), differing media about the progenitor (e.g. Wang & Loeb 2000) and the refreshing of the shock wave from continued energy injection from the central engine (Rees & Mészáros, 1998) , but, nonetheless the basic formalism remains unchanged.

1.2.4 Optical Light Curves

To date the majority of light curves for the optical transients (OTs) of GRBs approximately follow the power-law decline expected for standard synchrotron models, typically the early lightcurve falls

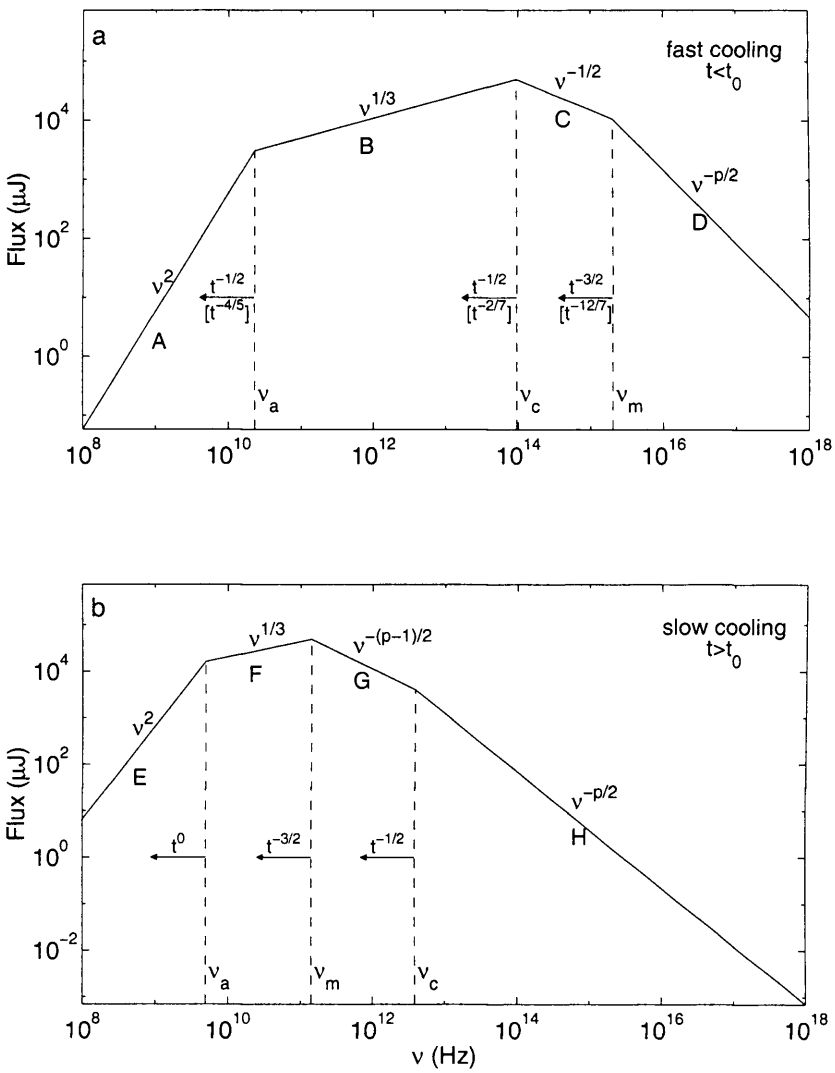

Figure 1.7: The expected spectral energy distribution of a GRB afterglow (taken from Sari, Piran & Narayan, 1998) which is modelled as a relativistic shock which forms a power-law electron energy distribution. Below ν_a self absorption is important and the fireball is optically thick. The locations of each of the breaks decrease with time as is indicated on each plot. The overall shape of the spectrum can be split into two components depending on the location of the cooling break ν_c with respect to the peak frequency (ν_m). Broadly speaking this represents the evolution of the fireball at early (fast cooling) and late (slow cooling) times.

as t^{-1}. On a timescale of hours to days an achromatic steepening of the light curve to t^{-2} is often observed. This break, is most likely a result of the jet geometry of the explosion. An observer viewing a relativistic jet observes a region whose size is Γ^{-1}. There are many of these regions across the jet (formally $(\theta\Gamma)^2$, where θ is the intrinsic opening angle of the jet) and they are causally disconnected. As the fireball expands the value of Γ decreases and the size of the observed region increases (at the same time the number of causally disconnected regions decreases). At the point where $\Gamma^{-1} = \theta$ the entire jet becomes causally connected, the jet begins to expand sideways and the lightcurve declines more rapidly, typically at around t^{-2}. At very late time the associated supernova may brighten and add to the observed flux at the GRB position. Finally there is also an additional component due to the host galaxy.

Therefore the flux seen at any given time is

$$F_{tot} = F_{OT} + F_{SN} + F_{Host} \tag{1.2}$$

The host contribution is typically removed by the subtraction of a late time data point from the earlier data, although it can normally also be neglected for early time data where $F_{OT} >> F_{Host}$. The SN component is commonly modeled on SN1998bw, but with the overall normalisation and light-curve stretch allowed to be free within some range (hence accounting for plausible ranges in Nickel yield and explosion geometry). Thus the full form of a typical afterglow is

$$F_{tot} = At^{-\alpha(t)} + BF_{SN}(z, Ct) + F_{Host} \tag{1.3}$$

Where A is a normalisation for the power-law (afterglow) component, α is the decay rate of the afterglow, which itself can vary with time, typically exhibiting a steepening (increasing α) on a timescale of a few days, commonly interpreted as the jet break[§]. B is the normalisation of the SN component, normally with respect to SN 1998bw and typically lies in the range $0.1 < SN1998bw < 1.2$, C represents the speed of the SN, typically in the range $0.7 < SN\ 1998bw < 1.2$. A commonly used alternative to using these scaling factors is to substitute the SN template to that of another SN, often SN 2002ap (a type Ic supernova exhibiting a similar lightcurve shape to SN 1998bw but approximately 10 times fainter) or SN 1994I (also a type Ic but both 10 times fainter and 40 % faster than SN 1998bw). The host value cannot be predicted a priori and is different for each burst, it must therefore either be neglected or obtained from a deep late time image.

[§]Though it should be noted that not all bursts follow perfect power-law behaviour, some require additional powerlaw components or have "bumpy" structure imposed on the lightcurve

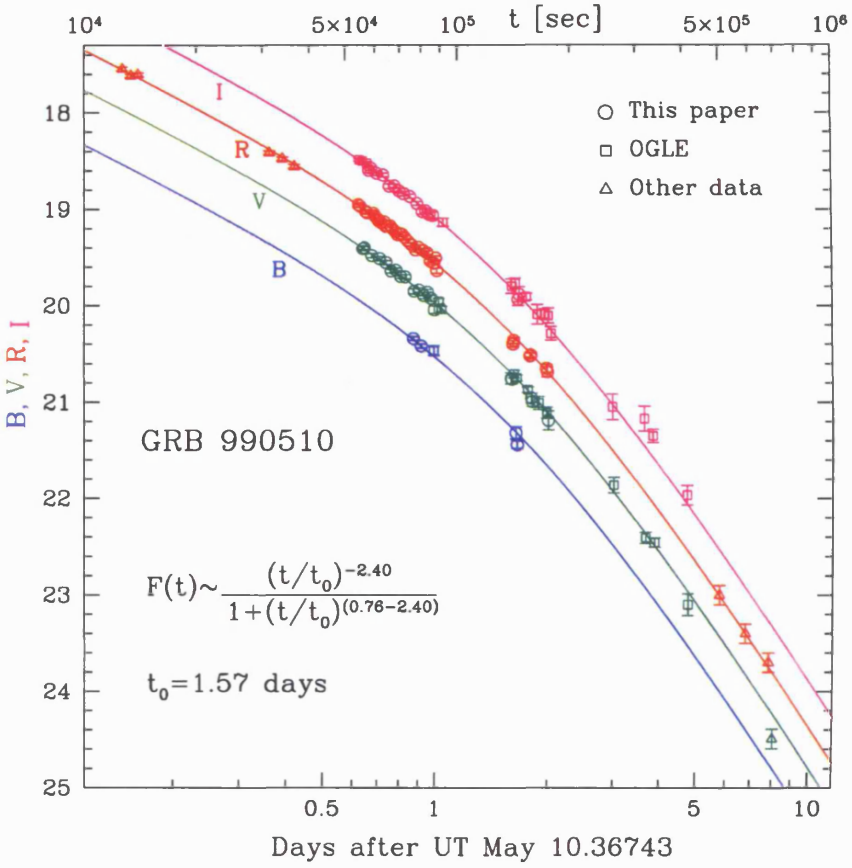

Figure 1.8: From Harrison et al. 1999. The optical light curve of GRB 990510 (Stanek et al. 1999; Harrison et al. 1999) showing a smooth steepening of the lightcurve, probably related to the lateral expansion of the GRB jet.

An afterglow lightcurve, demonstrating the behaviour of the well sampled afterglow of GRB 990510 is shown in Figure 1.8.

1.3 Host Galaxies

Deep follow-up of the positions of GRB afterglows with *HST* has revealed the presence of host galaxies in essentially all cases. The observed magnitude of these host galaxies ranges from $21 < R < 30$ with a median magnitude of $R = 25$ (e.g. Hogg & Fruchter 1999). Despite their faintness, many of these host galaxies do have spectroscopic redshift measurements since strong emission lines are often observed

in their spectra and it is possible to obtain redshifts from absorption spectra while the afterglow is bright. Additionally they have blue colours and appear to be star forming galaxies at high redshift. The positions of GRBs in their host galaxies are frequently aligned with star forming regions (although see chapter 6 for more details).

The GRB host galaxies are potentially powerful diagnostics of the high redshift universe. The majority of techniques for locating high redshift galaxies are subject to significant selection effects due to the fact that they are flux limited and contain inherent biases due to the presence (or not) of dust. For example, many high redshift galaxies have been found by the Lyman-break technique making use of the presence of a strong photometric break between bands and blue colours redward of this break. Additionally, many have been found by narrow band surveys searching for Lyman-α in emission. However these searches find galaxies only in narrow redshift bins, are flux limited, and can be confused by the presence of dust, which makes the Lyman break galaxies difficult to identify and largely extinguishes Lyman-α. However sub-mm studies rely on the presence of significant dust for detection of galaxies but miss those with all but the most extreme star formation rates. In contrast, the presence and properties of a GRB host galaxy can be inferred from the absorption spectra of its bright afterglow, even in cases where the host cannot be seen, furthermore the γ-ray and X-ray emission are largely immune to the effects of dust and gas.

Since GRBs (at least the long duration variety) are the result of the collapse of massive stars then they should be tracers of massive formation. The selection function of host galaxies should therefore trace the star formation rate. The galaxy type, morphology and colour in turn allow an inference as to the type of galaxy in which much star formation occurs, in theory independent of the magnitude of the galaxy or its dust content (GRBs can be seen where host galaxies cannot, and the X-ray afterglow can also been seen through large dust columns). Therefore GRBs should allow a selection of all types of star forming galaxy. [¶]

[¶]The caveat to this statement is that it assumes that GRB progenitors are indicative of *all* star formation. There is now some evidence that GRBs in fact favour low metallicity environments. Should this be the case then GRB host galaxies select only a *fraction* of massive star formation. This is discussed in more detail in chapter 6.

1.4 GRBs as Probes of Environments

The immense energies of GRBs make them visible over great distances, while their luminosity (both of the prompt γ-rays, and afterglow) allows many physical processes to be studied. This includes studies of extreme accretion rates onto black holes, the structure of the immediate circumstellar environments around the progenitor star and the nature of the sight-line between the observer and the burster. There are also tantilising hints of GRBs' power as cosmological probes; the narrowness of the distribution of true energy release for the bursts indicates that they could be used as standard candles (Frail et al. 2001; Bloom et al. 2003; Ghirlanda et al. 2004) and their extreme luminosities mean they can be seen out to very high redshifts. Therefore GRBs are likely to become the tool of preference for studies of high redshift environments.

1.4.1 GRBs as probes of stellar physics

The core collapse of the massive star which creates each long GRB allows a glimpse of the final moments of the stellar life cycle for some of the most unusual stars. The progenitors of long GRBs are most likely Wolf-Rayet stars that have lost the majority of their hydrogen envelope creating a baryon free environment that the GRB can penetrate (Hjorth et al. 2003; MacFadyen, Woosley & Heger 2001; Mirabal et al. 2003). In the standard picture, the afterglow of a GRB is caused by the interaction of the expanding shock with the interstellar or circumstellar environment about the progenitor star, and is formed by external shocks beginning at a distance of $\sim 10^{14}$ cm from the collapsing star. The matter at this distance is the mass which has been lost from the star over the ~ 100 days before the GRB. Therefore as the afterglow ploughs through this environment its temporal and spectral properties are related to its structure. For example, the multiwavelength afterglow can discriminate between a constant density interstellar medium or one which has been crafted into a r^{-2} profile by the outflowing stellar wind. Furthermore, inhomogeneities in the ISM can be probed by fine structure within the optical lightcurve.

Additionally wind-like features can be seen in absorption line spectra of the afterglow, and the relative velocities of these components directly imply the pattern of mass loss from the progenitor star and can be used to place strong constraints on its evolutionary path.

Finally, studies of the properties of the supernovae themselves allow the collapse of GRB progenitors to be placed in context with other stellar core collapse events. The lack of hydrogen and helium lines directly implies that the stellar envelope has been lost, either through a wind or via binary interactions, while the brightness of some of the supernovae indicates a high level of metal production and the collapse of a very massive stellar core, most likely to a black hole.

1.4.2 GRBs as probes of galactic and intergalactic structure

GRBs necessarily illuminate their sight-lines, both through their host galaxies and the intergalactic medium (IGM). Therefore, objects both within the host galaxy and intervening absorbing media can be probed via the afterglow itself. As GRB afterglows themselves have a well known underlying power-law spectrum, changes in the shape of this underlying spectrum allow the extinction curve of the host galaxy to be measured while absorption lines imprinted upon it can reveal the chemical composition of both the host galaxy and intervening absorption systems.

GRB afterglows offer a method complementary to studies of Damped Lyman-α (DLA) systems seen in quasar absorption line spectra. The hydrogen columns seen in GRBs form a broad range, from $10^{18} - 10^{22}$ cm^{-2}, indeed the observed column in several GRBs (e.g. GRB 030323, GRB 050401 and GRB 050730) is higher than is seen in any Quasar spectrum. As well as providing the hydrogen column narrow metal lines seen in absorption within these spectra allow accurate measures of the metallicity of the host galaxy to be made. This is remarkable since the host galaxies themselves are frequently very faint, and the afterglow enables detailed chemical and dynamical studies that are impossible with the currently available instrumentation.

1.4.3 GRBs as cosmological probes

The luminosity of GRBs allows them to be viewed at extreme redshifts as well as through the dust and debris commonly associated with star formation. There exist numerous possible cosmological uses for GRBs, the most important of which are:

The location of Pop III stars: Population III stars are the first generation of stars to form after the big bang. It is expected that due to their low metallicity they will be very massive and may give rise

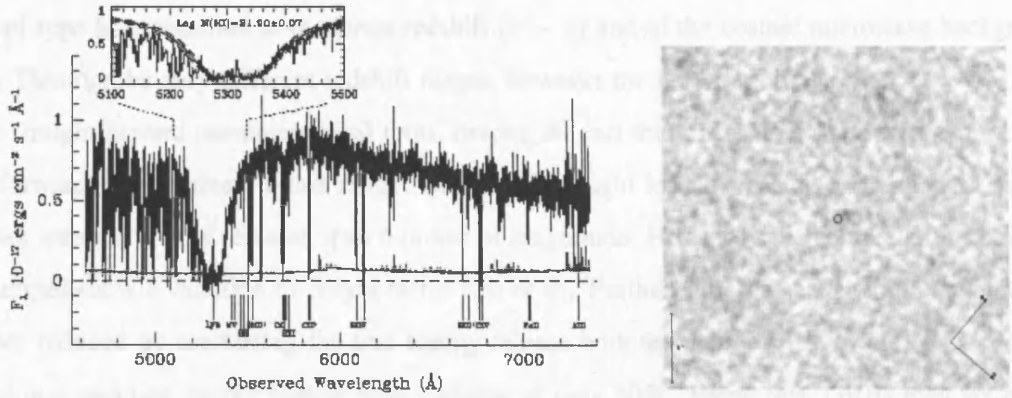

Figure 1.9: From Vreeswijk et al. 2004: The Very Large Telescope spectrum of the GRB 030323 afterglow, taken after 24 hours (left) and the host galaxy, imaged with the *Hubble Space Telescope* after 3 months when the afterglow has faded. The host has R$\sim$ 28. However, despite this, analysis of the afterglow allowed the redshift of the GRB, metallicity and dust content of the host galaxy to be accurately determined.

to bright GRBs. As such it may be possible to locate the first generation of star formation directly via GRBs.

The ionisation history of the universe: About 300,000 years after the big bang the universe underwent recombination, with the constituent protons and electrons forming hydrogen atoms. However, as seen today the universe is largely ionised. At some point a process of reionisation occurred which brought the universe out of the cosmic dark ages. It is commonly thought that this was caused by the first stars although this remains to be demonstrated. The presence of significant absorption blue-ward of Lyman-α in the spectrum of $z = 6$ quasars (the so called Gunn-Peterson trough) implies that the universe contained a significant fraction of neutral gas at this time. However probing the evolution beyond $z = 6$ is difficult since quasars become rare and galaxies too faint. GRBs on the other hand may still be bright at these redshifts and enable a direct measurement of the Gunn-Peterson trough and thus the ionisation history of the universe.

The universal equation of state: The currently most popular cosmological model involving the presence of dark energy and past epochs of both acceleration and deceleration is based primarily on observations of type Ia supernovae at moderate redshift ($z \sim 1$) and of the cosmic microwave background (CMB). These probe very different redshift ranges, however the important range of $1 < z < 10$ contains no straightforward cosmographical tools, despite the fact that differing cosmologies can be most straightforwardly determined in this range. GRBs at first sight look like being poor standard candles since their inferred energy releases span 6 orders of magnitude. However when corrected for beaming their energies show a variation of only a factor two or so. Furthermore the scatter in this relation can be further reduced by correlating the true energy release with the peak energy of the νF_ν spectrum, resulting in a standard energy budget with a scatter of only 30%. Using this, GRBs may yet enable detailed cosmographical measurements to be made over a wide range of redshifts.

1.5 This thesis

The work presented in this thesis investigates the broad subject of "Gamma-Ray Bursts and their Environments". The aim is to investigate the relationship between GRBs, massive stars and massive star formation at high redshifts. This is pursued through a variety of means which includes the study of individual afterglows, associated supernovae and a large survey of GRB host galaxies.

In chapters 3 and 4 I present studies of the supernovae associated with GRBs. Chapter 3 presents an analysis of the supernova light in the afterglow of GRB 020410, this afterglow was very faint and undiscovered by early optical observations, instead its bright supernova was located in deep *HST* images, representing the first optical afterglow to be found from an orbiting platform. The supernova is found to be an SN Ic, and is 2 magnitudes fainter than the prototypical SN 1998bw, and demonstrates the breadth of the luminosity function of associated supernovae

Subsequently in chapter 4 I investigate the relationship between XRFs and supernovae. XRFs are the most extreme of the burst populations emitting essentially all of their energy in the X-ray, rather than γ-ray band, although their emission properties form a continuum with GRBs they have not been studied in great detail due to a paucity of afterglow identifications. Chapter 4 presents a very deep search for supernovae in two XRFs and finds no evidence in either case, this is surprising since many models of XRFs place them at lower redshifts than GRBs, where supernova signatures should be easier to

see. It is possible that again this result indicates the breadth of the supernovae luminosity function, demonstrating that the massive stars which collapse to produce GRBs do not all have identical (or even near identical) energetics.

In chapter 5 I describe the discovery, and subsequent observations of GRB 030115 and its host galaxy. GRB 030115 is one of the most extreme GRB events seen to date, exhibiting very red colours (R-K=6), unheard of for other afterglows. The host galaxy, like the GRB afterglow is also very red, in contrast to other GRB hosts. These observations indicate that GRB 030115 may represent a transition object between the relatively unextinguished GRBs which have been observed to date and a sample which are much more heavily obscured. Furthermore the galactic environment in which GRB 030115 was found is most likely a rich high redshift cluster, in itself a rarity but especially so for a GRB.

Chapter 6 presents a detailed comparative study between the host galaxies of supernovae and those of GRBs. Since both GRBs and core collapse supernovae are caused by the collapse of massive stars it is natural to use these galaxies to test environmental dependencies that may favour the production of GRBs. Knowledge of this is important since it informs much of our understanding about the stars which create GRBs, the galaxies where we might expect to find young, GRB remnants and perhaps most importantly the extent to which GRBs can be used as star formation rate tracers at higher redshifts. The results of this study are surprising and show that GRB host galaxies are typically less luminous and smaller than those of core collapse supernovae, the most likely explanation for this is that GRBs are preferentially formed in low metallicity environments and thus are not un-biased tracers of star formation rate.

Finally I present a summary of the work presented in this thesis in the broader context of GRB astronomy, indicating the advances in knowledge that this work has enabled. I end with a discussion of the future steps which will be taken, both in the context of extending the work presented in this thesis, but more generally the future path of GRB astrophysics as it finally enters maturity and the *Swift* era.

Chapter 2

Methods and Observational Strategies

2.1 Locating GRBs

Of all the transient astrophysical phenomena which are currently studied GRBs are perhaps the most observationally demanding. The GRB trigger only ever lasts for a few seconds and, by necessity the detector is based on an orbiting platform. The afterglow of the GRB affords a slightly longer response but obtaining the maximum scientific return still involves obtaining multiwavelength observations in the seconds to minutes following the burst. follow-up of GRB is therefore dependent on three highly important steps.

1. The detection of the GRB by the orbiting observatory (e.g. *INTEGRAL, HETE-2, Swift*)
2. The rapid dissemination of this position to the world.
3. The triggering of multiwavelength facilities to search for the afterglow.

This task has recently become significantly more straightforward with the launch of the *Swift* satellite, which is capable of performing tasks 1 & 3 independently of task two. However the majority of the data presented in this thesis were obtained prior to the launch of *Swift* and it is therefore appropriate to describe the observing scenarios which were followed at this time.

2.1.1 Detecting GRBs

GRBs are currently detected by a large number of different instruments, including those which obtain crude positions via time delays and those which have limited "imaging" capability. To date GRBs have been detected by a number of instruments on board a wide range of satellites, including BATSE, *BeppoSAX*, *INTEGRAL*, *HETE-2*, *RXTE* and most recently *Swift*. The Interplanetary Network (IPN), which consists of a number of non-imaging spacecraft set out across a large region of space has also had success in the localisation of bursts since the large time delays between the detection of the burst by different spacecraft (some of which are as distant as Mars) allows for the accurate triangulation of the burst position. The bursts presented in this thesis were discovered by the *BeppoSAX* Wide Field Camera and GRB Monitor (GRBM) and the *HETE-2* Wide Field X-ray Monitor (WXM) and Soft X-ray Camera (SXC). These instruments are briefly described here.

2.1.2 BeppoSAX

BeppoSAX was designed to be a general purpose X-ray Astronomy satellite allowing observations over a very wide range of energies from 0.1-200 keV. Specifically, there were two general sets of instruments concentrating on narrow and wide field observations respectively. The Narrow Field Instruments (NFI) consisted of a Medium Energy Collimator and Spectrometer (MECS), which operated in the 1-10 keV energy range, a low energy version operating in the 0.1-10 keV region (LECS) and a high energy detector (2-300 kev). All of these cameras could be pointed simultaneously at a given source to allow a wide range of spectral information to gathered in a single observation. However for GRB studies the most important feature of *BeppoSAX* was its Wide Field Cameras which had a large (400 square degree) field of view, enabling a large fraction of the sky to be covered at any time in the 2-28 keV energy range. In addition to the WFCs the anti-coincidence shield was also used to detect higher energy photons and acted as a GRB monitor (GRBM) thus enabling approximately 10-12 bursts per year to be localised to a few arcminutes. *BeppoSAX* was also capable of slewing to new targets on a timescale of a few hours, the NFI instruments could provide $\sim$ 1 arcminute positions for the X-ray afterglows of many GRBs, refining the error obtained from the WFCs. Indeed this procedure has been followed by *Swift*, albeit in a much accelerated form.

2.1.3 HETE-2

HETE-2 was designed with the primary science goal to locate and characterize GRBs, and was launched on 9th October 2000*. Although a small mission, it contained three main instruments, the FREGATE γ-ray monitor, the Wide-field X-ray monitor (WXM) and Soft X-ray Camera (SXC), this provided *HETE-2* with a energy range from $\sim 2 - 500$ keV while the WXM delivered error boxes which were typically 10-30 arcminutes the SXCs positionally accuracy could be as good as one arcminute. The rate of detection by *HETE-2* has gradually risen since launch and is now stable at around 20 bursts per year, although the large error boxes which arise from WXM bursts have in practice reduced the number of well studied bursts to ~ 10 per year.

Both *HETE-2* and *BeppoSAX* used essentially two types of trigger on GRBs, those which were based on an increase in the count rate in the GRB monitor on *BeppoSAX* or FREGATE on *HETE-2* and those which were "imaged" and thus had associated positions. The latter type are those of most interest since they enable afterglow searches at longer wavelengths.

2.2 Distributing Information: The GCN Network

Once a GRB has been detected the next important task is to inform observers on the ground of its position and other vital properties (significance of the detection, flux, fluence, duration). This is currently done via the GCN (Gamma-Ray Bursts Co-ordinate Network). Individual satellites communicate with this network via NASAs Tracking and Data Relay Satellite System (TDRSS). The information is rapidly downlinked and subsequently sent out to the community via a set of notices which are transmitted via email, socket connection and mobile phone/ pager connections. Each satellite which communicates with the network has a variety of different notices which can be sent depending on nature of the trigger. For example many GRBs are detected but not "imaged", meaning that there is no accurately known position, however this may still be of interest to some groups who may be searching for high energy γ-rays from ground based arrays, or perhaps for neutrino signatures from the burst. Notices are distributed based on the best currently available information although vital properties (such as the position) may be refined over time, each successive refinement then generates a new notice. A given

*HETE-2 was the replacement for HETE-1 which unfortunately failed to correctly decouple from in launch system in 1996

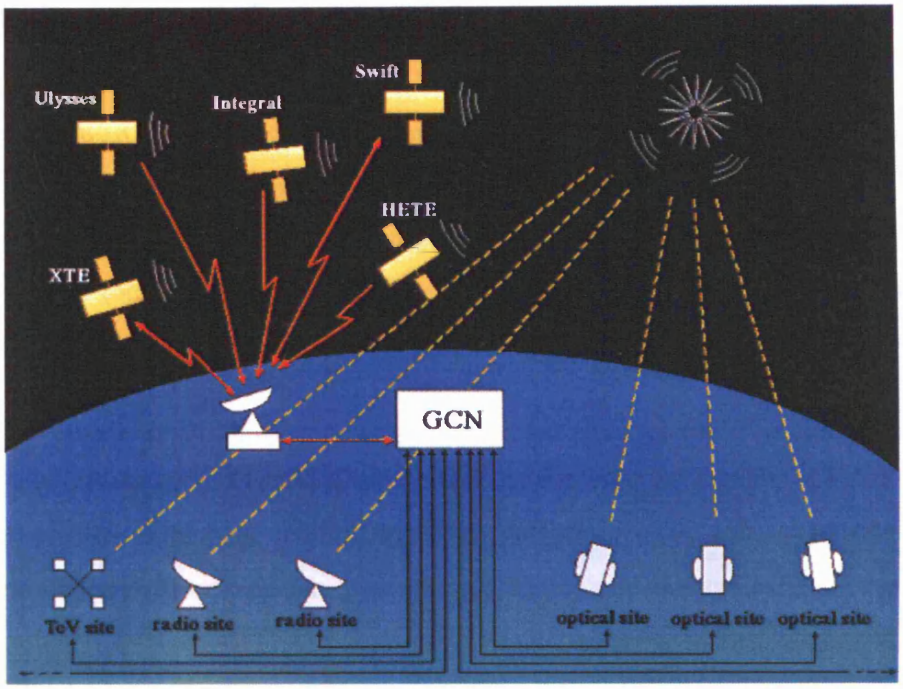

Figure 2.1: A schematic diagram of the Gamma-Ray Co-ordinate Network (GCN), the system uses the TDRSS system to rapidly disseminate positions for GRBs detected by a large number of satellites including those which are designed specifically for GRB astronomy and others which contain γ-ray detectors.

burst may have several position notices as the position is gradually improved both by further on-board processing and by ground based analysis. In addition to alerting human observers on the ground to a GRB trigger, these notices can also be used to directly trigger observations. Robotic telescopes can be linked to the system so that position notices trigger rapid, automated observations without the need for human intervention. This has been attempted for several years now with robotic telescopes of varying size, up to and including the 2m robotic telescopes sited on La Palma, Hawaii and in Australia.

Operating in tandem with the notice system are the GCN circulars. These are not automatically generated but are written individually by observers to quickly disseminate important results to the rest of the community, a service which is very useful for the planning and implementation of further observations. The circulars are used for a variety of purposes, the most important of which are the reporting of positions, magnitudes or redshifts for GRB afterglows in a fashion which is much more timely than refereed publication but enables a given discovery to be associated with those who made it.

2.3 The need for speed

GRB emission can be split broadly into prompt and afterglow components. Physically these components correspond to internal (prompt emission) and external (afterglow emission) shocks. The prompt emission from GRBs typically lasts only a few seconds, while the afterglow emission can be seen for days (and sometimes even months) after the explosion itself. However extracting the maximum information out of each GRB requires rapid responses from multiwavelength observatories.

Studies of the prompt emission outside the γ-ray band are probably the most taxing observation to obtain at many wavelengths. They require that alert notices must be transmitted to the observatory within a few seconds of the burst starting. The telescope must then respond and be able to take data within a few seconds of receiving this alert. Due to these constraints the only telescopes to locate prompt emission to date are small, robotic telescopes that can slew at high rates (several degrees per second), because of their limiting size they are only capable of locating prompt emission from very bright GRBs. For example the ROTSE instrument located prompt optical emission from GRB 990123 at 9th magnitude (Akerlof et al. 1999).

Afterglow emission from GRBs significantly outlasts the prompt component, however rapid response is still important. The afterglows fade as powerlaws, typically getting a magnitude fainter for every factor two in time. Therefore, while they can been seen by large telescopes for several days after the burst it is only possible to obtain high signal to noise observations, spectroscopy and polarimetry at early times, while the afterglow is bright. Additionally the fireball evolution proceeds most rapidly at early times and thus dense sampling of the afterglow in the minutes to hours after the burst is vital to reconstructing the properties of the explosion.

2.4 The role of Optical and IR observations

The location of optical/IR counterparts was amongst the most important questions in GRB astronomy throughout the 1990s and was thought of as the holy grail during this time. The rationale for this was that the location of GRBs at optical wavelengths offered the possibility of resolving the distance scale to the GRBs by allowing a precise astrometric position to be derived and for redshift measurements to

be made. Furthermore since the optical wavebands have historically been the best studied it also places the GRBs in context, since it is possible to ascertain if they are associated with stars, galaxies, nebulae etc.

Optical observations are still exceptionally important today. Spectroscopic observations of either the afterglow or the host galaxy still provide the only reliable mechanism for obtaining the redshift of the GRB. This remains possibly the single most important parameter to obtain for a GRB since it enables the energetics of the burst to be understood and is also of great importance for future statistical studies of bursts for star formation rate studies.

The large number of optical observatories and their geographical spacing makes it possible to create densely sampled multi-colour light curves for GRB afterglows. Such observations cannot easily be performed at other wavelengths (although the launch of *Swift* does now allow for similar coverage at X-ray wavelengths). Creating long baseline, densely sampled multi-colour lightcurves is important for several reasons. Primarily these observations allow the temporal behaviour of the afterglow to be accurately constrained, most importantly by locating the time of any achromatic steepening in the lightcurve which is indicative of the lateral expansion of the jet and provides its collimation angle. However further structure in the lightcurve can also be indicative of structure within this jet, or in the medium into which the fireball is expanding. Finally the combination of optical observations with those taken at X-ray, sub-mm and radio wavelengths allows the complete evolution of the fireball to be calculated, fixing the true energetic parameters of the burst and testing the theoretical models for the afterglow production.

2.5 *HST* observations and this thesis

The Hubble Space Telescope (*HST*) plays a major role in our understanding of GRBs due to its ability to obtain very deep images at the diffraction limit. This enables the afterglows of GRBs to be followed to very late times when beyond the limit of ground based telescopes. Also due to the invariant point spread function (PSF) the afterglow can easily be isolated, even from a relatively bright host galaxy, making precise photometry of the late afterglow possible. These late time measurements can be used to fix the late time slope and provide strong evidence for beaming (e.g. Fruchter et al. 1999). A second important aspect is that, again due to the diffraction limited imaging, *HST* enables a study of

the morphological properties of the host galaxies of GRBs (e.g. chapter 6), since these galaxies have typical scale lengths of order 1 arcsecond, these observations can only be performed with *HST*.

HST observations are used throughout this thesis and form an important component of each chapter. The insights which they allow into the nature of the host galaxies and the late time behaviour of afterglows are crucial to the scientific results that are presented. As the general reduction processes and methods are largely the same for each observation the techniques are described here, while specifics to each dataset are provided in the relevant chapter.

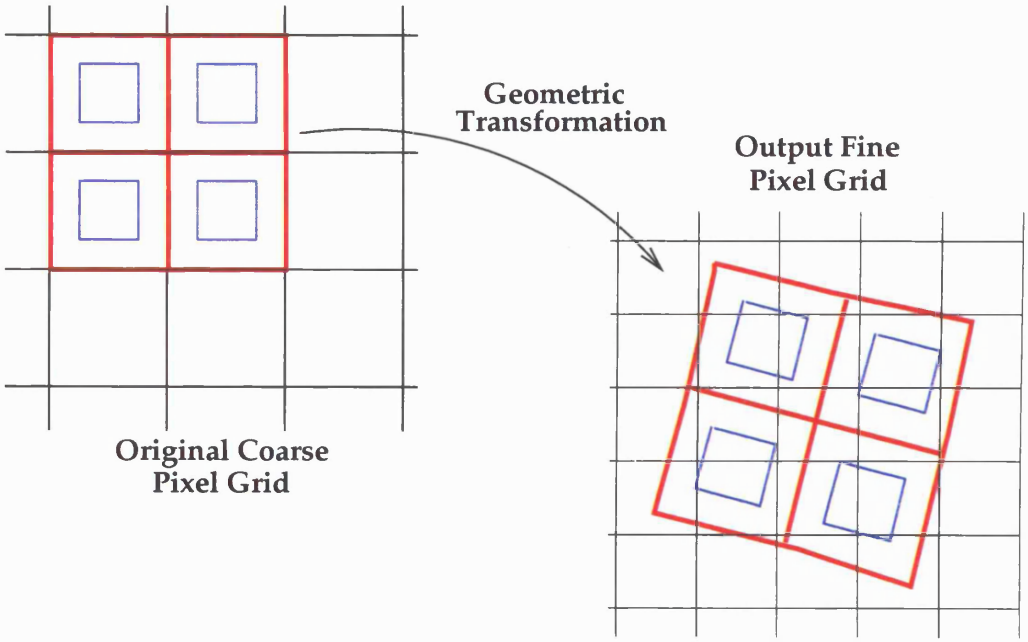

Figure 2.2: From Fruchter & Hook, 2002, showing the process of drizzling. The initial image, taken on a coarse output grid (i.e. the detector itself) is placed through a geometric transformation during which the physical size of the input pixel is shrunk by a factor PIXFRAC. The individual pixels then "drizzle" down onto an output grid with a smaller pixel size, with the contribution of the input pixel to given output pixel weighted by the area overlap. Using a set of sub-pixel dither positions allows a well sampled output image to be obtained.

The work presented here makes use of data taken by several imagers onboard *HST*. The Space Telescope Imaging Spectrometer (STIS) is capable of obtaining both deep imaging and slit spectra in the optical and ultraviolet. It contains CCD and MAMA (Multi-Anode Microchannel Array) detectors for operation in the optical and UV (with both near and far UV MAMA detectors). Although it was a workhorse instrument for UV observations (until the Advanced Camera for Surveys (ACS) was in-

stalled in servicing mission 3B), it was also the most sensitive imager on the telescope. Used without a filter (the 50CCD, or Clear mode) it was capable of very deep imaging, while a long-pass filter could provide limited colour information. Deep images presented in this thesis have been obtained via STIS for the afterglows of GRB 020410 and XRF 011030 and 020427, as well as for many of the host galaxies presented in chapter 6.

The Advanced Camera for Surveys (ACS) was installed during servicing mission 3B and has now replaced STIS as the most sensitive imager on *HST*, providing deep multiband imaging from 200nm to one micron and a large (202 $\times$ 202 arcsecond) field of view, split across two large Wide Field Cameras. It also has a high resolution camera (HRC) which operates primarily in the UV. Essentially all observations of bursts which have occurred since July 2002 have been taken with ACS.

The Near Infrared Camera and Multi-Object Spectrometer (NICMOS) has been used to obtain deep IR images of GRB 030115 in the F110W(J), F160W(H) and F222M(K) bands. NICMOS actually contains several cameras with different pixel scales and differing sensitivities, as well as GRISM spectroscopy and coronographic capabilities. The NIC3 camera was used for observations of GRB 030115 since it is the most sensitive of the cameras and is appropriate for observations of faint extended objects.

Finally some of the data presented in Chapter 6 have been obtained using the Wide Field Planetary Camera 2 (WFPC2). This camera has been used as the workhorse imager for *HST* for much of the mission lifetime. It consists of four chips, three wide field camera (WFC) chips which are identical and a fourth planetary camera which has a finer pixel scale than the wide field chips. All of the GRB observations have placed the GRB host galaxy on one of the wide field camera chips, normally at the corner of the WFC3, which is essentially at the centre of the camera.

2.6 Reduction and combination of dithered observations - Drizzle

Dithering is now common practice in astronomical observations. It has long been used at IR wavelengths to aid sky subtraction, and shifts of optical detectors by an integer number of pixels are a simple way to overcome bad or hot pixels, ensuring that the same region of the sky/object does not land on them in consecutive exposures. More recently the use of sub-pixel dithers (i.e. those which shift the detector by an intentionally non-integer number of pixels) have become widely used.

The point spread function of *HST* is undersampled in effectively all of its cameras, while this does not necessarily represent a problem it was recognised during the planning for the Hubble Deep Field that the use of sub-pixel dithers would allow for a degree of PSF recovery. An algorithm for doing this was therefore created and has since become the standard for the reduction of *HST* imaging data from all of the cameras. All of the *HST* data presented in this thesis has been processed through this algorithm, known as drizzle (Fruchter & Hook 2002).

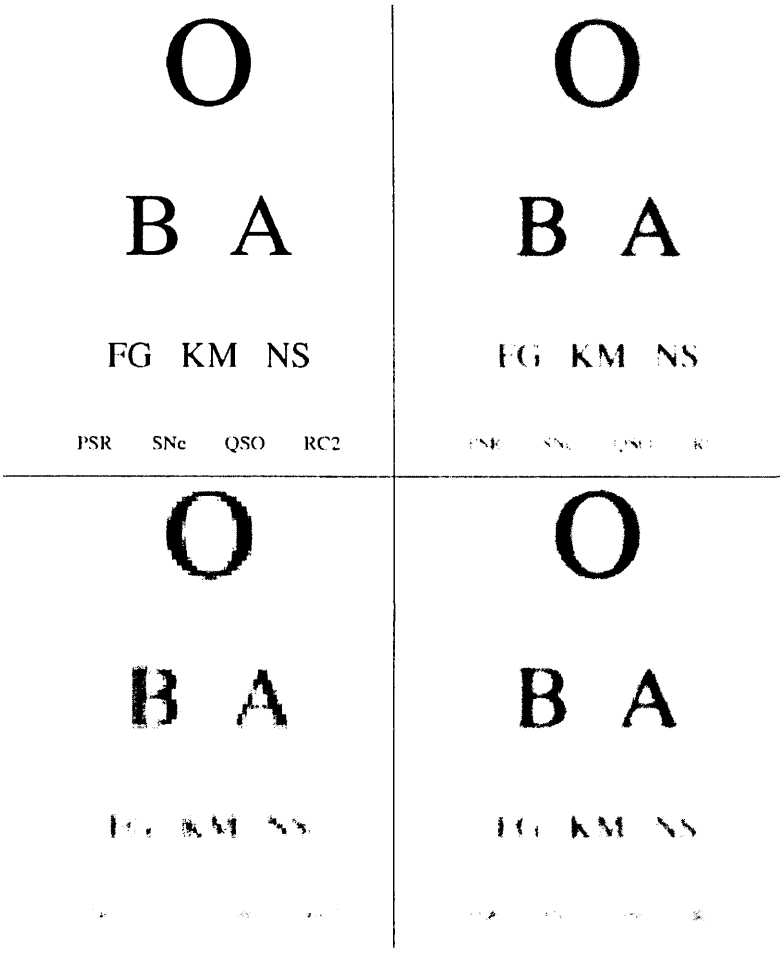

Figure 2.3: The "great eye chart in the sky", from Fruchter & Hook 2002. These four panels show (top left) an ideal input image, accurately representing an ideal image. (top right) the image convolved with the optics of *HST* and WFPC2, (bottom left) the image sampled by the pixel scale of WFPC2 and (bottom right) the image when reconstructed via drizzling.

The image which is produced from any given observation is the result of the convolution of the true image, with the telescope optics and detector. This is shown in figure 2.3. For ground based observations the PSF is typically limitied by atmospheric seeing, however for *HST* is diffraction limited. Drizzle

uses a set of sub-pixel dithers to re-sample the observation onto a smaller output pixel grid than the input, thereby recovering some of the details lost due to the undersampling of the PSF by the detectors. It is not, however, a deconvolution routine and does not aim to increase the resolution.

The fundamental principle of drizzle is relatively straightforward, at the time of observation the telescope is dithered by a small, non-integer number of pixels between each exposure. At the reduction stage these images are then aligned and the input pixels are reduced in size with respect to the input pixel by a factor of typically 0.6-0.7 (known as PIXFRAC). Each of these new smaller pixels then "drizzles" down onto an output grid of even finer pixels (with an even smaller SCALE). Performing this process using a number of dither positions allows a high quality image to be obtained on a smaller pixel scale and is shown schematically in Fig 2.2. The precise values of PIXFRAC and SCALE are determined by the number of dither positions available and the properties of the detector used.

2.7 GRB vital properties

As described earlier GRB emission can be split into two broad components relating to the prompt and afterglow phases. Alternatively, they can also be split into those which are intrinsic to the GRB itself (such as its energy release or beaming angle) and those which are observed (such as its redshift of peak flux). A summary of the different properties is provided below, although it is not intended to be exhaustive. It is split broadly into properties which must be derived from observations, and those which (at least in theory) can be directly observed.

- θ_j - the opening angle of the GRB jet, which is normally in the range 3-20 degrees
- Γ - the Lorentz factor of the ejecta. This is an evolving number which at the time of the burst may be several hundred though drops to ~ 1 on a timescale of weeks to months after the bursts.
- n - the particle density of the ISM/CSM around the progenitor. It is commonly assumed to be either uniform or to vary as r^{-2} as would be the case for a stellar wind.
- p - the powerlaw index of the electron energy distribution $N(\gamma_e) \propto \gamma_e^p$, is the value which determines the shape of the fireball spectrum.
- E_{iso} the energy release of the GRB if its emission is assumed to be isotropic.

- E_{true} the **actual** energy release of the GRB, when corrected for beaming (sometimes called E_γ, this is found to cluster around 10^{51} ergs, comparable to the energy release of supernovae.

In addition to these parameters there are also a number of observed values which are commonly used to derive the properties described above. These are:

- ν_c - the frequency of the cooling break which represents the age of the fireball. The time for electrons to cool is dependent on their frequency, higher frequency electrons cool more rapidly, with time progressively lower frequency electrons cool, as such the cooling break moves to lower frequency as $t^{1/2}$. At the time of the jet break ν_c freezes.
- ν_m - The frequency of peak emission
- ν_a - The self absorption frequency. Below this frequency the fireball is optically thick and behaves as a black body.
- E_p - The peak energy of the νF_ν spectrum of the GRB, it typically lies at around 100-1000 keV although for X-ray Flashes can be as low as 5 keV.
- t_{90} - the duration over which 90 % of the fluence of the GRB is detected. It does not start from zero and run to 90 % but rather excludes the first and last 5% of the fluence. Comparable numbers are sometimes quoted for 50% of the flux t_{50} etc.
- z - The redshift of the burst, determined either via absorption line spectra of the afterglow or from emission lines in the host galaxy.
- $S_{E_1-E_2}$ - the observed fluence of the GRB in a given energy band running from E_1 to E_2, the quoted energy range is dependent on the instrument which detected the GRB and may be e.g. 15-350 keV for *Swift*.
- t_b - the measured time of a steepening in the lightcurve, normally attributed to the later expansion of the jet when $\Gamma = 1/\theta_j$.

Part II : Supernovae in GRBs

Chapter 3

GRB 020410: A Gamma-Ray Burst Afterglow Discovered by its Supernova Light

3.1 Introduction

The discovery of SN 2003dh underlying GRB 030329 finally provided definitive evidence that at least some GRBs were associated with energetic type Ic supernovae. The high velocity SN 2003dh was very similar to SN 1998bw which was found in the error box of GRB 980425 some 5-years earlier. However GRB 980425/SN 1998bw was a highly unusual event, quite unlike any other GRBs seen to that date, leading to speculation that this event was part of a separate class of event. In contrast GRB 030329 was a "classical" GRB, highly energetic and occurring at cosmological distances, therefore the discovery of SN 2003dh confirmed that these explosions could also be associated with stellar death.

However this result did not answer all of the questions remaining about the GRB-SN connection. Are all GRBs associated with supernovae? If so, are the supernovae all of the same type, or is there a diversity of supernova properties? Can the properties of the supernovae be used to constrain the nature of the GRB progenitors? To fully answer these questions it is necessary to find signatures of supernovae at distances too great to reach with direct spectroscopy. Supernova spectra peak in the rest-frame

optical, so supernovae become hard to observe at high redshift where optical observations probe rest-frame ultraviolet light. Furthermore, the host galaxy is often brighter than the supernova, making precise photometry difficult.

Most supernovae associated with GRBs have been discovered only by their contribution to the intermediate time lightcurve of the GRB afterglow. The contrast between GRB and supernova is very large at early times since supernovae rise gradually from the time of core collapse, reaching a peak magnitude days to weeks later, while GRB afterglows are at their brightest soon after the time of trigger, falling monotonically thereafter. At later times, as the afterglow fades and the supernova brightens the fading of the afterglow can appear to have slowed down, or even been reversed with a brightening of the supernovae. At the same time, the colour becomes dominated by the supernova spectrum, which is typically more red than the power-law spectral energy distribution of the afterglow at early times. Such "supernova bumps" have now been seen in several GRB afterglows, including GRBs 980326, 970228, 991208, 011121, and 020405 (Bloom et al. 1999; Castro-Tirado et al. 1999; Galama et al. 2000; Castro-Tirado et al. 2000; Greiner et al. 2003; Garnavich et al. 2002; Bloom et al. 2002; Price et al. 2002; Masetti et al. 2003). They are in general adequately fit by the colours and brightnesses of high-velocity Type Ib/c supernovae such as SN 1998bw.

Here I show that the GRB 020410 was likely associated with a high-velocity supernova of type Ib/c at a redshift $z \sim 0.5$. The source brightened between ground-based observations taken after one week and those taken with *HST* after one month, late time observations also show a red colour, typical of supernovae. Fitting of the observed lightcurve implies that the peak absolute magnitude of the underlying supernova was $M_V \sim -17$, approximately 2 magnitudes fainter than SN 1998bw. Similar, faint supernovae may underlie many long GRBs, but would remain undetected in typical followup campaigns.

3.2 Observations

GRB 020410 was detected by the *BeppoSAX* Wide Field Camera 2 (WFC) on 10 April 2002 at 10:41:20 UT (Gandolfi 2002). The Gamma-Ray Burst Monitor (GRBM) was switched off at the time of the burst and thus no high energy ($>$ 28 keV) data were recorded by *BeppoSAX*. However the burst was detected by *Konus-Wind* in waiting mode (it did not trigger the instrument, although the lightcurves

were recorded and could be recovered, once the GRB time was known)*. In the 19-300 keV band it had a duration of $\sim 600s$ and was best fit with a powerlaw with slope $\Gamma = -1.9$, it had a peak flux of 8×10^{-8} ergs s^{-1} cm^{-2} and fluence 1.3×10^{-5} ergs cm^{-2} in the 19-1270 keV band. The lightcurves in the 19-77, 77-330 and 330-1270 keV energy bands are shown in Figure 3.1.

BeppoSAX observations with the Narrow Field Instruments (NFI) began 20 hours after burst, with a second epoch obtained after 54 hours. These observations revealed the presence of a slowly fading X-ray point source (Gandolfi 2002a,b; Nicastro et al. 2002) with a decay best fit as $t^{-0.82}$; Nicastro et al. 2004), the initial error radius was two arcminutes, however this was further refined to a 20 arcsecond radius error box 8 days after the burst.

Based on both the prompt emission observed by the WFC and the afterglow properties it was suggested that GRB 020410 was an X-ray Flash (XRF) (Nicastro et al. 2002). XRFs are defined as burst which have a higher X-ray fluence than γ-ray fluence (Lamb et al, 2003). In order to compare the properties of this burst which was observed by *Konus-Wind* with those of the bulk GRB/XRF population (now observed by *HETE-2*) the expected fluence in the 7-30 (S_X) and 30-300 (S_γ) keV band was calculated based on the observed powerlaw slope of $\Gamma = -1.9$. It is then possible to calculate the ratio $\log(S_X/S_\gamma)$. X-ray rich GRBs and XRFs are defined as having $\log(S_X/S_\gamma) > -0.5$ and > 0 respectively. For GRB 020410 a value of $\log(S_X/S_\gamma) = \log(5.58 \times 10^{-6}/1.066 \times 10^{-5}) = -0.28$ is determined, which places GRB 020410 in the X-ray rich GRB category. With a fluence of 1.3×10^{-5} ergs cm^2 (19-1270 keV) the fluence of GRB 020410 lies in the upper quartile of the bursts reported by Barraud et al (2003). However none of the bursts with higher fluence are as X-ray rich. Indeed the measured $\log(S_X/S_\gamma)$ value of -0.28 is actually typical of the fainter bursts (for which $\log(S_X/S_\gamma) = -0.25 \pm 0.07$) Barraud et al (2003).

A comparison of early optical observations with Digital Sky Survey images initially failed to find any counterpart (Castro-Tirado et al. 2002; Kilmartin & Gilmore 2002). However, after the discovery of the transient with *HST* a reanalysis of images obtained six hours after the burst at the 0.6m Microlensing Observations in Astrophysics (MOA) telescope in New Zealand by Nicastro et al. (2004) revealed a 4-σ detection of an OT at the position of the *HST* transient, with a magnitude of R$\sim$ 21 (see also Figure 3.2). This detection confirms the fading source seen in the *HST* images is the afterglow of the GRB,

*The detection of the GRB by *Konus-Wind* was first reported by Nicastro 2002 at the "Gamma-Ray Bursts in the Afterglow Era" conference

and is not an unrelated supernova found in the field. No radio afterglow was detected to a 4-σ limiting flux of 200 μJy at 8.7 GHz (Frail et al. 2002). The properties of the prompt γ/X-ray emission and of the X-ray afterglow are discussed in detail in a paper by Nicastro et al. (2004).

The 40 arcsecond diameter error box of GRB 020410 was imaged with *HST*/STIS in 50CCD/CLEAR mode on 8 May and 14 June 2002. The dithered datasets were retrieved from the *HST* archive† after on-the-fly processing had been applied. These datasets were then drizzled (Fruchter & Hook 2002) onto an output grid with pixels half the linear size of the native pixels (i.e 0.025" on a side) using `pixfrac = 0.7`. Due to the invariant point spread function of *HST* a direct subtraction of two aligned images can be performed in which non-varying objects cleanly subtract yielding small residuals while variable objects can easily be seen, even against bright galaxies where visual inspection would not discern the presence of the transient. Performing this process on the first two epochs of imaging of GRB 020410 revealed a transient object approximately 10" from the centre of the refined *BeppoSAX* error circle. The source was subsequently imaged again with STIS on 22 July 2002 and 18 April 2003. It was also imaged with the Advanced Camera for Surveys (ACS) using the Wide Field Camera (WFC) in the F606W and F814W filters on 24 July 2002. The ACS images were also drizzled onto an output grid using the same parameters as for the STIS data. A log of the observations is shown in Table 3.1.

The *BeppoSAX* error circle of GRB 020410 was imaged by the 3.6m telescope at La Silla/ESO seven days after the burst. Images were obtained in U,B and R filters in 1.4" seeing, with the R-band exposure being the deepest observation. These images were bias subtracted and flat fielded in the normal way, within *IRAF*. Examination of the images reveals no evidence for any source at the position of the OT (see below for further details).

3.2.1 Photometry and Light Curve

In order to create a lightcurve free from host galaxy contamination the late time STIS image of the field of GRB 020410 obtained 373 days after the burst was used as template to subtract from the earlier data (see Figure 3.2). Each frame was aligned using 8 point sources in common to each image (and the IRAF task GEOMAP) and then drizzled onto a common reference frame The accuracy of this alignment is $\sim$ 0.2 drizzled STIS pixels (or 0"005). A small (0"1) aperture was used to determine the flux from

†http://archive.stsci.edu

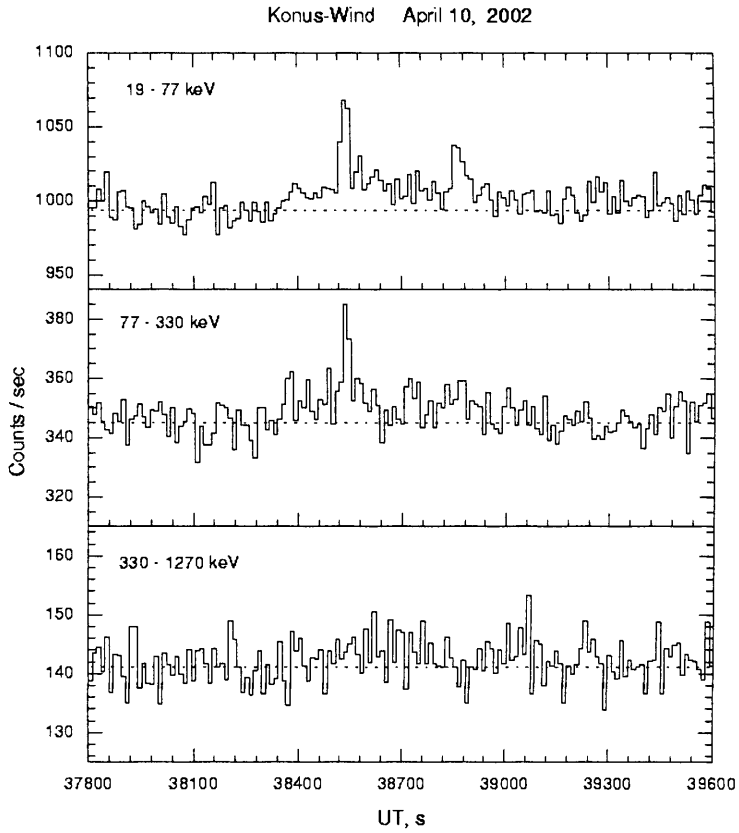

Figure 3.1: The lightcurve of GRB 020410 as seen by Konus-Wind.

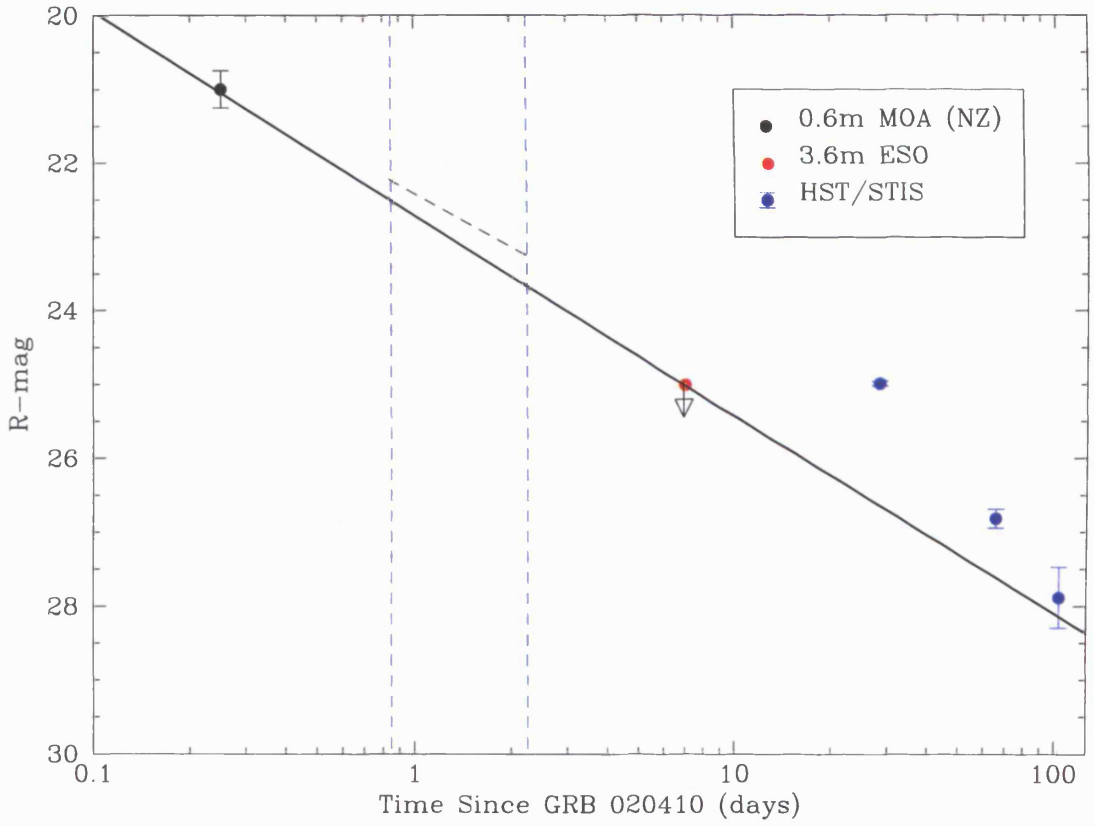

Figure 3.2: The lightcurve of GRB 020410: The early detection from the Microlensing in Astrophysics 0.6m telescope (MOA) (Nicastro et al. 2004) is shown along with the non-detection at $t = 7$ days. The solid black line shows the maximal afterglow contribution under the assumption that it decays as a single power-law. The true afterglow contribution may lie well below this line, especially if the jet break occurs between t=1 and 100 days. Also shown are the times of the two *BeppoSAX* observations (dashed vertical lines) and the X-ray slope determined from them (dashed diagonal line). The position of the X-ray afterglow is arbitrary and is for illustrative purposes. The R-band magnitudes are calculated based on the observed spectral slope at $t = 100$ days $F_\nu \propto \nu^{-2.7}$.

t_b (days)	Inst./Filter	Exp. Time (s)	V-mag	V-mag - host	counts	K_{BS}	K_{VS}
6.895	ESO 3.6m R	1800	$R > 25$	-	-	-	
28.0635	STIS/50CCD	8392	25.35	25.39± 0.02	2.40(2.30)±0.03	-0.177	0.289
65.0635	STIS/50CCD	8315	26.91	27.22± 0.13	0.51(0.43) ± 0.04	-0.308	0.582
102.820	STIS/50CCD	8315	27.45	28.29± 0.41	0.26(0.17) ± 0.03	-0.285	0.484
372.215	STIS/50CCD	8233	28.69	-	-	0.09 ± 0.03	-
104.035	ACS/WFC F606W	3680	27.81(AB)	-	0.30 ± 0.03	-	-
104.371	ACS/WFC F814W	3680	26.75(AB)	-	0.45 ± 0.04	-	-

Table 3.1: Table of observations of GRB 020410, showing the time of each observation, the observed magnitude (or limiting magnitude). Also shown in the case of the STIS images are the measured magnitudes of the OT before and after the host has been subtracted and the relevant K-corrections to correct from Bessel B & V filters to that of STIS. These are based on the observed spectrum of SN 1998bw, which is spectroscopically similar to that of both supernovae 1997ef and 2002ap and indeed SN 2003dh (GRB 030329). The uncertainty quoted is based simply on the uncertainty in the measured number of counts in the aperture, and does not reflect the potential uncertainty in the underlying spectrum. * numbers in parenthesis indicate the host subtracted counts. Magnitudes have not been extinction corrected, the correction is $\sim$ 0.37 magnitudes to $F606W$ and 0.31 magnitudes to F814W.

the afterglow. An aperture correction was then applied in order to allow for the light from the afterglow which is not included in the measurement aperture. This correction was determined via comparison with two isolated point sources in the STIS field which exhibit a similar colour to the afterglow (the colours are determined from the ACS data). Aperture photometry was then performed on each of these stars using 0"1 and 1" apertures. Having corrected for the light within the 1" aperture the total flux for a point source was calculated assuming $F_{\infty} = 1.096 \times F_{1''}$.

A zero point for the image obtained at the ESO 3.6m was obtained by comparison to stellar sources in common to both the 3.6m and ACS images. The observed colour of stellar sources in F814W and F606W was measured and a single powerlaw spectrum was assumed between the two bands. A Johnson R magnitude was then extracted assuming this spectral slope within IRAF/SYNPHOT Using this method a 3σ upper limit of R=24.10 at the position of the afterglow is determined. The *HST* images (see Figure 3.3) show that the OT is offset from a nearby galaxy by 0"65. These two sources are blended at the resolution of the ground based observations, therefore their integrated magnitude was $R \geq 24.1$, 7 days after the GRB. A magnitude for the nearby galaxy based was derived based on its measured magnitude in each of F606W and F814W and its F606W-F814W colour of 0.95. This is converted to an R-band magnitude via IRAF/SYNPHOT, this yields R=24.45 $\pm$ 0.21. This can be compared to the flux in a 1" aperture measured on the ESO 3.6m image which contains both this galaxy and the position of the optical transient. Their integrated magnitude is fainter than R= 24.10. Using this, and the known magnitude of the nearby galaxy, a 3-σ upper limit on the magnitude of the afterglow is $R \geq 25.0$ at t_b =6.8 days. Using 10 sources within 2 arcminutes of the GRB position a marginally deeper 3-σ upper limit of $R = 24.2$ is found, in order that the estimates remain conservative, in what follows the shallower limit implied by calibration against the *HST* data is assumed.

In order to determine a "Johnson/Cousins" V or R magnitude from our broadband STIS/50CCD image it is necessary to assume a spectrum of the object. The early time colour of the object is poorly constrained since it is only present in a single R-band image. However given the predicted rate of decline of the afterglow there is minimal contamination from it at the time of the first *HST* observation. Therefore, after host subtraction, the measured flux is from the supernova only. Thus K-corrected magnitudes are derived from the assumed spectra of the SN (see below) and the observed number of counts (via the method of Nugent, Kim & Perlmutter 2002). The magnitudes and counts are listed in Table 3.1.

The position of the transient was determined from two USNO CCD Astrograph Catalog (UCAC) stars which lie in the field of the ACS image. The mean position based on the two available images (F814W and F606W) is RA= $22^h\ 06^m\ 32.18^s$ Dec =-$83^d\ 49'\ 27.81''$ (J2000) with an accuracy of $\sim$ 0"2. This position is offset from the center of the *BeppoSAX* NFI error box by approximately 10", fully consistent with the 40 arcsecond diameter 90% error box (Nicastro et al. 2002).

The magnitude of the transient at the time of the first STIS observation is $R = 24.90 \pm 0.03$. This limit is slightly brighter than the limit obtained at day 7, implying that the transient re-brightened in this period. Although within the photometric errors the decay is marginally consistent with being flat over the period of 7 to 25 days, such a flat decay slope has never been observed and is not predicted under standard models. It is, therefore, more likely that the afterglow emission faded and then brightened due to the emergence of the underlying supernova. Based on the non-detection at ESO, the mean decay rate between the first detection and the non detection at one week is steeper than $t^{-1.1}$, somewhat faster than the observed X-ray decay flux of $t^{-0.82}$ (Nicastro et al. 2004). Were the slopes identical, which would be the case if they both lay on the same section of the fireball spectrum (i.e. were not separated by the cooling break), then a break would be implied between the second *BeppoSAX* observations and those at ESO. This would not be unexpected since the majority of GRB afterglows have average decay rates faster than t^{-1} over the first week. However, the lack of optical coverage over this period means that strong conclusions cannot be reached.

The magnitude of the OT in the final ACS epoch is determined using aperture photometry. A small (0"1 radius) aperture is used, to minimize the effect of the underlying host, which will likely have a different spectrum to the GRB afterglow and therefore change the observed colour. The magnitude is subsequently corrected to the true magnitude by comparison to a point source in the image. Assuming a foreground extinction of E(B-V) = 0.13 the observed colour using this small aperture is F606W-F814W = 1.03 $\pm$0.06 mag, corresponding to a spectral slope of $\nu^{-2.7}$. The use of a larger aperture (0"25) resulted in a colour of F606W-F814W = 0.53 $\pm$0.10 mag. This change is due to the contamination of the measurement by the host galaxy and implies that the host is very blue; typical of GRB hosts in general (Fruchter et al. 1999; Le Floc'h et al. 2003). It is possible to estimate the contribution to this measurement of the galaxy directly underlying the supernova using the final two epochs of STIS imaging, the first of which is roughly simultaneous with the ACS images (Δt = 2 days, at $t \sim 100$ days). The contribution of the host galaxy to the first of these STIS images will be approximately the same as to the ACS data, allowing a crude separation of host and SN in the ACS observations. The

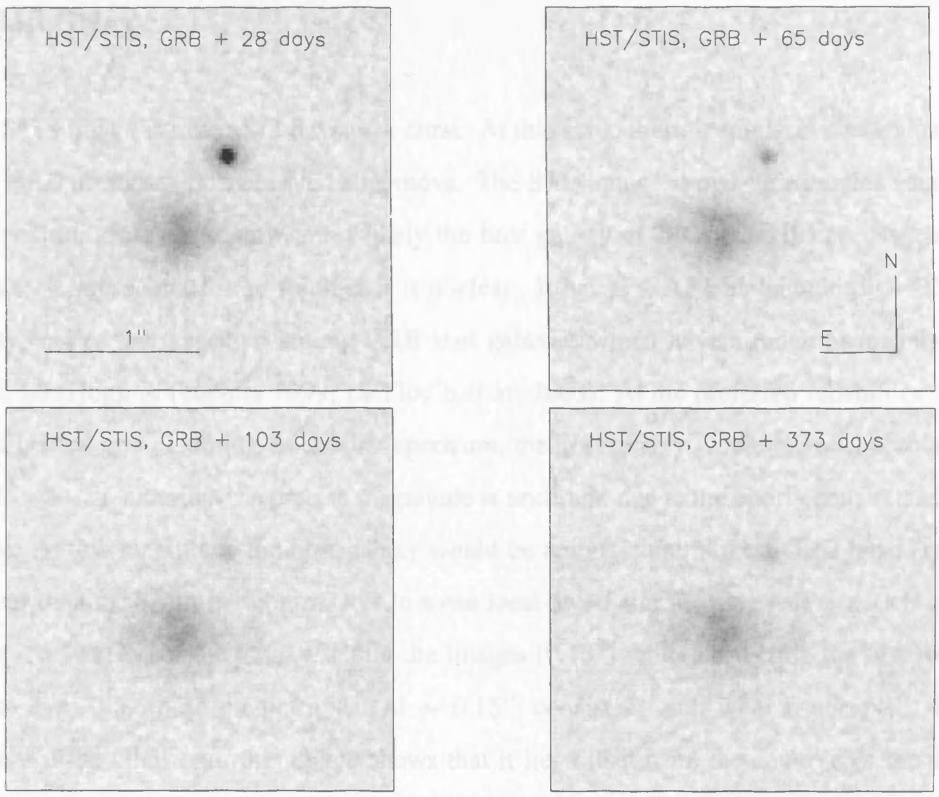

Figure 3.3: Postage stamp STIS images of the OT of GRB 020410 showing the fading behavior of the transient over the year between the first and last observation. In the final image (bottom right) the afterglow /supernovae contributes no light. The object directly underlying the position of the afterglow is interpreted as the host galaxy of GRB 020410. This image is used as a template to subtract from the previous epochs in order to obtain a lightcurve free from host galaxy contamination.

contribution of the host galaxy to this epoch of STIS imaging was $\sim$ 30 %. Assuming that this fraction of light was also the contaminant in the F606W image, and that the host galaxy directly under the SN is the same colour as the outlying regions. The estimated colour of the SN is then F606W - F814W = 1.13 $\pm$ 0.14 mag. This result assumes that the colour of the host galaxy is the same directly under the SN as in outlying regions. However as the host galaxy contributes only 30 % of the light the result is not sensitive to small changes in the underlying colour. Bluer underlying colours would result in a slightly redder supernova, while a reddened underlying population would produce a bluer SN. The lightcurve is shown in Figure 3.2, with the early detection in New Zealand, from Nicastro et al. (2004) and the ESO data, along with the points from STIS.

3.2.2 Host Galaxy

The final STIS image is taken 373 days post burst. At this stage there is minimal contamination from either the GRB afterglow or associated supernova. The STIS image shows an extended source underlying the position of the afterglow, most likely the host galaxy of GRB 020410. Its association with the galaxy $\sim$ 1 arcsecond to the south-east is unclear. It has a V(AB) magnitude of $\sim 27.5 \pm 0.2$, which is typical of that expected among GRB host galaxies which have a range of magnitudes from $21 < R < 30$ (Hogg & Fruchter 1999; Le Floc'h et al. 2003). At the preferred redshift ($z = 0.5$, see discussion below) and assuming a starburst spectrum, the host galaxy would have an absolute magnitude of $M_V \sim -14$, although the precise magnitude is uncertain due to the poorly constrained spectrum of the host. At this magnitude the host galaxy would be amongst the faintest GRB hosts, two magnitudes fainter than the SMC, but comparable to some local dwarf star forming galaxies such as IC 1613. The measured FWHM of the galaxy within the images (0.13") while correcting the observed size of IC 1613 to $z = 0.5$ would predict a size of $\sim$ 0.15", consistent with what is observed. Projecting the position of the GRB onto this image shows that it lies offset from the centroid of the underlying host galaxy by approximately 0"03 $\pm$ 0"01. At $z = 0.5$ the GRB would have occurred within 200pc of the galaxy centre. Using a large aperture (0"25 radius) on the ACS images the observed colour is F606W-F814W = 0.53 $\pm$ 0.10. At the epoch of the ACS observations there remains contamination from the supernova (which is red, with (F606W-F814W)$_{supernovae}$=1.03 $\pm$0.06). The colour of the host galaxy is estimated by subtracting the contribution of the supernova within the 0.25" aperture. This contribution is determined by correcting the measured flux in a 0"1 aperture to that in a 0.25" for a point source, using a stellar source in the image which exhibits similar colours to the supernovae to calibrate this correction. The host galaxy magnitude is then $F_{host} = F_{obs} - F_{SN}$. This results in an AB magnitude of 28.13 $\pm$ 0.10 mag in F606W and 27.67 $\pm$ 0.11 mag in F814W and a colour of F606W-F814W = 0.44 $\pm$0.15 magnitudes. These magnitudes underestimate the true brightness of the galaxy since the host galaxy immediately under the supernova has been subtracted.

The relationship between the host galaxy directly underlying the position of the GRB, and the brighter galaxy, offset 0"6 to the south-west (see Figure 3.3) is unclear. There may well be no physical association. However if there is then the GRB occurred offset from the nucleus of this galaxy by 3.6 kpc and lies on a relatively faint region of the host, this is unusual for GRB events (which typically lie on bright regions of their hosts, see e.g. Chapter 6). However, if the nearby galaxy were the host galaxy then the

absolute magnitude of the host system would be $M_V \sim -18$, similar to the LMC.

3.3 Supernova lightcurve fitting

In order to determine what, if any, supernova lightcurves could fit the optical photometric data spectral templates of different supernova sub-types were constructed. The templates used for the SN Ia and SN II lightcurves can be found in Nugent, Kim & Perlmutter (2002) and Gilliland, Nugent & Phillips (1999) respectively. For the SN Ib/c subtype, the template was based on the spectra of SN 1998bw. These spectra and their temporal evolution are similar to those of supernovae 1997ef and 2002ap, two other well known high-velocity SN Ib/c. The templates were constructed from the extinction corrected spectra of SN 1998bw, and foreground extinction for GRB 020410 was factored into these templates for calculations of the K-corrections.

Figure 3.4 plots the lightcurves of a normal SN Ia over the redshift range $0.25 < z < 1.25$ as they would appear in the STIS 50CCD clear filter. It is clear from this figure and the data in Table 3.1 that the only possible scenario in which the OT could be associated with a SN Ia is at a redshift greater than 1.0. Supernovae Ia at lower redshifts could only approach the magnitudes seen for this event at very late times during the tail of the supernova lightcurve. At these epochs the decay of the lightcurve is nicely modelled by a decline of 0.017 magnitudes per day in the rest-frame B- or V-band divided by the factor $(1 + z)$ over a period of several hundred days (Caparello et al. 1997 for example). However, this is not a good match for the lightcurve of the OT as it declines by 0.05 mags per day between days 28 and 65 and 0.02 mags per day between day 65 and 102.

As seen in Figure 3.4 a SN Ia at a redshift of 1.0 can nicely reproduce the STIS lightcurve if the first *HST* data point was taken near maximum light. However, this possibility can be rejected by consideration of the ACS photometry in the F606W and F814W filter taken at day 104. The observed colour was ≈ 1.1 mag. However, for supernovae Ia at this redshift and late-time epoch, the flux in the restframe ultraviolet has practically vanished and thus the flux in the F606W filter would as well. Based on the templates, the colour for a SN Ia with $z \geq 1$ at these epochs would be > 2.2 mag between these filters. Thus a SN Ia at any epoch and redshift is not able to reproduce all the observed data for the OT. In addition to this, in order for a SN Ia to reproduce the observed light curve, the SN and GRB could not have been simultaneous but the SN would have to occur several days before the GRB.

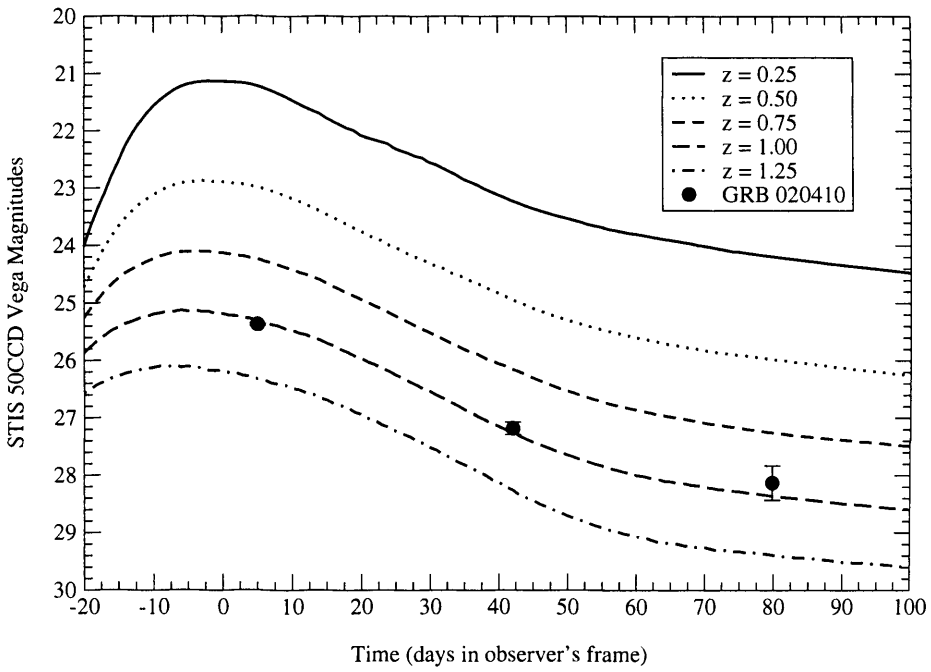

Figure 3.4: The lightcurves of normal supernovae Ia as a function of redshift. Templates are from Nugent, Kim & Perlmutter (2002) and the STIS points are plotted based on the K-corrections for SN Ia spectra discussed therein. The only redshift at which an SN Ia provides a reasonable fit to the data is $z = 1$. However, the late time colour of the object rules out this possibility, since SN Ia would be much redder. Zero days corresponds to the B-band maximum of an SN Ia. At $z = 1$ the SN and GRB could not have been temporally coincident. Galactic extinction along the line of sight to GRB 020410 has been folded into the SN Ia template such that the solid lines represent what would be expected of an SN Ia at each redshift when seen at the galactic extinction measured for GRB 020410.

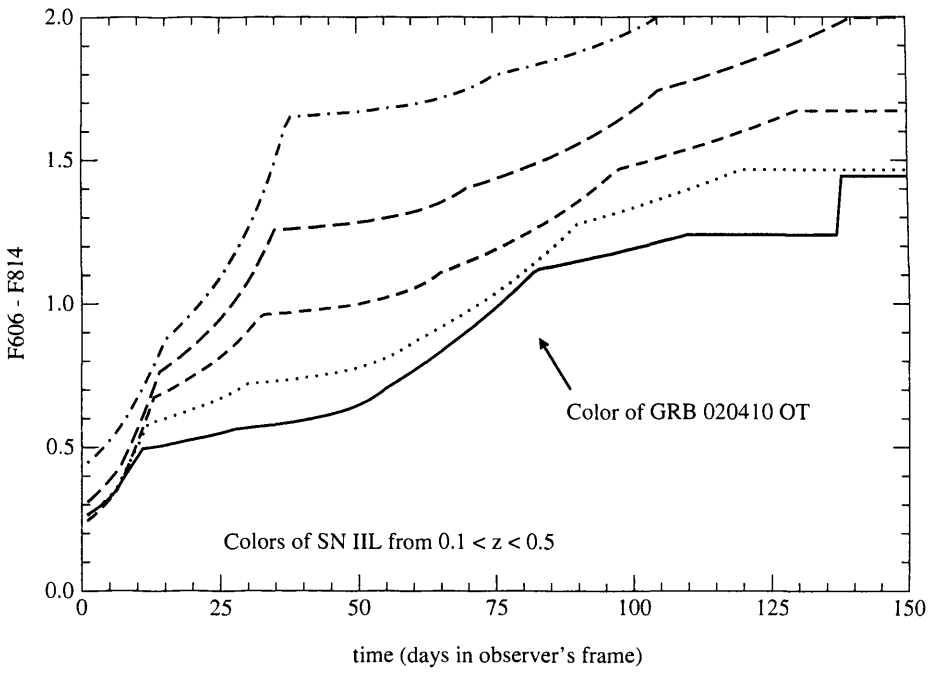

Figure 3.5: The colour evolution of supernovae IIL over a range of redshifts (0.1 (dot-dashed line) $\leq z \leq 0.5$ (solid line)). This clearly shows that the observed late time colour of the OT of GRB 020410 can only be explained by a low redshift ($z \leq 0.2$) event. However, in this case the luminosity would not fit the observed luminosity function of SN IIL.

As for supernovae II the mere shape of the lightcurve rules out plateau-like events. The only possible fit to a linear-like event, based upon the colours, would be at very low redshift, $z < 0.2$, as seen in Figure 3.5. However, at these redshifts the intrinsic brightness of the supernova would be $M_B \approx -14.0$. This is unheard of for linear events which are usually representative of the brighter portion of the SN II population such as SN 1979C (Branch et al. 1981; de Vaucolours et al. 1981). Further Richardson et al. (2002) find that none of their sample of 16 SN II-L events have $M_B > -16$. For a full discussion of supernova absolute magnitudes see Richardson et al (2002). In addition, as seen in Figure 3.6, the fit to an average linear template at these redshifts is quite poor.

The only good fit to the OT based on an underlying supernova is seen in Figure 3.7. Here the high velocity supernovae Ic 1997ef (Iwamoto et al. 2000), 1998bw (Galama et al. 1998; McKenzie & Schaffer 1999) and 2002ap (Pandey et al. 2003; Gal-Yam, Ofek & Shemmer 2002) have been shifted

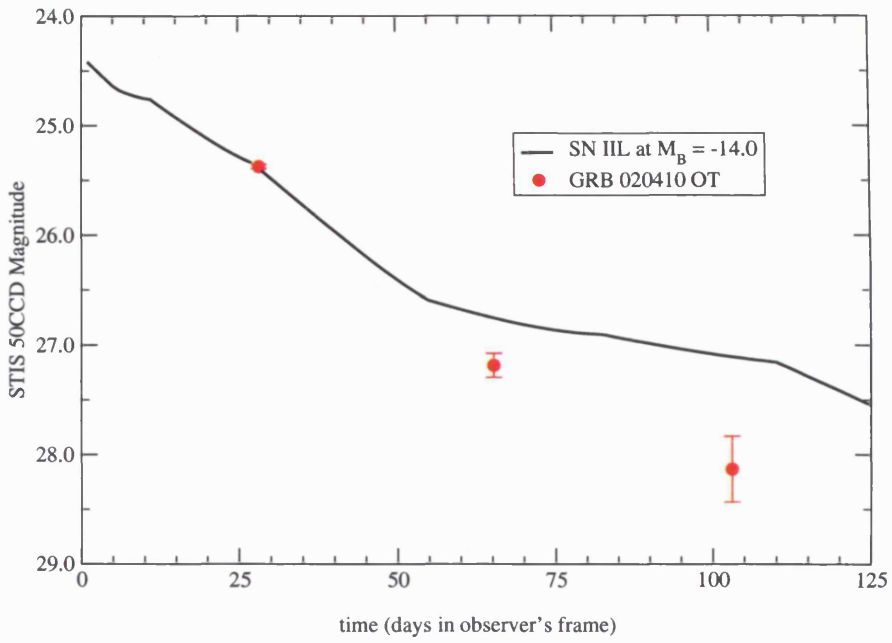

Figure 3.6: A $z = 0.2$ SN IIL, (the only redshift and magnitude allowed based on the measured colour) overlayed with the *HST* magnitudes. As can be seen, the late time behavior is poorly modelled by this type of supernova.

to a redshift of $z = 0.5$ with the explosion date set to be coincident with the observation of the GRB signal from 020410 (cosmology of $h = 0.7, \Omega_M = 0.3$ and $\Omega_\Lambda = 0.7$). All three supernovae follow a very similar spectral evolution to the template so that differences in the K-corrections between the various supernovae will be negligible. The observed lightcurve for the OT is nicely reproduced as is the colour at day 104. Both supernovae 1997ef and 2002ap have peak magnitudes of $M_V \approx -17.4$, which is where the OT is found to lie given the choice of cosmology. SN 1998bw is more than 2 magnitudes brighter than SN 1997ef and SN 2002ap, so the peak of its lightcurve has been shifted down correspondingly. Some variation in the lightcurve shape and decline on the tail between these supernovae is seen, demonstrating that within the expected variability of these types of supernovae Ic a good match could be found to the late time light curve of GRB 020410

Figures 3.8 and 3.9 demonstrate how the data constrain the redshift. Assuming that the explosion date is coincident with the date of the GRB detection. Brightness (blue) and colour (black) of a high-velocity

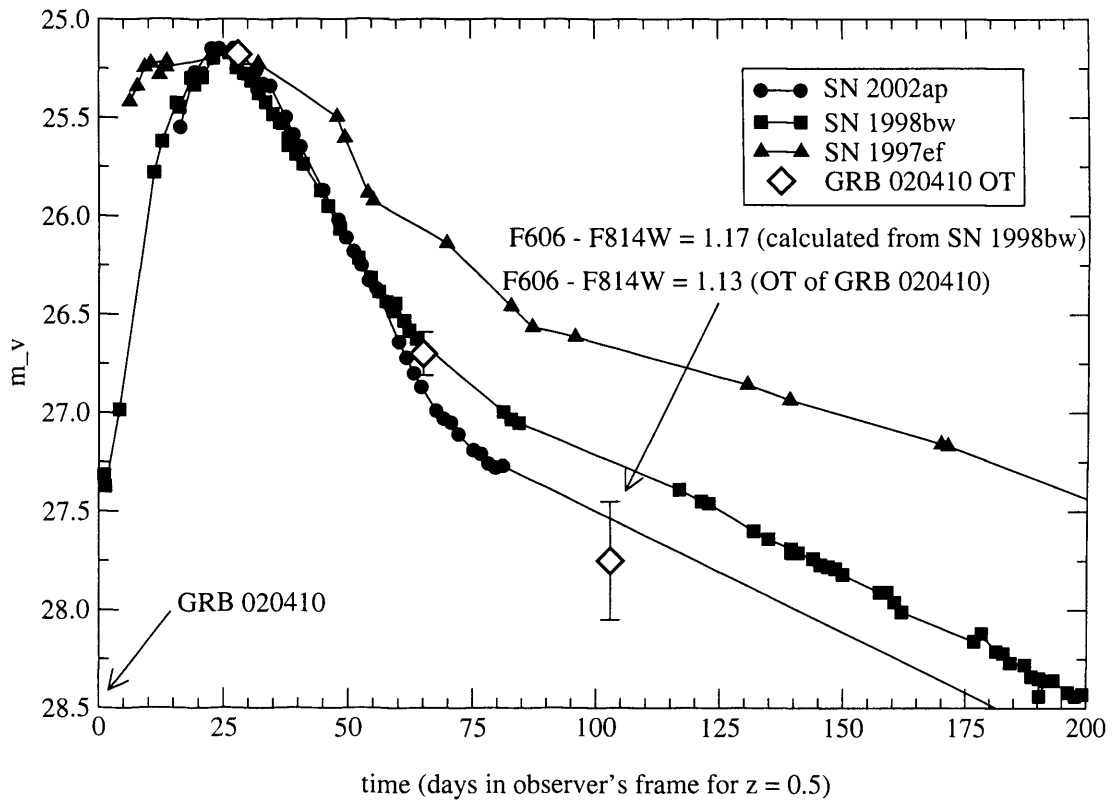

Figure 3.7: A fit to the STIS data points for OT of GRB 020410. The data are modelled with the lightcurves of supernovae 1997ef (Iwamoto et al, 2000), 2002ap (Gal-Yam, Ofek & Shemmer, (2002); Pandey et al. (2003)) and 1998bw (Galama et al. 1998; McKenzie & Schaefer, 1999), redshifted to z=0.5. The afterglow curve is well reproduced by the first two supernovae while SN 1998bw (which is intrinsically 2 magnitudes brighter) has been shifted down in brightness in order to examine the diversity in lightcurve shapes for high-velocity supernovae Ib/c. The data from SN 2002ap have been supplemented by the late time data of Foley et al (2003), and as such the exponential decay is plotted through these points, although they are beyond the range of the plot. A correction for galactic extinction has been applied to the template spectra.

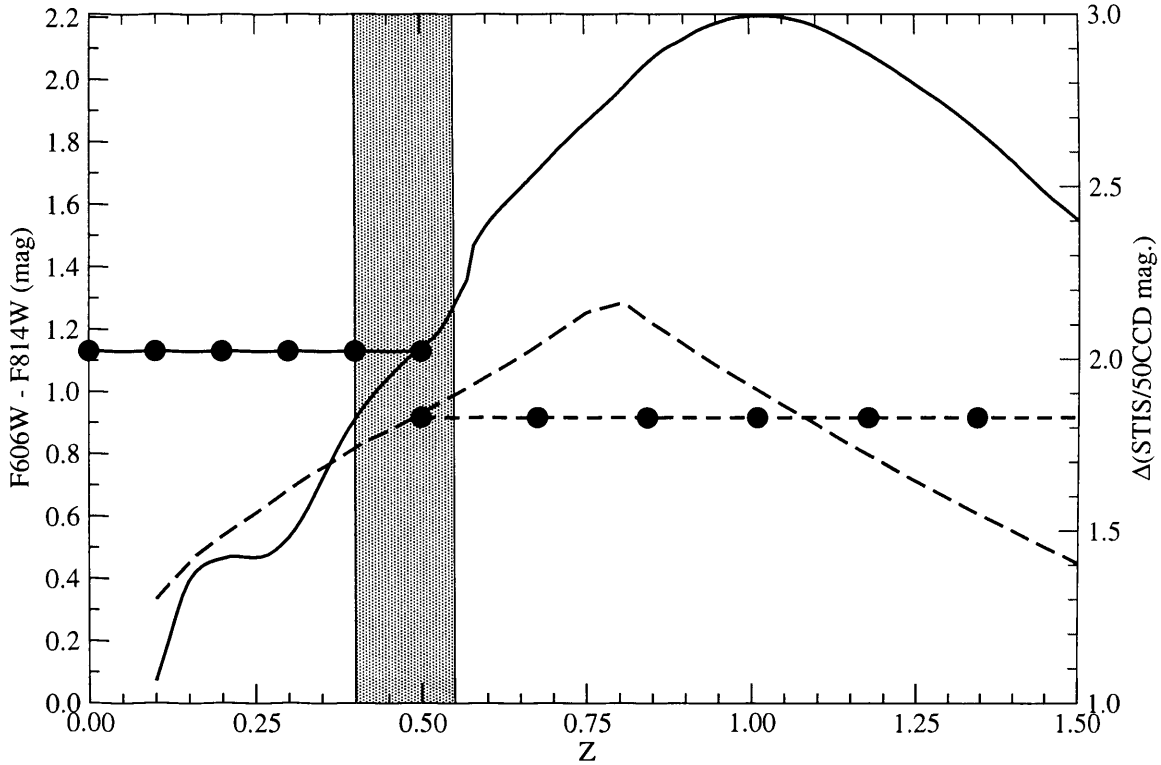

Figure 3.8: Assuming that the explosion date is coincident with the date of the GRB detection, the plot shows the colour (solid line) and brightness change (dashed line) for a high velocity SN Ib/c as a function of redshift, along with the inferred values from the *HST* observations The Δ(STIS/50CCD) mag value is based on the expected change in magnitude of a SN 1998bw and SN 2002ap like SN between the first two epochs, over this time period both SN 1998bw and SN 2002ap show very similar evolution, see Figure 3.7). Due to the steepness of the colour–redshift relationship, the only reasonable redshift range is $0.45 < z < 0.60$. The resulting peak brightness is $M_V \approx -17.4$, assuming the aforementioned cosmology, which is more consistent with the peak brightness of supernovae 2002ap and 1997ef rather than SN 1998bw. The colour-redshift relation is based on the late time colours of the SN ($\sim$ 100 days) where all SN Ic show very similar colours.

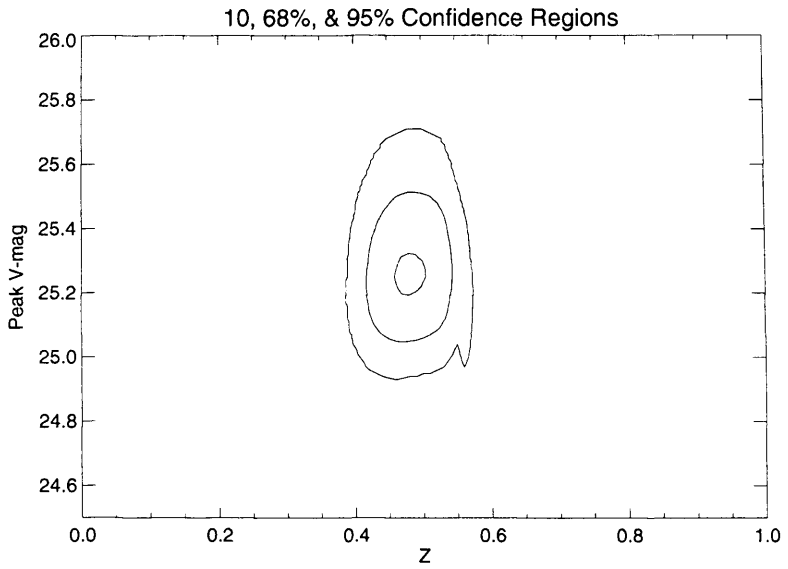

Figure 3.9: The redshift confidence range for the supernova associated with GRB 020410, assuming that the GRB and supernovae are temporally coincident and that the supernovae has a SN 1998bw-like spectrum and zero host galaxy extinction

SN Ib/c are plotted as a function of redshift along with the *HST* observations. Due to the steepness of the colour–redshift relationship, the only reasonable redshift range is $0.45 < z < 0.6$. The resulting peak brightness, given this redshift range, is $M_V \approx -17.4$.

The data were also compared to a more normal set of supernovae Ib/c such as supernovae 1993J (IIb) and 1994I (Ic). These supernovae are characterised by much lower expansion velocities, indicative of less energetic explosions. They also have significantly more rapid declines after maximum light, although both SN 1993J and 1994I reach a peak brightness comparable to supernovae 2002ap and 1997ef. Given colour information for the OT at the earlier epochs it would have been possible to distinguish between these supernovae and their high velocity counterparts quite easily, since their colours before and at maximum show some variety. However, given the choice of filters and the corresponding uncertainties in the observations, the late-time colours for all these supernovae are indistinguishable. The fact that supernovae 1993J and 1994I decay much more rapidly in the optical (Lewis et al. 1994; Richmond et al. 1996) than the OT could be used as evidence against more normal SN Ib/c being associated with this OT. However, given the diversity in both the rise-times and decline rates of core-collapse supernovae, this difference cannot be used as strong evidence of an exclusive association of this OT with a high-velocity SN Ib/c. The strength of the redshift constraint ($0.45 < z < 0.6$) is a product of

both colour and lightcurve shape. This is reasonable as the local sample of type Ib/c supernovae (SN 1994I, 1997ef,1998bw and 2002ap) have effectively identical late time colours. At present these are the best spectral models available, but the sample is still small at present. The caveat to this result is, therefore, that should a larger sample of SN Ib/c spectra reveal differing late time (> 50 day) colours then the redshift range (and hence peak magnitude) determined for GRB 020410 could be significantly affected.

The detection of a supernova associated with GRB 020410 was largely possible due to the intrinsic faintness of the afterglow. For example, despite deep *HST* observations Price et al (2002) were only able to place a constraint of 1.34 magnitudes fainter than SN 1998bw on any supernova in the lightcurve of the nearby GRB 010921. The difficulty for this burst was assessing the contrast between the afterglow and supernova light, such that a faint supernova could not have been seen. However the absolute magnitude of SN 1998bw was $M_V = -19.35$ (Galama et al. 1998), while both supernovae 1997ef and 2002ap were in excess of 2 magnitudes fainter, and would have remained invisible in the lightcurve of GRB 010921. In contrast, the faintness of the afterglow of GRB 020410 allowed a better separation of afterglow and supernova light. The implied intrinsic magnitude of the supernova underlying GRB 020410 was similar to that of SN 2002ap and SN 1997ef and provides evidence that supernovae significantly less luminous that SN 1998bw can also give rise to GRBs. Furthermore it is possible that supernovae of comparable brightness may be present in the afterglows of low-redshift GRBs for which no definitive supernova signature can be found.

Supernova are not the only possible explanations for the late time bumps seen in GRB afterglows. Esin & Blandford (2000) and Reichart (2001) consider the possibility that the bumps may be due to dust echos. In this model the late time bump is caused by re-radiation, or reflection of the early optical afterglow from dust which lies beyond the sublimation radius of the burst. However, for a dust echo to have the same appearance as a supernova, must be somewhat fortuitous. It has to mimic both the colour and the time of peak emission of a supernova. In all cases where a re-brightening of the lightcurve has been observed it can be well fit by an underlying supernova which occurred approximately temporally coincident with the GRB, making dust echoes an unlikely explanation. Furthermore the multicolour dataset available for the afterglow of GRB 970228 allowed Reichart (2001) to demonstrate that dust echoes were not a valid mechanism for the production of the observed bump.

3.4 Comparison with other GRBs

The implied magnitude of GRB 020410 at 1 day is R$\sim$ 22.5. This places GRB 020410 as one of the fainter GRB afterglows discovered thus far. Its magnitude at one day places it in the fainter quartile of GRBs observed prior to *Swift* [‡]. However its decay rate (at least in the X-ray) was $\sim t^{-1}$, typical for GRBs in general, implying that GRB 020410 "started faint" (i.e. $R > 21$ after 6 hours), rather than "faded fast" as has been seen for some bursts [§]. The afterglow could easily have remained unidentified (and the burst classified as "dark") were it not for the *HST* observations taken 28 days after the burst. This is apparently consistent with the conclusions of Fynbo et al. (2001) that many bursts which are classed as optically dark are in fact simply missed since current searches are neither sufficiently rapid nor deep enough to discover the OT. In any case, this burst could certainly be classified among the "optically dim" GRBs.

Some models of dark and optically faint GRBs attribute their optical faintness to extreme extinction in their host galaxies, as may be expected if they are quite dusty. This would be typical of low redshift starbursts. To date the exact nature of host extinction and its effect on the bursts is unclear. For example in the well studied case of GRB 010222 (Galama et al. 2003) the multi-band optical data is well fit by a very low extinction, somewhat in conflict with the SCUBA observation implying that the galaxy is a ULIRG with $A_V \sim 5$ magnitudes (Frail et al. 2002). Another clear disagreement comes from the dark GRB 000210, where a high hydrogen column density (N_H) was measured from the X-ray afterglow (Piro et al. 2002) and sub-mm observations imply a high dust content (Barnard et al. 2003; Berger et al. 2003) whereas optically its host galaxy shows $A_V \sim 0$ (Gorosabel et al. 2003). Similarly dust extinction has been suggested as an explanation for the very red afterglow of GRB 000418 (Klose et al. 2000) and the non-detection of the afterglow of GRB 020819 (Klose et al. 2003). However the host galaxy extinction in the case of GRB 000418 is, similarly to GRB 000210 very low ($A_V \sim 0.2$; Gorosabel et al. 2003b). Only in the case of GRB 030115, which is discussed later in this thesis does a very red afterglow appear to be located in a very red (and highly extinguished) galaxy.

If the optical faintness of the GRB 020410 afterglow were due to extinction in the host, this may

[‡]For example its magnitude at one day is similar to is similar to that of GRBs 980329, 980613, 000630, 020124, 021211 and 030227 (Reichart et al. 1999; Gorosabel et al. 1999; Fynbo et al. 2000; Hjorth et al. 2003; Berger et al. 2002; Fox et al. 2003; Castro-Tirado et al. 2003, respectively)

[§]Two examples of the fast fading variety of GRB are GRBs 020124 and 021211

explain its observed red colour at late times: the presence of a dusty host would significantly redden the normally blue ($\sim \nu^{-1}$) afterglow spectrum, whilst (as with the cases above) the global (host galaxy) colours could remain very blue. However, the re-brightening of the afterglow of GRB 020410 cannot be explained simply by a dusty host galaxy (unless the dust echo model is also inferred), further the observed colours of the SN are not consistent with those of SN 1998bw with significant extinction. With 2 magnitudes of additional extinction (the necessary extinction such that an event as bright as SN 1998bw would appear as faint as SN 2002ap) SN 1998bw would have F606W-F814W = 2.0 so extinction is not a valid method of obtaining both a faint afterglow and faint supernovae. It is therefore unlikely that there is significant extinction within the host galaxy along the line of sight to GRB 020410.

Zeh et al. (2004) have carried out a survey of all low-z GRBs and find that their intermediate time afterglows can be fit with SN 1998bw-like templates with a modest dispersion in their peak luminosities and rise times. The peak luminosity of a type Ic supernova is determined by its Nickel yield. A fainter supernovae corresponds to a lower Nickel production. The faintest supernova within the Zeh, Klose & Hartmann (2004) sample (for which there is a positive detection) is $\sim$ 40 % as bright as SN 1998bw. The supernova associated with GRB 020410 is only $\sim$ 15 % as bright and is as such the faintest supernovae yet seen associated with a GRB, this would correspond to a Nickel yield of $\sim$ 0.05 $M_{\odot}$. There are also now three cases of bursts whose "bump" spectra and light curves may be better fit with SN 1994I-like supernovae (GRB 021211, Della Valle et al, 2003; XRF 030723 Fynbo et al, 2004; GRB 020305, Gorosabel et al, 2005). However due to the lack of early colour information or spectroscopy it cannot be determined if GRB 020410 lies in this class.

3.5 Conclusions

The re-brightening and colour of the afterglow of GRB 020410 present strong evidence for an associated supernova. Both the excess and the colour of the afterglow have been modelled with various supernovae templates which clearly demonstrate that the only acceptable fit is that of an SN Ib/c at $z \approx 0.5$.

This GRB was unusual in that its initial discovery was done via photometry with *HST* taken one and two months after the burst, after early ground based observations had failed to detect a transient. Were it not for these deep, late-time observations, this burst would have been classified as a dark GRB, for which

only an X-ray afterglow was found. These early optical searches were conducted using small telescopes to depths no greater than the Digitized Sky Survey. Hence a change in the search strategies to include much deeper, later-time imaging may be successful in locating OTs associated with GRBs. However, in order for this method to be successful, the error boxes will need to be well defined in order to limit both the time spent searching and to eliminate unrelated, serendipitously discovered supernovae. The launch of *Swift* and its ability to deliver X-ray positions accurate to $\sim$ 6" will be pivotal to this work since the chance of unrelated supernovae is such small error boxes is very small. Dark *Swift* GRBs should be monitored to deep limits over long time frames to search for rising supernovae.

Finally it should be noted that the presence of a supernova component, whose magnitude is significantly fainter than SN 1998bw (by 2 magnitudes) has dramatic implications for the searches for similar signatures in other afterglows. It is possible that such supernovae could be present in the afterglows of many long GRBs. For example, the well constrained upper limit for an underlying supernova to GRB 010921 of 1.34 magnitudes fainter than SN 1998bw remains consistent with a supernova of similar magnitude to that underlying GRB 020410. This stresses the need for accurate photometry of the late time afterglows of many GRBs if the breadth of the luminosity function for underlying supernovae is to be understood.

Chapter 4

The Supernova - X-ray Flash connection: A deep search for supernova signatures in XRF 011030 and 020427

4.1 Introduction

X-ray Flashes (XRFs) occupy the extreme left (lower energy) wing of the peak energy distribution of Gamma-Ray Bursts (GRBs). While GRBs radiate the majority of their energy in γ-rays (with a peak of their νF_ν spectra (E_p) at $\sim$ 200 keV, Preece 2000), XRFs are characterized by peak energies below 50 keV and an X-ray fluence in excess of that observed in γ-rays. XRFs were discovered with the *BeppoSAX* Wide Field Cameras (Heise et al. 2001a) and constitute approximately 1/3 of the total burst population (Lamb et al. 2004). The physical mechanisms driving XRFs and their observed differences to GRBs are some of the key questions in the field today.

Of the many competing theories relating to the origin of XRFs, the most popular is that XRFs are produced when a classical GRB is observed "off-axis", so that the highly collimated ejecta (i.e., the highest energies and harder photons) are not seen (Yamazaki, Ioka & Nakamura, 2002; Rhoads 2003; Dado et al. 2004). Alternatively, models invoking either an increase of the baryon load within the fireball itself (Dermer, Chiang & Böttcher 1999; Ramirez-Ruiz & Lloyd-Ronning 2002; Meszaros et

al. 2002; Huang, Dai & Lu 2002) or low efficiency (high baryon load) shocks (Zhang & Meszaros 2002; Barraud et al. 2003) can also produce XRFs.

One interesting consequence of all of the models above, is that they predict a distance distribution for XRFs which is foreshortened with respect to that of GRBs, since XRFs emit a fraction of the energy of the GRB itself. This hypothesis seems to be supported by the analysis of GRBs with known redshifts, whereby the event peak energy (E_p) scales as $E_{iso}^{1/2}$, i.e. softer GRBs have lower isotropic energies (Amati et al. 2002; Lloyd-Ronning & Ramirez-Ruiz 2002). Qualitative arguments on XRF distances were presented by Kouveliotou et al. (2004), where a comparison of the energetics of the X-ray afterglows of GRBs and XRFs suggested that, were the latter placed at high redshift (e.g. $z = 1.5$), their luminosities would rival those of the brightest GRBs, suggesting a closer proximity for XRFs.

However, determining the true distances of XRFs has proven to be exceptionally difficult observationally. Only two XRFs have so far been associated with optical afterglows, XRF 020903 (Soderberg et al. 2004) and XRF 030723 (Fynbo et al. 2004). Of these only the former has a measured spectroscopic redshift ($z = 0.25$; Soderberg et al. 2004) while the latter has only a redshift limit ($z < 2.3$) with the suggestion of low redshift based on the presence of a supernova like component it its late time light curve (Fynbo et al. 2004). A third possible case, GRB/XRF 031203 is not yet settled, as there is an ongoing debate on the true nature of this nearby event ($z = 0.105$), which was originally classified as an XRF based on its X-ray brightness (Watson et al. 2004) as inferred from the discovery of a halo from dust scattering in our own Galaxy (Vaughan et al. 2004). However, an analysis of its high energy spectrum recorded with *INTEGRAL* (Sazonov et al. 2004) revealed an $E_p \sim 190$ keV, apparently inconsistent with that inferred from the dust halo. The paucity of distance measurements thus prevent definitive conclusions on the XRF distance distribution from being derived.

The spectroscopic signatures of type Ic supernovae seen in GRB 030329/SN 2003dh (Stanek et al. 2003; Hjorth et al. 2003) and the discovery of photometric bumps in many GRB optical afterglow light curves (e.g. Zeh, Klose & Hartmann 2004) strongly support the collapsar model (Woosley 1993), whereby the majority of long duration GRBs are the result of core collapse supernovae. Should XRFs be associated with supernovae, as seen in GRBs, but found at typically lower redshifts, it should be possible to constrain their distances by the detection of a supernova brightening in their X-ray located host galaxies. This can be the case where an optical afterglow is seen (e.g. XRF 030723; Fynbo et al. 2004) or in some cases where there was no apparent optical afterglow (e.g., GRB/XRF 031203; Bersier et al. 2004;

Thomsen et al. 2004;Cobb et al. 2004; Gal-Yam et al. 2004; Malesani et al. 2004).

In this chapter I present deep *HST* observations of the locations of two XRFs. Direct subtraction of these deep observations places very deep limits on any transient optical source found at the locations of the X-ray afterglows to both XRF 011030 and 020427. Indeed neither of these bursts exhibited measurable optical emission at any epoch. The limits obtained via the *HST* data place strong constraints on the contribution of underlying supernovae to each XRF. Various scenarios to explain the lack of optical emission are considered including bursts which lie at higher than expected redshift, behind significant dust column or are associated with faint supernovae.

Date	Δt^b	t_{exp} (ks)	Counts^c	Γ	N_H (10^{21} cm^{-2})	F_x^c
XRF 011030						
2001 Nov 09.728	10.46	46.6	374	1.31(8)	1.02	1.06 $\times 10^{-13}$
2001 Nov 29.464	30.19	19.9	16	1.3(4)	1.02	1.07 $\times 10^{-14}$
XRF 020427						
2002 May 06.225	9.08	13.7	56	1.3(2)	0.29	5.1 $\times 10^{-14}$
2002 May 14.154	17.00	14.6	24	2.1(3)	0.29	1.2 $\times 10^{-14}$

Table 4.1: Properties of the X-ray afterglows of XRF 011030 and 020427, ^{a} values in parenthesis correspond to 68% uncertainty, ^{b} days since burst, ^{c} measured counts and unabsorbed flux (erg s^{-1} cm^{-2}) between $0.3 - 10$ keV, ^{d} Galactic value (Dickey & Lockman,1990) , indicates that the spectral index is determined by a joint fit to both data sets.

4.2 Observations

XRF 011030 was detected with *BeppoSAX* on 2001 October 30, 06:28:02 UT (Gandolfi 2001) with an initial error circle of $r = 5$ arcminutes. It had a long duration ($t_{90} \sim 1000s$), an apparently low E_p (< 40 keV; Heise et al. 2001b) and a fluence of 9×10^{-7} ergs cm^{-2} ($2 - 28$ keV). The field surrounding XRF 011030 was imaged with the WIYN 3.5m telescope on 2001 November 1, 2, and 3, reaching limiting magnitudes of R$\sim$ 23.5 on each occasion. Image subtraction failed to locate any afterglow candidates to these limits; a stacked image indicated that no optical afterglow was present to R>24 (Rhoads et al. 2001). Radio observations with the VLA, however, did identify a fading source

as the possible afterglow of XRF 011030 (Taylor et al. 2001). The field was imaged by *Chandra* at two epochs on 2001 November 9 (47.21 ks) and 29 (20.12 ks), with the Advanced CCD Imaging Spectrometer S-array (ACIS-S). Comparison of the two epochs revealed a variable source within the *BeppoSAX* error box at at RA =20:45:36.00, DEC =+77:06:01.09 (Harrison et al. 2001; Bloom et al. 2003), approximately 1.2 arcseconds from the location of the radio source; the *Chandra* source was then identified as the X-ray counterpart of XRF 011030 (Fruchter et al. 2002a).

XRF 020427 was detected also with *BeppoSAX* on 2002 April 27, 3:48:40 UT and was classified as an XRF by its $(10-28)$ to $(2-10)$ keV hardness ratio, which indicated an X-ray rich event (in't Zand et al. 2002). Optical observations taken after the burst failed to locate the afterglow to a limit of I=21.7, 51 hours after the burst (Jakobsson et al. 2004) . For this work the field of XRF 020427 was observed on 2002 May 11 with the 1.54m Danish Telescope at La Silla, Chile in the R-band with a total exposure time of $9\times$ 300 seconds (Table 4.2) a limit on the afterglow emission of of I>22.0 was found at this time. Radio observations of the XRF field also failed to find any counterpart (Wieringa et al. 2002). XRF 020427 was also imaged with the *Chandra* ACIS-S array on 2002 May 6 (13.92 ks) and 14 (14.76 ks). Comparison of the two observations revealed a bright, rapidly declining source within the *BeppoSAX* error circle at RA = 22:09:28.22, Dec=-65:19:32.03 (Fox 2002a,b; Bloom et al. 2003). VLT observations of the counterpart obtained in June 2002 show a blue colour complex of galaxies underlying the position of the X-ray transient (Castro-Tirado et al. 2002). Amati et al. (2004) presented a comprehensive analysis of all available X-ray data on this burst. The prompt event had an $E_p < 5$ keV and a duration $t_{90} \sim 60$s, and its fluence was 5.8×10^{-7} ergs cm^{-2} $(2-28$ keV); the best fitting pseudo-redshift was $0.1 < z < 0.2$ (Atteia 2003; see also section 4).

For each XRF the *Chandra* data were reprocessed and spectra extracted using *CIAO* version 3.0.2 and *CALDB* version 2.26. Both images were searched over a region 4.2 $\times$4.2 arcminutes (512 $\times$ 512 pixels) centered at the *BeppoSAX* source location; within this radius, there is only one clearly decaying source, already identified as the XRF afterglow. The spectrum for each burst was fit using the C-statistic (appropriate for low count data; Cash et al. 1979); the spectra were unbinned and the (negligible) background was not subtracted. The resulting counts, spectral indices and fluxes are shown in Table 4.1.

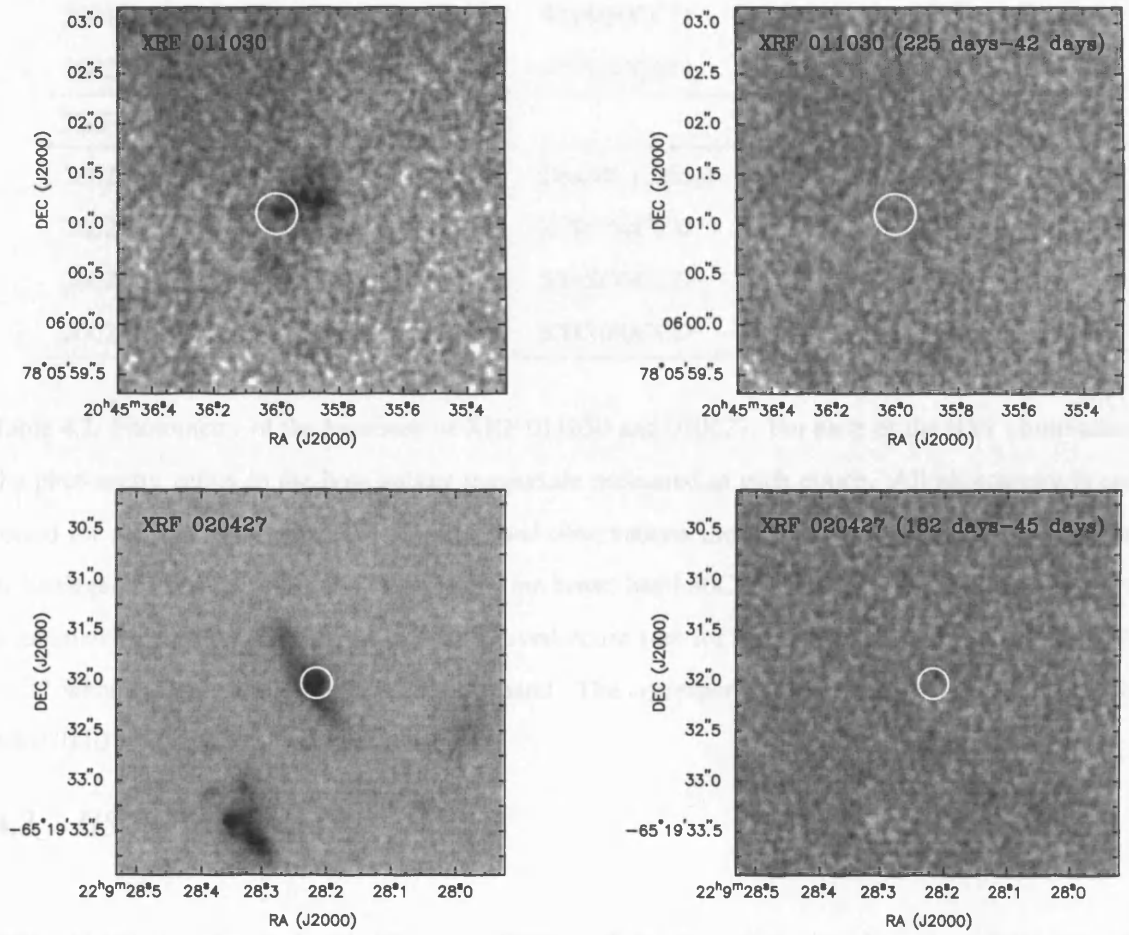

Figure 4.1: The host galaxies of XRFs 011030 and 020427 (left column) and the results of difference imaging on each of their fields (right column). For each XRF the images were obtained with STIS. The two subtracted images are taken approximately six months apart and show no evidence for any excess emission at either epoch, placing limits of $V \sim 28.5$ for the combination of afterglow and supernovae approximately 40 days after each burst. In each image North is up, and East to the left.

Date	$\Delta t = t - t_0$ (days)	Inst/Filter	Exp Time (s)	Mag
XRF 011030				
2001 Nov 1.221	0.952	WIYN/R	3000	> 22.5
2001 Nov 3.132	2.862	WIYN/R	3000	> 22.2
2001 Dec 12.175	42.905	STIS/50CCD	8640	25.31 ± 0.10
2002 June 12.602	225.380	STIS/50CCD	7505	25.30 ± 0.10
XRF 020427				
2002 May 11.607	14.447	Danish 1.54m/I	2700	> 22.0
2002 June 10.762	44.603	STIS/50CCD	8640	24.44 ± 0.05
2002 June 14.734	48.575	STIS/50CCD	4781	24.45 ± 0.05
2002 Oct 26.011	181.852	STIS/50CCD	8392	24.44 ± 0.05

Table 4.2: Photometry of the locations of XRF 011030 and 020427. For each of the HST observations the photometry refers to the host galaxy magnitude measured at each epoch. All photometry is corrected for galactic extinction. For R and I band observations the corrections are based on the values of Schlegel, Finkbeiner & Davis (1998). For the broad band 50CCD images the extinction correction is estimated based on the change in the observed count rate for a typical GRB host galaxy shape of $\nu^{-0.8}$ when folded through the 50CCD passband. The corresponds to $A_{50CCD} = 1.17$ and 0.06 for XRF 011030 and 020427 respectively.

4.3 *HST* Observations

XRF 011030 was observed with *HST* using STIS on 2001 December 12 and again on 2002 June 12. The first of the STIS observations were obtained in both the 50CCD and Long-Pass (LP) filters, while the second was obtained only with 50CCD. The field of XRF 020427 was imaged with *HST* also using STIS in the 50CCD mode 2002 June 10 and 14; LP images were also obtained at the June 14 epoch. A final epoch was obtained on 2002 October 26, again using the 50CCD filter. Table 4.2 shows the log of the *Hubble Space Telescope* observations. Both XRF datasets were retrieved from the *HST* archive* and were combined and cleaned of cosmic rays using the drizzle routine (Fruchter & Hook 2002). Dithered images were drizzled onto a grid with pixels of size 0.025 arcseconds, half the native STIS pixel, using a value for `pixfrac` of 0.7. All observations were aligned with the IRAF routine

*http://archive.stsci.edu

`geomap` using point sources in common in each *HST* image and then redrizzled onto an aligned output grid. A log of *HST* and all ground based optical observations is shown in Table 4.2.

4.3.1 Astrometric Alignment

To accurately position the *Chandra* sources on the *HST* image the *Chandra* field has to be precisely aligned with that of *HST*. The STIS field of view of only 50 arcseconds typically contains an insufficient number of sources to assure such an alignment and, therefore, it is necessary to use ground based intermediate images. The data obtained at the WIYN (XRF 011030) and Danish 1.5m (XRF 020427) telescopes respectively are used for this purpose. Each of these fields was initially aligned to the USNO-A2 catalogue and positions were estimated for all objects for which an apparent optical counterpart was identified within 0.5 arcseconds of a *Chandra* source. A first alignment of the X-ray to the optical sky was then performed using the *Chandra* header coordinates. Finally, relative astrometry between the ground based observations and the *HST* images was performed, using eight and ten common point sources between each field (for XRF 011030 and 020427, respectively). As a result, it is possible to place the X-ray counterparts of XRF 011030 and 020427 onto the *HST* images with a positional accuracy of $\sim$ 0.2 and 0.15 arcseconds, respectively.

These positions agree with those reported by Fruchter et al. (2002a,b) and Bloom et al. (2003) and confirm their identification of the host galaxies. The positions of the X-ray afterglows for both XRFs are coincident with the stellar fields of their host galaxies with blue global colours (Bloom et al. 2003). The host of XRF 020427 also appears to have several neighbour galaxies of similar magnitude, colour and morphology indicating that it may be part of a galaxy group. The blue colours of each XRF host galaxy are similar to those of other GRB hosts, and imply relatively young stellar populations and little dust (see e.g. Trentham et al. 2002; Le Floc'h et al. 2003; Christensen et al. 2004).

To search for optical variability of the X-ray sources, direct image subtractions of each of the XRFs was performed. Due to the invariant point spread function of *HST* it is possible to directly subtract aligned image without the need for additional manipulation of the data via "PSF matching" algorithms as is necessary for ground based data. Thus by direct subtraction of images obtained at $\sim$ 40 and 180 days, strong constraints can be placed on underlying supernova emission. To increase the depth of the final subtraction for XRF 020427 the data of June 10 and 14 were drizzled together onto a single first

epoch image. The resulting difference image was then searched using SExtractor (Bertin & Arnouts 1998), with a signal to noise threshold of 5σ and a Gaussian mask with FWHM = 3 pixels, to mimic the *STIS* point spread function (PSF). No variable object was found in either field, with the exception of saturated stellar objects, which leave clearly detectable residuals. The subtractions are shown in Figure 4.1. To define the depth of these subtractions artificial stars were created within the first epoch image with magnitudes in the range $27 < V < 30$, and a FWHM equal to the STIS PSF. The difference images containing these fake stars were then searched with the same method described above. 100% of the artificial stars were recovered at $V = 28.7$ in the XRF 020427 image, and 95% of those at $V = 28.5$ in the XRF 011030 field (at a 5σ detection level).

This sensitivity difference is mostly due to a larger number of saturated objects in the field of XRF 011030 than for XRF 020427; when artificial stars land on (or near) these objects, it is not possible to recover them. Moreover, the depth of XRF 011030 images is slightly lower. The "true" limit for XRF 011030 further diminishes to $V \sim 27.6$ when the large foreground extinction (E(B-V) = 0.4) towards this source is considered. For XRF 020427 the smaller extinction (E(B-V)=0.03) has little effect on the limiting magnitude. These limits, and the constraints they place on the optical afterglow and supernova emission from each XRF are discussed in the next section.

4.3.2 Lack of residual optical emission at 40 days after the burst trigger

Assuming that there is a supernova associated with each XRF, the flux seen at the location of the burst at a given time is the sum of the afterglow, supernova and host galaxy. The host galaxy component can be removed by the subtraction of a late time image after both afterglow and SN have faded. For GRBs with bright optical afterglows their magnitude at $\delta t = 10$ days after trigger, is in the range $22 < R < 25$ (see e.g. Figure 2. of Fox et al. 2003); assuming a fast decaying trend (t^{-2}) this would imply that the majority of these afterglows would be somewhat brighter than $R = 28$ after 40 days. In the case of XRF 011030 and 020427 the putative sum of afterglow + SN at 40 days is fainter than $V \sim 28.5$. This is not surprising, however, since many GRB afterglows are often not seen at optical wavelengths (so called "dark" bursts), and a more careful examination is necessary to determine if this lack of emission is unusual.

Under the standard fireball model (see Mészáros 2002 for a review) GRB afterglows are described by

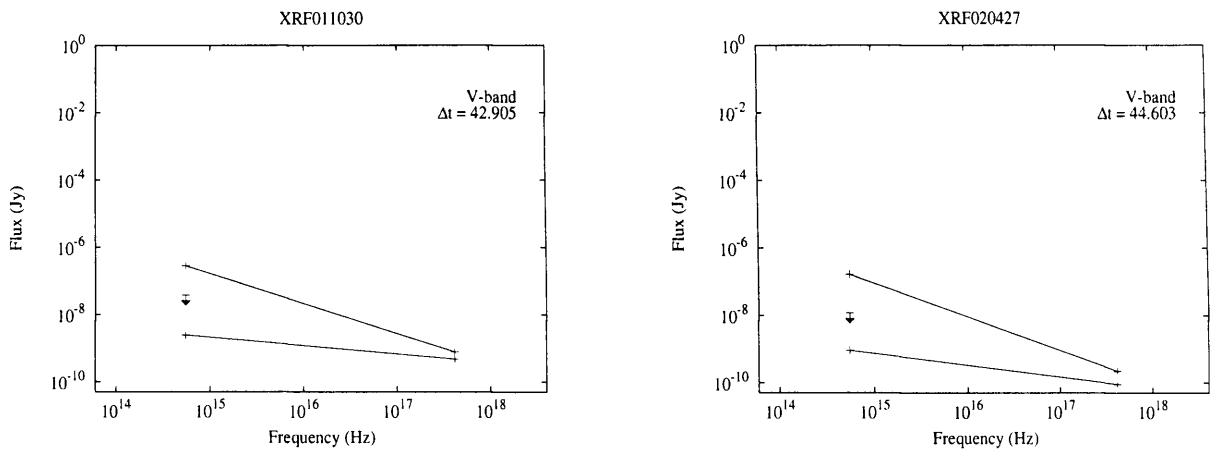

Figure 4.2: The extrapolation of the X-ray afterglows of XRF 011030 (left) and XRF 020427 (right) into the optical waveband (STIS). The optical limits shown are derived from extrapolating the X-ray observations both temporally and spectrally to the optical observations. This was done using the powerlaw indices from the X-ray observations, and allowing for a possible cooling or jet break between the epoch of the X-ray and optical observations, such that the final optical limits derived are the extremes of all possible allowed scenarios (see Rol et al. 2004).

a synchrotron spectrum, which can be represented to first order by a set of gradual power-laws with breaks at frequencies representing the cooling of the fireball (ν_c), the peak frequency of the electrons (ν_p) and the self-absorption frequency where the fireball becomes optically thick (ν_{sa}) (see Figure 1.7). It is therefore possible to extrapolate between wavebands under the premise of this model. Such extrapolations are potentially of great value for bursts unseen at optical wavelengths since, based on the properties of the X-ray afterglow, it is possible to predict the expected optical flux. This may differentiate between truly dark events (i.e. ones for which the expected optical emission is brighter than observed limits) and the ones which are not seen due to insufficient depth of the observations (Fynbo et al. 2001). Groot et al. (1998) first attempted such a method for the dark GRB 970828 and found that extrapolating the X-ray slope into the optical regime predicted significant optical flux, while none was seen. However, such predictions need to take account of the possible presence of ν_c between the optical and X-ray frequencies and therefore the optical to X-ray spectral flux is not well constrained but falls within a range of values for a given burst; thus the distinction between dark and bright bursts is not sharp but is populated with "gray" bursts, events which fall between the extremes of the extrapolations (Rol et al. 2004). Applying the same method of extrapolation to XRF 011030 and 020427 showed that the existing optical limits for both bursts lie below the most optimistic estimates

from the X-ray afterglow of each burst, but above the limits derived using a worst case scenario (the most rapid possible decay and the presence of a cooling break between optical and X-ray bands). Thus these non-detections can be explained without recourse to additional extinction (and always assuming a fireball spherical expansion); this is evident in Figure 4.2, where it is clear that the limiting flux for XRF 020427 falls well within the extrapolation of the limits obtained from the X-rays. For more details of this method, the reader is referred to Rol et al. (2004).

To determine the limits on underlying supernovae for each XRF, spectral templates were created based on the SN 1998bw spectra first reported by Patat et al. (2001)[†]. Since observations at a fixed observer time correspond to different rest frame times, for each redshift considered the template spectrum taken closest to the rest frame time corresponding to the observer time of the *HST* data was used. In cases where temporally coincident spectra were not available, the closest available spectra were used, normalized against the observed photometry of SN 1998bw at that time (using the light curves of Galama et al. 1998) and K-corrected them to the appropriate redshift corresponding to the fixed observer time. The expected number of counts from these spectra within the STIS/50CCD passband were then calculated by convolving them with the STIS response with *synphot*. At this stage the effect of Galactic extinction for each XRF field was also included based on the tabulated E(B-V) from Schlegel, Finkbeiner & Davis (1998). Thus the expected number of counts from a SN 1998bw like supernova for each XRF field at various redshifts was obtained.

The optical spectra available for SN 1998bw extend only to $\sim$ 3000Å. Therefore, they are of limited use at higher redshifts, where the rest frame ultraviolet component is observed. Moreover, very few studies exist to date of the UV-spectra of type Ic supernovae, in particular temporally resolved studies, which would be ideal for the comparisons presented here (a generic feature of most supernovae is a suppression of the UV-flux due to the blanketing effect of metals). Therefore, limits on the UV component of the SN flux have been computed via two different methods. The first is to assume zero flux below 3000Å (rest frame); while this is clearly underestimating the true flux, it provides a firm lower limit on the expected brightness of the supernova within the redshift limits studied. The second method is to use the available UV spectroscopy of SN 2002ap (a typical Ic supernova), taken with *STIS* on 2002 February 1 using the G230L grism. This spectroscopy shows a substantial decrease in flux from $\sim 3000 - 2000$ Å as expected and also seen in SN 1994I (Millard et al. 1999). The flux was then

[†]These templates were taken from the database of supernovae spectra maintained at http://tor.nhn.ou.edu/~ suspect/index.html

rescaled so that it is matched to the flux seen with ground based spectra at $\sim$ 3000Å. Although these spectra should provide a reasonable measure for the UV flux for type Ic supernovae it should also be noted that the spectrum of SN 2002ap was taken at an early epoch ($\sim$ 5 days) and possible evolution of the features may change the spectral shape at later epochs. However, as time resolved UV spectroscopy is not available for any high velocity Type Ic SNe, it is not possible to determine if this early shape is maintained into later epochs.

SN 1998bw was a very bright Type Ic event; fainter Type Ic supernovae are more common locally and it is likely that their overall distribution may be bimodal (Richardson et al. 2002). Although it is not clear that all Type Ic supernovae produce a GRB, the ones firmly (i.e. spectroscopically) associated with GRBs are comparable in brightness to SN 1998bw (e.g. Hjorth et al. 2003; Stanek et al. 2003; Garnavich et al. 2003). However as demonstrated in the previous chapter and elsewhere (e.g. Price et al. 2002; Zeh et al. 2004) there is growing evidence that GRBs can be associated with fainter supernovae which are more typical of the mean luminosity of SN Ib/c. The faintest of the local high-velocity type Ic supernovae is SN 2002ap. This supernova exhibits similar spectral and temporal evolution to SN 1998bw (with a slightly faster rising lightcurve, e.g. Fig 4 of Foley et al. 2003) and was 2 magnitudes fainter than SN 1998bw although still one magnitude brighter than the faintest type Ic ever seen (Richardson et al. 2002). This supernova was used as a template to study what might be expected as a limiting magnitude from fainter supernovae. The predicted magnitudes are not strongly dependent on the UV-flux below $z \sim 1$ as can be seen in Figures 4.3 & 4.4 (upper panels), where the evolution of the magnitude of SN 1998bw and SN 2002ap at various redshifts in the two XRF fields are plotted. However, the limiting magnitude beyond this is a sensitive function of the unknown UV-flux, and the true magnitude may be somewhat different; a hard upper limit is set by the assumption of zero UV flux.

The evolution of the expected magnitudes for supernovae with differing properties is shown in Figures 4.3 & 4.4 (for XRF 011030 and 020427 respectively). For XRF 011030 a faint type Ic supernova association, such as SN 2002ap, would fall below the detection limit of the observations at $z \sim 1$, while a SN 1998bw type would have been seen out to $z \sim 1.5$. For XRF 020427 both supernovae would be visible up to $z \sim 1.2$, and again only a SN 1998bw type could be seen beyond $z \sim 1.5$. However, for $z > 1$ the rest frame UV light from the supernova is very sensitive to the host galaxy extinction, such that a moderate $A_V \sim 1$ could extinguish the supernova contribution (see also Figures 4.3,4.4, lower panels). Further, the true colours of type Ic supernovae are not well constrained in the rest

frame UV. For most supernovae the colours evolve from blue to red, with bluer bands experiencing peak light before the red. Some supernovae associated with GRBs, however, have exhibited blue (rest-frame UV) peak colours (e.g., SN2001ke/GRB 011121; Garnavich et al. 2003; Greiner et al. 2003) implying that they have a significant UV-component, while many Type Ic supernovae (including SN 1994I and SN 2002ap) have a large UV decrement due to metal line blanketing. This approach, therefore places only a lower limit on the expected emission from supernovae at these redshifts.

The limiting magnitudes placed on underlying supernovae depend not only on the observed spectra but also on the shape of the light curve of the associated supernova. Local type Ib/c supernovae show a range of light curve properties including some which evolve faster than SN 1998bw (e.g. SN 1994I) and some which evolve slower (e.g. SN 1997ef). A fast evolving supernova would have decayed further at the time of the observations, while a slower one would be closer to peak (or even at peak if viewed at higher redshifts). To explore the possible effect of light curve shape on the derived supernovae limits the same K-corrections as described above were performed but on supernovae which evolved 30 % slower, and 30 % faster than SN 1998bw. In each case the UV-flux estimates for SN 2002ap were maintained. A faster evolving supernova would drop below the visibility limit at $z \sim 0.8$ for XRF 011030 and at $z \sim 1.1$ for XRF 020427, assuming the same peak magnitude as SN 2002ap ($M_V = -17.2$). A slower evolving supernova (again with a peak brightness similar to the one of SN 2002ap) would be seen out to $z = 1.3$ and $z = 1.5$ for XRF 011030 and 020427, respectively. It should also be noticed that these estimates assume that the supernova light at the time of the second epoch observations is much fainter than at the first. This is so far the case for *all* type Ib/c SNe known (for example SN 1998bw would have fallen by more than a factor 10 in the period between the observations considered here); it is clear, however, that these estimates depend on the SNe light curve shape and would provide different limits in the (unlikely) event of e.g., SN Ib/c light curves exhibiting a plateau.

4.4 Discussion

The X-ray light curve decay indices (assuming a power law decay starting at $t = 0$ for each burst) are $\alpha = -2.0 \pm 0.3$ and $\alpha = -1.4 \pm 0.4$ for XRF 011030, 020427, respectively. These slopes are both comparable to those observed in typical GRB X-Ray afterglows, which at late times lie in the range $-1 < \alpha < -2$ with a best fit of $\alpha = -1.69$ (Kouveliotou et al. 2004). Unfortunately the sample

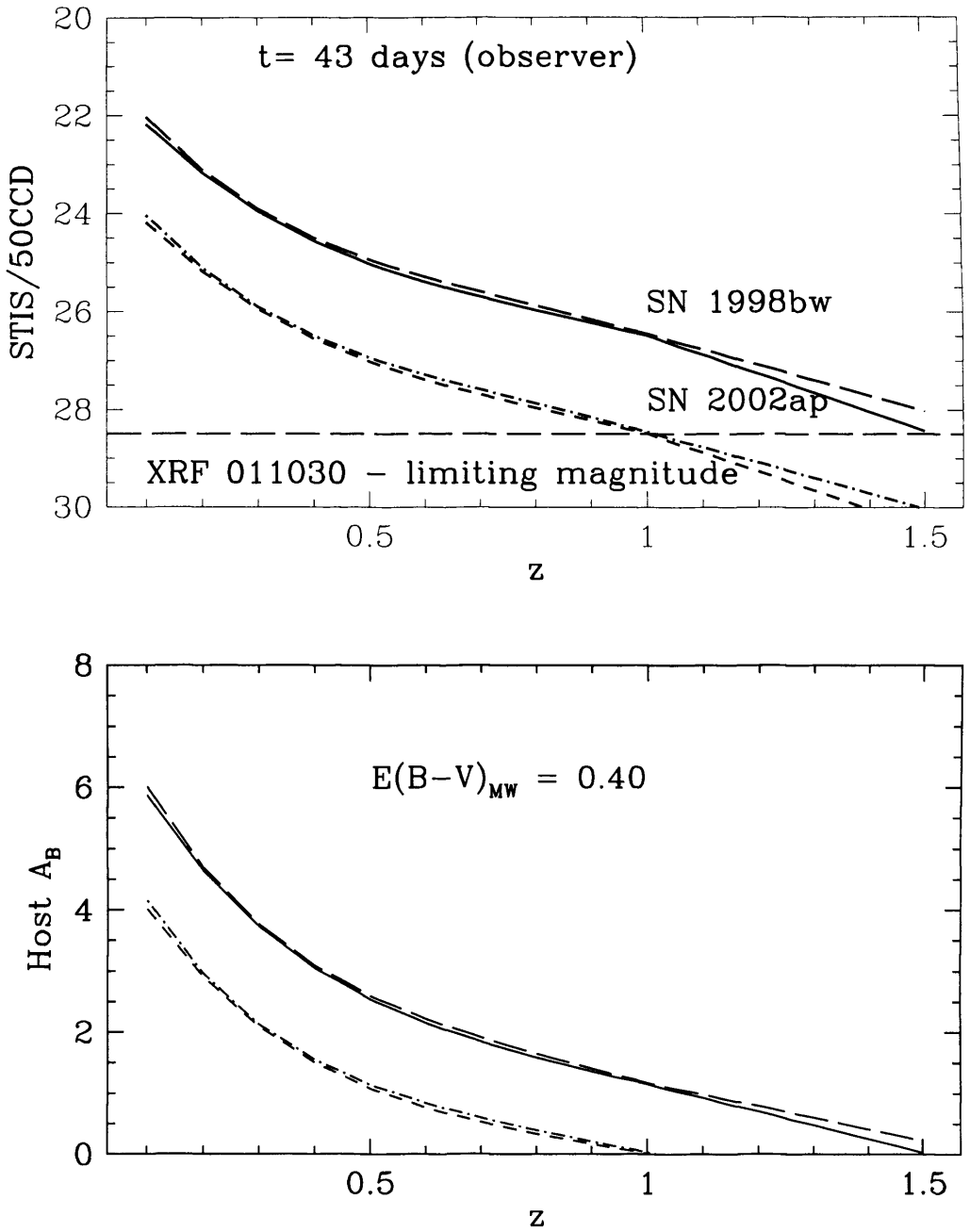

Figure 4.3: *upper panel*: The predicted magnitude of SN 1998bw and SN 2002ap at various redshifts in the XRF 011030 field and at a fixed observer time. Two lines are shown for each supernova, the lower line (solid for SN 1998bw, dashed for SN 2002ap) show the extrapolations assuming zero flux for $\lambda < 3000$Å, while the upper line shows the magnitudes assuming that the UV-flux had a spectral shape as determined from SN 2002ap. The horizontal line corresponds to the limiting XRF magnitude calculated in this Chapter. *bottom panel*: The required rest frame B-band extinction within each XRF host galaxy such that either a 1998bw or a 2002ap like SN could be hidden. The two lines again represent different methods of treating the UV component of the supernova flux.

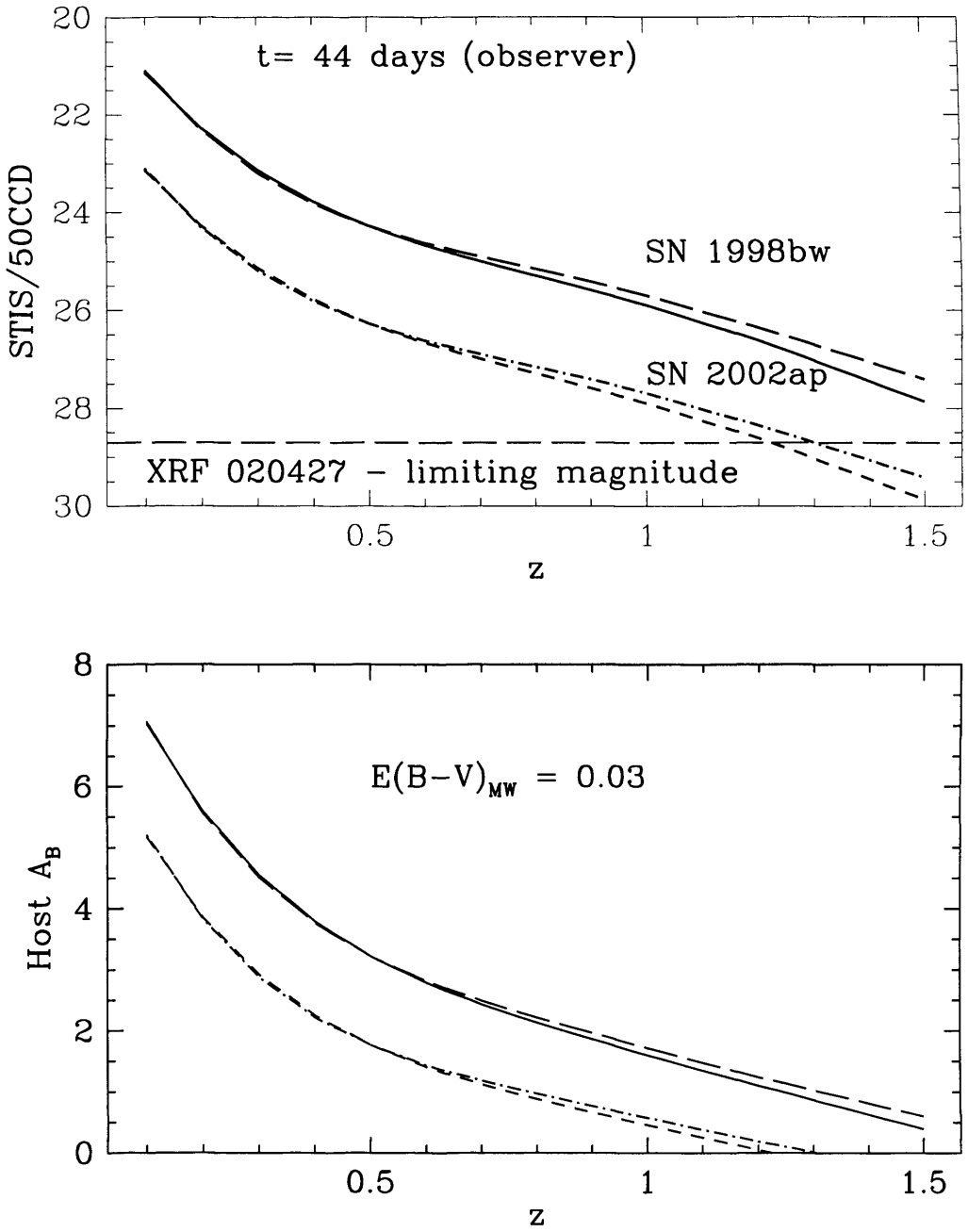

Figure 4.4: As for Figure 4.3, but for the XRF 020427 field. Note the limits shown in each figure (dashed line in the upper panel) are the raw observed limits not corrected for Galactic extinction, since the extinction is considered when the spectra are folded through the instrument response. (i.e. the expected magnitude plotted in the upper panel is that expected for the Galactic extinction relevant for each XRF).

of known redshift XRF afterglows with multi-epoch X-ray imaging is very limited with a possible exception of the still debated GRB/XRF 031203, which exhibits a large X-ray flux as well as a high peak energy (Vaughan et al. 2004; Watson et al. 2004; Sazonov et al. 2004). The fluxes observed for XRF 011030 and 020427 are also similar to the typical GRB fluxes at $z \sim 1$ at similar epochs (see Kouveliotou et al. 2004 for a full discussion of X-ray afterglow properties). For either XRF afterglow, however, to have a luminosity similar to GRB 980425 or GRB/XRF 031203 they would have to be exceptionally close ($z \sim 0.1$); conversely, if placed at redshifts higher than $z \sim 1.5$, they would become among the most intrinsically luminous afterglows yet observed (Kouveliotou et al. 2004).

It is interesting to investigate how off-axis models apply to XRFs. Off-axis models predict that the early X-ray light curves will differ significantly from those of on-axis events. Specifically, the light curves should start substantially fainter and then rise as the core of the on-axis material slows down and comes into the observer's line of sight. An observer at $\theta_{\rm obs} > \theta_0$, where θ_0 is the initial jet opening angle, sees a rising light curve at early times, peaking when the jet Lorentz factor is $\sim 1/\theta_{\rm obs}$, and approaching that seen by an on-axis observer, at later times. Therefore, under this model it would be expected that at the time of the X-ray observations the XRF afterglow luminosities, if located at $z < 1$, should be smaller than those of classical, on-axis GRBs. For XRF 020427 early *BeppoSAX* observations imply that the afterglow decayed approximately monotonically from an early stage, and thus is incompatible with a sharp edge seen off-axis (see e.g. Ramirez-Ruiz & Madau 2004); the lack of early X-ray data for XRF 011030 prevents quantitative conclusions from being drawn. Another possibility for XRF 020427 is that the jet does not have sharp edges but wings of lower energy and Lorentz factor that extend to large θ. Such a picture of the jet is consistent with the relativistic studies of the collapsar model by Zhang, Woosley, & MacFadyen (2003) and Ramirez-Ruiz, Celotti & Rees (2002). The early emission detected by *BeppoSAX* in XRF 020427 would be then produced by material (on the wings) moving in the direction of the observer.

For a dirty fireball or an inefficient shock model the degree of collimation can be similar to that of a GRB, and an XRF can still be viewed directly down the jet-axis. The evolution of the XRF light curve could be similar to that of a classical GRB. Unfortunately the sparse multiwavelength afterglow coverage makes any quantitative analysis in this case unreliable.

GRB host galaxies show a broad range of absolute magnitudes and physical extents (e.g. Hogg & Fruchter 1999; Bloom, Kulkarni & Djorgovski 2002). For both XRF 011030 and 020427 the angular

size and absolute magnitude lie within the range seen for GRB host galaxies across a broad range of redshifts ($0.1 < z < 2.5$). Thus morphological or luminosity information cannot be used to constrain the distances to these galaxies.

There are several explanations can account for the lack of a supernova component, these are discussed in more detail below. The first option is that XRF 011030 and 020427 are accompanied by bright supernovae but lie at $z > 1.2$-1.5. At this redshift XRF 020427 would clearly violate the observed relationship between the peak of the νF_ν spectrum and the square root of the isotropic energy release ($E_p \propto E_{iso}^{1/2}$) reported by Amati et al. (2002), Lloyd-Ronning & Ramirez-Ruiz (2002) and subsequently Lamb et al. (2004) using data from *BeppoSAX*, *BATSE* and *HETE-II*, respectively. Under this scheme the lower peak energies for XRFs naturally result in a smaller isotropic energy, these less energetic explosions could not be seen at such large redshifts, and which would in turn result in a foreshortened distance distribution. To date it has been difficult to extend this relation into the XRF regime (especially at very low $E_p < 10$ keV) since only one XRF has a firmly established redshift (XRF 020903 at $z = 0.25$; Soderberg et al. 2003). However the existence of GRB/XRF 030429 at $z = 2.66$ (Jakobsson et al. 2004; Sakamoto et al. 2004) implies that some outliers do exist, although the E_p = 35 keV for this burst is not sufficiently low to be greatly constraining[‡]. Likewise the E_p limit on XRF 011030 of $E_p < 40$ keV does not provide a strong indicator of redshift. However for XRF 020427 the $E_p < 5$ keV does impose stronger limits. Amati et al. (2004) derive a best fit redshift range of $0.1 < z < 0.2$ for XRF 020427 and they notice that at the maximum allowed redshift ($z < 2.3$ based on the optical spectra of van Dokkum & Bloom 2003) XRF 020427 would not fit the E_p-E_{iso} relation since this would require $E_p > 100$ keV. If at $z > 0.5$, XRF 020427 lies outside the 90 % bounds of the Amati relation, assuming the latter is described by $E_p = 89(E_{iso}/10^{52})^{0.5}$ with a lognormal scatter of 0.3 (Butler et al. 2004). Notably, GRB 980425, also violates this relationship, with a very low E_{iso} and high E_p. In contrast, should XRF 020427 be at higher-z, it would be the most extreme of the outliers with low E_p and high E_{iso}.

Another straightforward explanation would be that these XRFs were not accompanied by a luminous supernova. While this is possible, it is puzzling, given the clear observational evidence for supernovae now seen in many low redshift, long duration GRBs, the possible association of an XRF with a supernova (XRF 030723; Fynbo et al. 2004) and the spectroscopic supernova signatures seen in GRB/XRF 031203.

[‡]Indeed it should be noted that the restframe properties of XRF 030429 would not classify it as a GRB

Further possibilities which can explain *both* a low redshift and the absence of a supernova are, (i) that the afterglows were heavily dust extinguished, (ii) that the associated supernovae were very faint, or (iii) that the supernova and XRF were not temporally coincident in each of these cases. Each of these options is considered in turn.

In the high extinction scenario both afterglow and supernova would not be seen due to the strong absorption of optical light. The colours of their host galaxies, however, imply that they contain little dust. For XRF 020427, this is confirmed by deep K-band imaging of the host galaxy that rules out very red colours; the limit is formally $R - K < 2.5$ (Bloom et al. 2003). The caveat here is that these observations do not probe the line of sight directly to the source of the burst, which could potentially be heavily extinguished. To investigate this possibility the extinction necessary in the host galaxy of each XRF to hide a SN as strong as SN 1998bw and SN 2002ap is plotted in the bottom panel of Figures 4.3 & 4.4. The assumed extinction law here is SMC like (Pei 1993), found to be the best fit to many GRB afterglows (e.g. Jakobsson et al. 2004; Holland et al. 2003). Similarly, the majority of GRBs do not show excessive extinction in their light curves and only GRB 030115 (discussed in the next chapter) has a significant optical dust column. Thus if these two XRFs do demonstrate heavy reddening, then they are very different from the optically bright GRBs.

One way of determining the possible extinction along the line of sight is to measure the hydrogen column density (N_H) from the X-ray data. Each XRF has a relatively low number of counts (see Table 4.1) and, therefore, the limits which can be placed are poorly constrained. However, in each case, the value found was marginally in excess (but consistent with) the Galactic value. The 95 % upper limits on the value of N_H (Galactic + host galaxy) were $\sim 3.5\times10^{21}$ cm^{-2} and $\sim 4\times10^{21}$ cm^{-2} for XRF 011030 and XRF 020427, respectively. Accounting for the Galactic column and using Bohlin et al. (1978) to convert from N_H to A_V, this implies an upper limit on the host galaxy extinction of $A_V < 1.7$ and $A_V < 2.5$ for XRF 011030 and XRF 020427, respectively. These poorly constrained limits are also consistent with zero host galaxy extinction; it should be noted, however, that the conversion between N_H and A_V is sensitive to the assumed dust to gas ratio and is, therefore, somewhat uncertain.

Since the extinction required to remove a supernova signature at low redshift ($z < 0.5$) is very large, and apparently incompatible with the measured dust columns, it is logical to consider if a fainter supernova could explain these observations. Richardson et al. (2002) conducted a survey of the absolute magnitude distributions of all types of supernovae; they found that the faintest SN Ic peaked at ap-

proximately $M_V = -16$. Assuming a similar light curve evolution to SN 1998bw, such a SN would have been visible at $z \sim 1$ with no host galaxy extinction. As the supernova peak light scales linearly with its Nickel yield, a very faint supernova would produce very little Nickel. The faintest local core collapse supernovae are of type II-P (again see Richardson et al. 2002), which approach $M_V \sim -14$; such supernovae would only be seen at low redshifts ($z < 0.5$). It is, however, by no means clear that such supernovae are capable of producing GRBs.

A final option is that the supernova and XRF are not temporally coincident. In the collapsar model (Woosley 1993) the GRB occurs within seconds of the supernova explosion, while other models have suggested that a longer delay could occur between the two events. For example in the supranova model (Vietri and Stella 1998) the GRB can be produced months to years after the SN. However, Long delays are not favored by observations of low redshift GRBs which support simultaneous explosions (Galama et al. 1998; Hjorth et al. 2003; Stanek et al. 2003). At moderate redshifts, the supranova model may be a viable explanation for the lack of supernovae associated with XRF 011030 and 020427, as a supernova occurring a few weeks before the XRFs would not have been detected; at very low redshifts ($z < 0.2$) the delay would have to be over 6 months.

4.5 Conclusions

Deep, multi-epoch *Hubble Space Telescope* observations of the fields of two XRFs have been presented. These observations, reaching depths of $V \sim 28.5$ would be sensitive enough to detect underlying supernovae such as SN 1998bw or SN 2002ap out to $z > 1$ even with moderate host galaxy extinction. At very low redshifts the extinction required to remove the supernova flux is very large, and incompatible with the measured column density in the case of XRF 020427. At higher redshifts XRF 020427 does not fit the E_p - E_{iso} relationship. This situation can be reconciled if the XRFs are situated locally behind large dust absorbing columns, if the supernovae are very faint, or if the SN and XRF are not temporally coincident. A final option is that GRBs and some XRFs do not represent the same physical process, and that they may be due to similar but physically distinct phenomena, where a supernova is not required for the latter.

Part III : GRBs and star formation

Chapter 5

Infrared and Optical Observations of GRB 030115 and its Extremely Red Host Galaxy: Implications for Dark Bursts

5.1 Introduction

Most ground-based GRB afterglow searches are pursued first at optical wavelengths. These have relied on either comparing a newly acquired image to an archival image (normally the Digitized Sky Survey) and locating any new sources, or on performing multi-epoch observations and identifying any variable sources within the GRB error box. In many cases both approaches have been used. Such searches have resulted in the discovery of approximately 60 GRB afterglows with about 50% and 35% being discovered by each of the methods respectively, and $\sim$ 15% being discovered by a combination of the two. One GRB afterglow was found by a colour-colour technique (Rhoads 2001; Gorosabel et al. 2002), exploiting the ability of multi-band observations to distinguish blackbody stellar spectra from the power-law spectra displayed by GRB afterglows.

The advent of small robotic telescopes that can slew automatically in response to GRB alert notices (e.g. ROTSE, Palomar 48-inch and the Liverpool Telescope) has increased the discovery rate of young and bright afterglows. For example, the afterglows of GRB 021004 and GRB 021211 were discovered

only minutes after the GRB trigger (Fox 2002; Fox et al. 2003a,b). These rapid-response campaigns have also substantially decreased the fraction of bursts that have no identified optical counterparts: the so called "dark bursts." Of the GRBs well localised by the Wide X-ray Monitor (WXM) on *HETE-2*, the optical counterpart discovery percentage is $\sim$ 60%, while for bursts localised by the Soft X-Ray Camera (SXC) the discovery rate is $\sim$ 90%, (see, for example, Lamb et al. 2003). There are possible selection effects: relatively bright and soft bursts are more easily localised by the SXC, and these smaller error boxes are easier to search to deep limits. Nevertheless, it appears that the dark burst fraction has decreased significantly from the $\geq$ 70% that was typical during the first few years of GRB observations, when localizations came more slowly and less accurately, from *BeppoSAX* and the Interplanetary Network (see e.g. Fynbo et al. 2001; Lazzati et al. 2002).

The decreasing dark burst fraction strongly implies that many dark bursts can be ascribed to slow alerts and non-optimal search strategies. Indeed, the optical flux limits for many dark bursts are actually above (or consistent with) the extrapolation of the X-ray afterglow into the optical waveband (as discussed in the previous chapter and in Rol et al. 2005). For the relatively small number of bursts that are still apparently "dark" despite deep and early optical limits, a number of plausible explanations have been widely discussed. Among these are:

1. The bursts occur at *very high redshift*. At redshifts, $z > 6$, the Lyman-α break moves through the optical window, making the burst dark to optical CCD observations. At moderately high redshifts, $3 < z < 5$, the burst may appear faint simply due to the large luminosity distance to the burst (e.g. GRB 020124 at $z = 3.20$; Berger et al. 2003; Hjorth et al. 2003b). The current record GRB redshift is $z = 4.5$ for GRB 000131 (Anderson et al. 2000) while the average is approximately $z = 1.1$ (Jakobsson et al. 2004). Furthermore, for several dark GRBs with good radio positions (eg. GRB 970828; Djorgovski et al. 2001) host galaxies have been identified at moderate redshifts ($z \sim 1$), indicating that very high redshift events cannot account for all optically dark GRBs.

2. The bursts occur in *highly obscured environments*, where local dust extinction results in the attenuation of optical photons, while allowing the high-energy X-rays and γ-rays to escape (Groot et al. 1998; Taylor et al. 1998). This might be the case, for example, where the host is a high-redshift ultra-luminous infrared galaxy (ULIRG). Although this explanation may be correct for some bursts, most attempts to fit extinction laws to GRB light curves find that the extinction is

low. If some afterglows are highly extinguished, why are there not more intermediate cases of moderately high extinction, which are still observed in optically detected samples? One complication is that X-ray and EUV radiation from the burst is expected to destroy the dust in the region surrounding the burst for distances up to $\sim 10-100$ pc (Waxman & Draine 2000; Fruchter, Krolik & Rhoads 2001). Such dust destruction may result in a "grey" extinction law, which may have indeed been seen in the SEDs of some bursts (e.g., GRB 010222, Savaglio, Fall, & Fiore 2003).

3. The burst afterglows are *intrinsically faint*, for example because they occur in a low density ambient medium (e.g., Taylor et al. 2000). The brightness of a given afterglow scales with the square root of the particle density (at least in the optical regime, which typically lies below the cooling break energy). Hence bursts occurring in low ambient density environments are expected to be much fainter than those occurring in dense molecular clouds. This is a common explanation for the lack of afterglows to the short GRBs, for which a popular theory is that they are merging compact objects (NS-NS or NS-BH); their relatively long progenitor lifetimes and natal kick velocities indicate that they are likely to be far from their original star-forming molecular cloud by the time they merge.

4. Another option is that the afterglows of dark GRBs simply *fade quickly*, so that they are too faint for optical observations to detect them after several hours. Most GRB afterglows fade as $\sim t^{-1}$ for the first 24 hours, with breaks to t^{-2} occurring hours to days after the burst. Current observations are biased towards locating more slowly fading afterglows, thus a population of more-steeply declining afterglows could remain undetected in many searches (e.g., GRB 021211, which, despite being detected at R= 15, had R>22 after 24 hours Fox et al. 2003; Crew et al. 2003).

Therefore, it is likely that dark bursts represent the manifestation of several physical phenomena. While the first two scenarios above have been used to motivate afterglow searches in the near-infrared, locating afterglows from bursts akin to the third and fourth options can be equally well done by early, deep optical observations.

As the connection between long-duration GRBs and supernovae is now secure (Hjorth et al. 2003; Stanek et al. 2003; Zeh, Klose & Hartmann 2004), it is expected that GRBs point to locations of star formation throughout the Universe. The determination of which of the explanations above is the domi-

nant origin of dark GRBs may thus shed light into the processes of star formation and its evolution. For example, were many dark GRBs genuinely at high redshifts, they would point to strong star formation even at very early ages in the Universe. While if most are actually in obscured environments at lower redshifts they would support models whereby much of the star formation in the Universe is obscured. Moreover, the type of their host galaxies, their environments and relative frequencies may also indicate where much of the star formation occurs.

The discovery and followup of GRB 030115 is presented here. This burst was heavily reddened with respect to a model power law SED and, in the optical, was the faintest GRB afterglow ever observed at similar epochs post-burst. The host galaxy of GRB 030115 lies at moderate redshift ($z \sim 2.5$) and has very red colours (R$-$K $\sim$ 5). It is therefore likely that GRB 030115 was reddened due to high local extinction. Furthermore, there is a significant overdensity of galaxies at the redshift of the GRB host possibly associated with the latter; this putative galaxy cluster is a mix of young, blue, star forming systems and red systems which are either dusty starburst systems or contain an older stellar population. This cluster, if confirmed, is the first associated with a GRB, and one of very few known at $z > 2$.

5.2 Observations

GRB 030115 was detected by the *HETE-2* satellite on 2003 January 15 at 02:44 UT, with a duration of $t_{90} = 17.8$ seconds (Kawai et al. 2003). The burst, classified as an X-ray Rich GRB*, was localised by both the WXM and SXC instruments with error circles of 5 and 2 arcmin radius, respectively. Early optical observations were acquired by several groups using 1-2 m class telescopes. Comparing these images with the Digitized Sky Survey revealed no new objects, placing an early ($\Delta t = t_{\rm obs} - t_0 \approx 2$ hour) limit on the magnitude of the afterglow at $R = 21$ (Castro Tirado et al. 2003; Blake et al. 2003). Data presented here were obtained from the Kitt Peak National Observatory (KPNO) 5 and 9 hours after the GRB in the infrared (J,H,K) bands, comparison of which revealed a fading IR source in all filters (see §5.2.1). Following the announcement of the IR counterpart (Levan et al. 2003), a re-inspection of early optical images obtained at Δt =2 hours revealed a marginal optical detection (Masetti et al. 2003). Further IR observations by Vrba et al. (2003) and Kata et al. (2003) confirmed the fading nature of the object, thus securing its association with GRB 030115. Early radio observations

*see http://space.mit.edu/HETE/Bursts/Data/

at 8.46 GHz (Berger & Frail, 2003) failed to detect the afterglow candidate at Δt =5 hours, specifically recording a flux density of $84 \pm 62 \mu$Jy. However, further observations at Δt =55 hours detected a weak source coincident with that of the afterglow, with a flux level of 94 $\pm$ 22μJy (Frail & Berger 2003). Radio observations were also undertaken at the Westerbork Synthesis Radio Telescope (WSRT) at 3 epochs between 1.5 and 12 days post-burst. Combining these data provided a $\sim 4\sigma$ detection of the radio transient at 4.9 GHz (Rol & Wijers 2003). Sub-millimeter observations were pursued with the SCUBA array on the James Clark Maxwell Telescope (JCMT) at 850 μm (Hoge et al. 2003) and the Max-Planck Millimeter Bolometer (MAMBO) and IRAM 30-m telescope at 1.2 mm (Bertoldi et al. 2003). These placed 3-σ limits at 850 μm and 1.2 mm of 6 mJy and 3 mJy, respectively. While these observations are relatively deep (for afterglow searches), and would have detected the host if it were very bright in the submm (cf., Smail et al. 2002), the few sub-mm detections of GRB host galaxies to-date (e.g., Barnard et al. 2003; Berger et al. 2003; Tanvir et al. 2004) have been at the 3 mJy level (at 850 μm), and so would not have been detected at these limits.

5.2.1 Infrared observations

Observations at the KPNO 2.1 m telescope were undertaken using the SQIID (Simultaneous Quad Infrared Imaging Device) which provides 4 simultaneous colours (J,H,K & L). The sensitivity in the nIR is significantly greater than that in the mid-infrared (L-band) and hence only the J, H and K images were used for analysis. A first epoch of observations was obtained 5 hours after the burst, with a second taken after 9 hours.

A PSF matched image subtraction was performed (using the ISISII code (Alard & Lupton 2000)). This led to the discovery of a transient source, seen to fade in the J, H and K bands. Astrometrically calibrating against the UCAC-2 catalogue provides a celestial position of RA=11:18:32.63, Dec=+15:02:59.9, with a positional accuracy of 0"1. The discovery images are shown in Figure 5.1.

Further IR observations were taken with INGRID at the William Herschel Telescope (WHT), and the NOTCAM on the Nordic Optical Telescope, both sited on La Palma, SOFI on the 3.6 m New Technology Telescope at the European Southern Observatory (ESO) La Silla site (J,H and K-band, 26 hours after burst), and finally at the Very Large Telescope (VLT, UT1) at ESO, Paranal, using the ISAAC array. All of these IR observations were reduced through the ORAC-DR pipeline (Cavanagh et al. 2003).

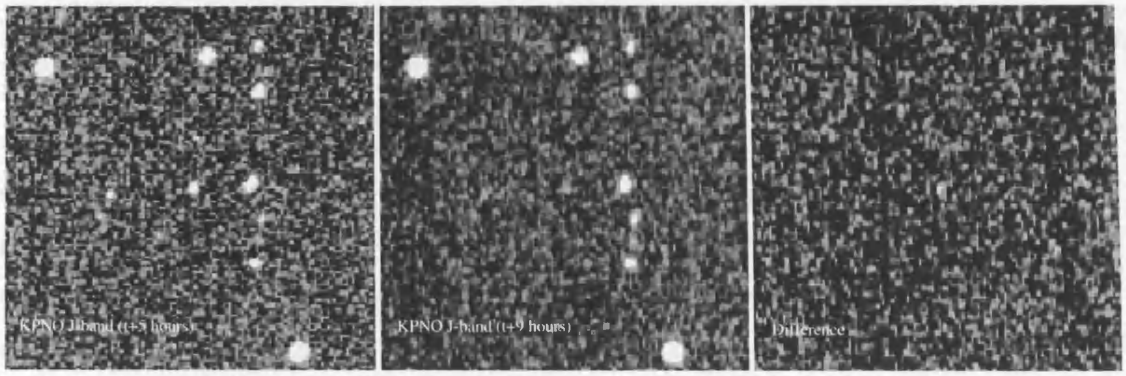

Figure 5.1: The discovery of GRB 030115: The left panel shows an image obtained with KPNO 2.1 + SQIID in the J band 5 hours after burst. The central shows an image obtained in the same configuration after 9 hours, and the right hand panel shows the results of a PSF matched image subtraction, the afterglow is at the centre of the image.

A summary is given in Table 5.1

5.2.2 Optical Observations of the GRB 030115 afterglow

Optical observations of the GRB 030115 error box were performed by several groups. However, these observations failed to reveal any possible candidates in comparison with the Digitized Sky Survey (Castro-Tirado et al. 2003; Masetti et al. 2003; Flaccomio et al. 2003; Lamb et al. 2003). Some of these data were deeper than the DSS and were re-examined once the afterglow position was known. Data obtained from the 1.82m Copernico Telescope at Δt =2 hours in poor seeing ($\sim$ 2.5") contain a weak (4σ) detection of the transient at this epoch from which a magnitude of R= 21.8 $\pm$ 0.3 is determined.

Further optical data were obtained at the VLT using the FORS2 instrument in V, R and I on 2003 January 16 (Δt =26 hours) and in R and I on 2003 January 17, using FORS1. All optical data were processed through IRAF in the usual manner, photometry of the afterglow on the resultant images is shown in table 5.1.

Δ_T (days)	Inst./Filter	seeing (")	mag	F_ν Jy	F_ν (Host Subtracted)
0.11	Asiago/1.82m/R	2.5	21.8 ± 0.3	5.5×10^{-6}	5.3×10^{-6}
0.21	KPNO2.1m/J	1.2	19.19 ± 0.11	3.31×10^{-5}	3.20×10^{-5}
0.21	KPNO2.1m/H	1.2	17.82 ± 0.09	7.52×10^{-5}	7.19×10^{-5}
0.21	KPNO2.1m/K	1.2	16.84 ± 0.05	1.19×10^{-4}	1.14×10^{-4}
0.38	KPNO2.1m/J	1.3	20.47 ± 0.27	1.02×10^{-5}	9.10×10^{-6}
0.38	KPNO2.1m/H	1.3	18.37 ± 0.16	4.53×10^{-5}	4.19×10^{-5}
0.38	KPNO2.1m/K	1.3	17.26 ± 0.08	8.12×10^{-5}	7.65×10^{-5}
1.11	WHT/H	1.3	20.29 ± 0.28	7.44×10^{-6}	4.10×10^{-6}
1.22	NTT/J	0.7	21.12 ± 0.19	5.59×10^{-6}	4.49×10^{-6}
1.23	NTT/H	0.7	20.69 ± 0.31	5.35×10^{-6}	2.01×10^{-6}
1.25	NTT/K	0.7	19.51 ± 0.15	1.02×10^{-5}	5.50×10^{-6}
1.14	VLT/FORS2/I	0.8	23.8 ± 0.20	8.00×10^{-7}	4.02×10^{-7}
1.17	VLT/FORS2/R	0.8	24.5 ± 0.20	5.49×10^{-7}	1.89×10^{-7}
1.21	VLT/FORS2/V	0.8	25.1 ± 0.30	3.88×10^{-7}	1.68×10^{-7}
2.10	NOT/NOTCAM/K	1.0	19.8 ± 0.3	7.24×10^{-6}	2.54×10^{-6}
2.12	VLT/ISAAC/K	0.7	19.8 ± 0.15	7.24×10^{-6}	2.54×10^{-6}
2.20	VLT/FORS1/I	0.8	24.0 ± 0.3	7.24×10^{-7}	-
2.24	VLT/FORS1/R	0.8	25.2 ± 0.4	2.40×10^{-7}	-
GCN data	Kato et al.	2003a,b			
0.86	IRSF/J		20.4 ± 0.2	1.16×10^{-5}	1.05×10^{-5}
0.86	IRSF/H		19.9 ± 0.3	3.90×10^{-5}	3.56×10^{-5}
0.86	IRSF/K		18.5 ± 0.2	2.44×10^{-5}	1.97×10^{-5}
1.96	IRSF/J		21.5 ± 0.5	4.2×10^{-6}	3.10×10^{-6}
1.96	IRSF/H		20.4 ± 0.4	6.7×10^{-6}	3.30×10^{-6}
1.96	IRSF/K		19.1 ± 0.1	1.4×10^{-5}	9.30×10^{-6}

Table 5.1: Table of observations of GRB 030115. Shown is the time since burst of each observation, the measured magnitude, flux and host subtracted flux. For the final two R and I band points, the flux levels are nominally above those measured for the host galaxy, but consistent within the measurement errors. All of the data points are corrected for foreground reddening E(B-V) = 0.024, assuming a MW extinction law.

5.2.3 *HST* observations of the GRB 030115 host galaxy

GRB 030115 was first imaged with the *Hubble Space Telescope (HST)* on 2003 February 10. At this epoch observations were made in F606W (broad V-R) and F814W(I) filters using the Advanced Camera for Surveys (ACS) Wide Field Camera (WFC) as well as in F160W(H) using NICMOS and the NIC3 camera. A second epoch of observations was acquired on 2003 April 24, in F814W(I) and F110W (J) filters. A final set of observations were obtained on 2003 June 16 and 20 in F435W (B) and F222M (K) filters, providing a complete set of B(V-R)IJHK photometry on the host galaxy of GRB 030115. The results of these observations are summarised in table 4.2.

Δt (days)	Inst./Filter	mag	F_ν (Jy)
26.466	*HST*/ACS/F606W	25.58 ± 0.05	2.00×10^{-7}
26.406	*HST*/ACS/F814W	24.83 ± 0.04	4.06×10^{-7}
26.268	*HST*/NICMOS/F160W	22.68 ± 0.08	2.55×10^{-6}
126.193	*HST*/NICMOS/F110W	24.08 ± 0.11	1.10×10^{-6}
127.672	*HST*/ACS/F814W	24.85 ± 0.04	3.98×10^{-7}
151.975	*HST*/ACS/F435W	25.99 ± 0.12	1.37×10^{-7}
156.071	*HST*/NICMOS/F222M	22.21 ± 0.15	4.70×10^{-6}

Table 5.2: *HST* photometry of the host galaxy of GRB 030115. The epoch of the observation (in days since the burst) is shown, as is the camera used and the observed magnitude in the AB-system, the flux which is corresponds to is also shown

The ACS data were calibrated "On-The-Fly" to produce flattened images. They were then drizzled (Fruchter & Hook 2002) onto an output grid with pixels 0.66 times the size of the native ACS pixel (this corresponds to $\sim$ 0.033"). The linear drop size (`pixfrac`) was set to one.

In order to estimate the contribution of the afterglow to the late *HST* observations the two F814W epochs taken at Δt =26 and 127 days respectively were aligned and subtracted. Performing relative astrometry between the VLT/ISAAC image and these images resulted in a position for the afterglow on its host galaxy accurate to $\sim$ 0.05". At this position a 3σ upper limit for the afterglow flux is F814W(AB) = 28.2 (at Δt =26 days). Based on the measured R-band magnitude of $R = 21.8$ at Δt =2 hours and the optical slope of $\alpha = -1.4$ the estimated magnitude of the afterglow would be $I \sim 31$ at the time of this observation and thus the non-detection is in accordance with what would be

RA(°)	Dec(°)	J	H	K
169.65241	15.06268	16.13 ± 0.02	15.63 ± 0.03	15.44 ± 0.10
169.64557	15.05777	15.84 ± 0.03	15.45 ± 0.01	15.36 ± 0.06
169.65432	15.04912	14.79 ± 0.02	14.15 ± 0.02	13.98 ± 0.02
169.61094	15.04204	15.93 ± 0.05	15.44 ± 0.04	15.08 ± 0.06
169.62917	15.03929	15.61 ± 0.05	15.17 ± 0.02	15.13 ± 0.06

Table 5.3: Secondary standard stars in the GRB 030115 field

expected by extrapolation of the early decay. Thus it is safe to conclude that all of the HST observations contain negligible afterglow contamination.

An additional possible cause of contamination could be a possible supernova. Supernovae spectra peak in the optical rest frame, which lies in the IR bands at the favoured redshift of GRB 030115 (see Section 5.3.1). This possibility cannot be tested directly since multi-epoch IR observations at late time do not exist. However, the expected flux even of an extreme event like SN 1998bw at $z \sim 2$ is < 0.05 μJy (F160W(AB) > 27). Therefore, it is highly unlikely that there is any supernova contamination in the IR images.

5.2.4 Photometry and Light Curve

Each of the IR fields was calibrated by the use of secondary standards within the field of view of all telescopes. These stars are listed in Table 5.3. Aperture photometry was performed on the standard stars and the afterglow candidate with the aperture being set to twice the Full Width Half Maximum (FWHM) of the image. The RMS scatter observed in the magnitudes of the standard stars in each of the observations (from that expected and tabulated in Table 5.3) is less than 0.06 magnitudes.

The lightcurve of GRB 030115 in J, H and K is shown in Figure 5.2. Using the first three epochs of data, before host contamination becomes important. The data are best fit with a broken power law with α_1 = 0.7, α_2 =1.8 and a break time between the two decay indices of $t_b \sim 9$ hours (where α_1 and α_2 are the pre, and post-break decay indices, referenced to the time of the burst). The spectral energy distribution of the burst, and its evolution is shown in Figure 5.3.

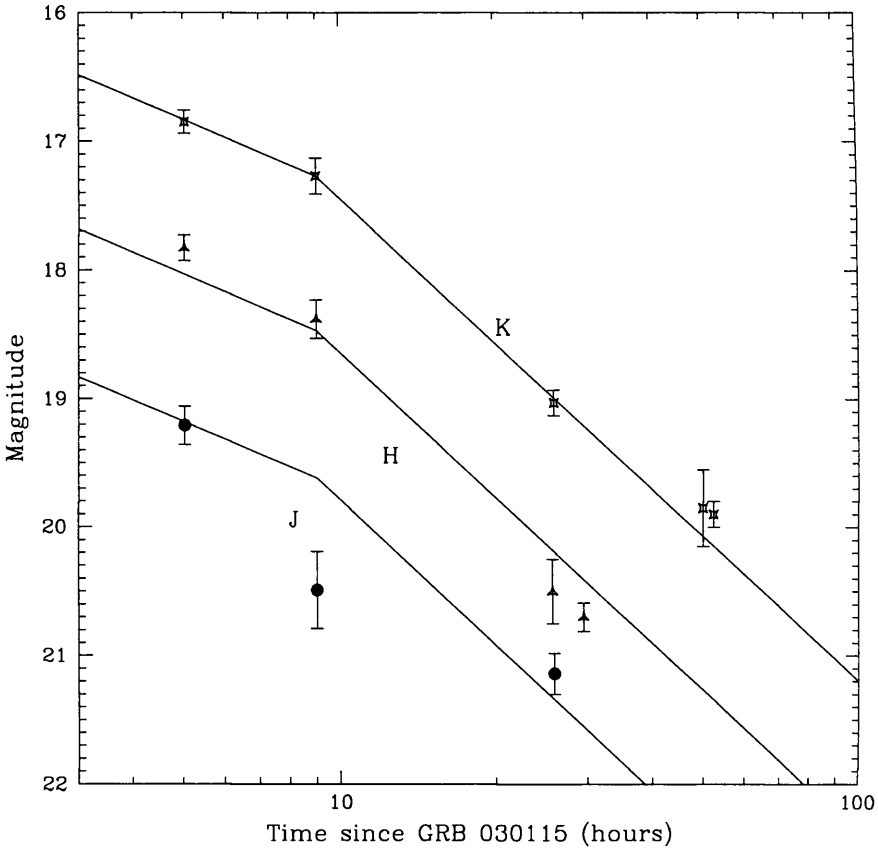

Figure 5.2: The nIR light curve of GRB 030115 in J, H and K. A broken power-law fit is shown and is a good fit to the H and K band light curves. The J band lightcurve does not fit this model due to the Δt =9 hour point.

5.3 The Host Galaxy – Photometric Redshift

The host galaxy of GRB 030115 (Figure 5.4) shows an irregular morphology. The host may be involved in a merger with a companion galaxy offset approximately 1" northeast of the host. The F435W image (the shortest wavelength used in this study) also shows some evidence for an edge-on disk through the host galaxy. Precise ISAAC astrometry shows the position of the afterglow at the southern end of this putative disk, with a positional accuracy of 0.05" (1σ). The host was observed with a complete filter set (B(V-R)IJHK) using both ACS and NICMOS. The results of the photometric analysis are shown in Table 5.2. The host has a very red R-K colour (5.35), far redder than any other GRB host observed to-date. This colour is dominated by a break between the J and H bands of 1.4 magnitudes (AB). It

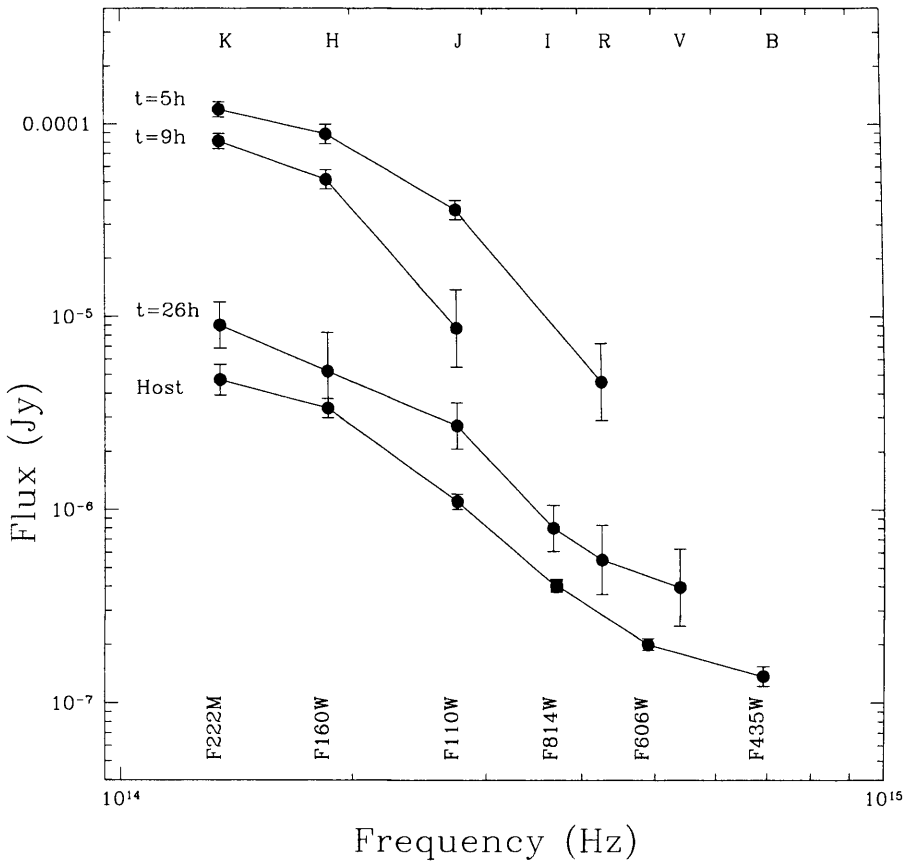

Figure 5.3: The evolution of the spectral energy distribution (SED) of GRB 030115 with time. Marginal evidence of colour evolution can be seen between 5 and 9 hours. However, the reality of this cannot be assessed since it is apparent in only one data point.

is possible that this represents the Balmer (4000 Å) break, which could indicate the presence of an underlying older stellar population, however it is not possible to distinguish unambiguously between a strong break as might be expected from an older population and a very steep slope which could be indicative of a younger, but obscured system.

Knowledge of the redshift of GRB 030115 is essential to our understanding of the afterglow, and hence to the issue of "dark" bursts. Despite attempts from the ground to obtain spectroscopy of the host galaxy, the results were inconclusive. Therefore a photometric redshift fit was attempted based on the available B(V-R)IJHK photometry. This method has the advantage that photometric redshifts are also possible for all other galaxies which fall within the field of view of both the ACS and NICMOS images.

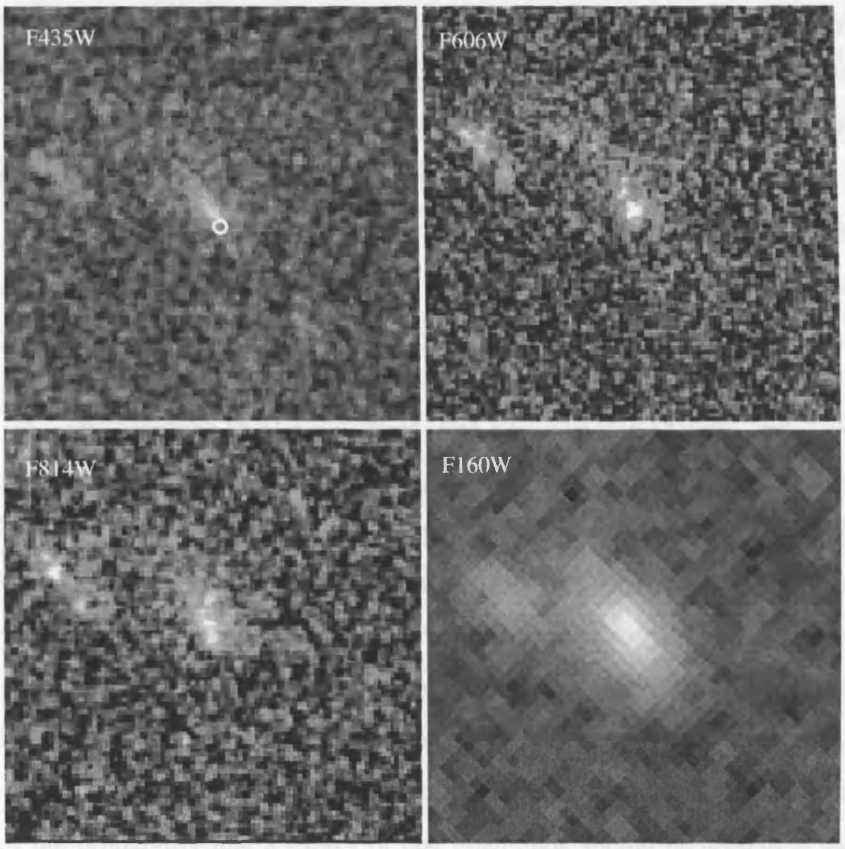

Figure 5.4: The host galaxy of GRB 030115 as seen by *HST* using ACS and NICMOS. The position of the afterglow is marked as a white circle of the F435W image (top left), with the radius of the circle marking the 1σ confidence level. The possibly interacting galaxy can be seen to the upper left (northeast) in each of the images).

The field of view of ACS is much larger than that of NICMOS (200 arcseconds on a side). The total area covered by both NICMOS and ACS observations is 0.51 arcminutes^2. Photometric redshifts were attempted for all galaxies in this region.

Two independent techniques have been used to determine photometric redshifts. The first is the template fitting method of HYPERZ [†]; the second is the Bayesian method of Benítez (2000) [‡]. They are outlined below but for more detail the reader is referred to Benítez (2000) (BPZ) and Bolzonella, Miralles & Pello (2000) (HYPERZ).

[†] see http://webast.ast.obs-mip.fr/hyperz/

[‡] see http://adcam.pha.jhu.edu/~txitxo/bpzdoc.html

HYPERZ is a template fitting photometric redshift code. It provides a maximum likelihood redshift by performing χ^2 fitting of the available photometry with a variety of spectral templates: Starburst (Stb), Elliptical (E), Lenticular (S0), Irregular (Im) and a set of spiral templates of type Sa through Sd. In addition to the photometric redshift and extinction measures it is also possible to obtain an estimate of the age of the stellar population of the host galaxy. It is also possible to vary the Initial Mass Function (IMF), although the affect of different IMFs when applied to GRB host galaxies has been found to be negligible (Gorosabel et al. 2003a,b; Christensen et al. 2004).

The Bayesian code (BPZ) works by making use of other available information information, rather than simply fitting templates. Bayesian techniques in general take advantage of the "a priori" knowledge which exisits before the fit. The probability of a given fit to the data being accepted is then not simply a function of the χ^2 per degree of freedom but of how the data compares to what was expected before to fit is performed. In the case of BPZ these priors take into account our knowledge of the expected physical parameters of galaxies, such as their luminosity function, redshift distributions, and galaxy type fractions. For the GRB 030115 field the prior used was based on the observed luminosity function of the Hubble Deep Field. Therefore, in addition to the template fitting performed by HYPERZ, BPZ also determines the probability that a galaxy of that magnitude should be present at the redshift suggested by the linear fit. This can be effective at clipping "unreasonable" redshifts when template fitting alone finds two or more plausible fits. For example, template fitting alone may find that a galaxy may lie at either $z = 0.1$ or $z = 2$, while the colours of different galaxy types at these two redshifts may be indistinguishable their absolute magnitudes will be very different, thus if the magnitude of the object falls outside a reasonable range based on the observed HDF luminosity function then its probability of being at that redshift is reduced.

Magnitudes for the photometric redshifts were determined by aligning and rebinning all of the ACS and NICMOS data to the same pixel scale, while preserving photometry (this was done via the IRAF tasks *geomap* and *geotran*). A detection mask was defined on the F160W image and extracted magnitudes from the same physical region in other filters. A complete set of photometry is thus obtained to H=25(AB). The ACS images are significantly deeper than those obtained with NICMOS and therefore contain many galaxies which are not contained within the catalogue based on IR detections. However in the absence of IR detections it is not possible to determine accurate photometric redshifts for these galaxies.

Based on these detection criteria, photometric redshifts for the host galaxy were found to be $z = 2.50 \pm 0.20$ for HYPERZ and $z = 2.70 \pm 0.25$ for BPZ. Individually, the best fit redshift of the neighbour was found to be $z = 2.65 \pm 0.30$ based on HYPERZ and $z = 3.0 \pm 0.30$ based on BPZ. The colours of the neighbour galaxy are very blue (F814W-F160W (AB)= 1) and are typical of star forming galaxies containing little dust. The best fitting spectral type of the host galaxy is that of a S0 in HYPERZ (Figure 5.5) and a Sb/c in BPZ. HYPERZ finds that the internal extinction within the host is moderately large $A_V = 1.0$ and that its dominant stellar population is old; 2.6 Gyr. This age determination is largely due to the strength of the Balmer break which lies between the J and H bands at this redshift. If this age determination were correct it would imply a redshift of formation of $z \sim 6.5$. However, this age should be treated with caution, since it has been noted that, for Extreme Red Objects (EROs), the photometric shape alone cannot adequately distinguish between dusty, star forming galaxies and those which harbor an older population of stars (Moustakas et al. 2004).

5.4 Comparison of the host properties with other GRB host galaxies

Given the very red colour of both host and afterglow, it is obviously interesting to compare GRB 030115 with other host galaxies. Chary et al. (2002) and Le Floc'h et al. (2003) have imaged a sample of GRB host galaxies in the IR (K-band). Their measurements allow the determination of the global (R-K) colour of the host galaxies and provide insight into the extinction and star formation rate. A important question relating to the nature of GRB hosts is whether these are typical of high-z galaxies which are selected by other techniques (e.g., sub-mm surveys). These surveys indicate that the majority of high-z star formation ($z \sim 2$) is obscured with a significant fraction likely taking place in galaxies analogous to the lower redshift ULIRGs. The optical counterparts to these sub-mm bright galaxies are often very red, massive systems. By contrast, typical GRB host galaxies are mostly blue and sub-luminous, though the latter may be due to the steep luminosity function of star-forming galaxies (Fruchter et al. 1999; Hogg & Fruchter 2000; Fynbo et al. 2002; Le Floc'h et al. 2003). The R-K colours of GRB host galaxies are therefore apparently distinct from those of the typically red sub-mm emitting galaxies, and the few GRB host galaxies which do show sub-mm emission do not show any significant optical properties to distinguish them from other GRB hosts (Berger et al. 2003). In fact a sub-mm emitter, like the host of the dark GRB 000210, can show low extinction in the optical-nIR having colours typical of the bluest host galaxies (Gorosabel et al. 2003a). The host of GRB 030115 is, however, very red

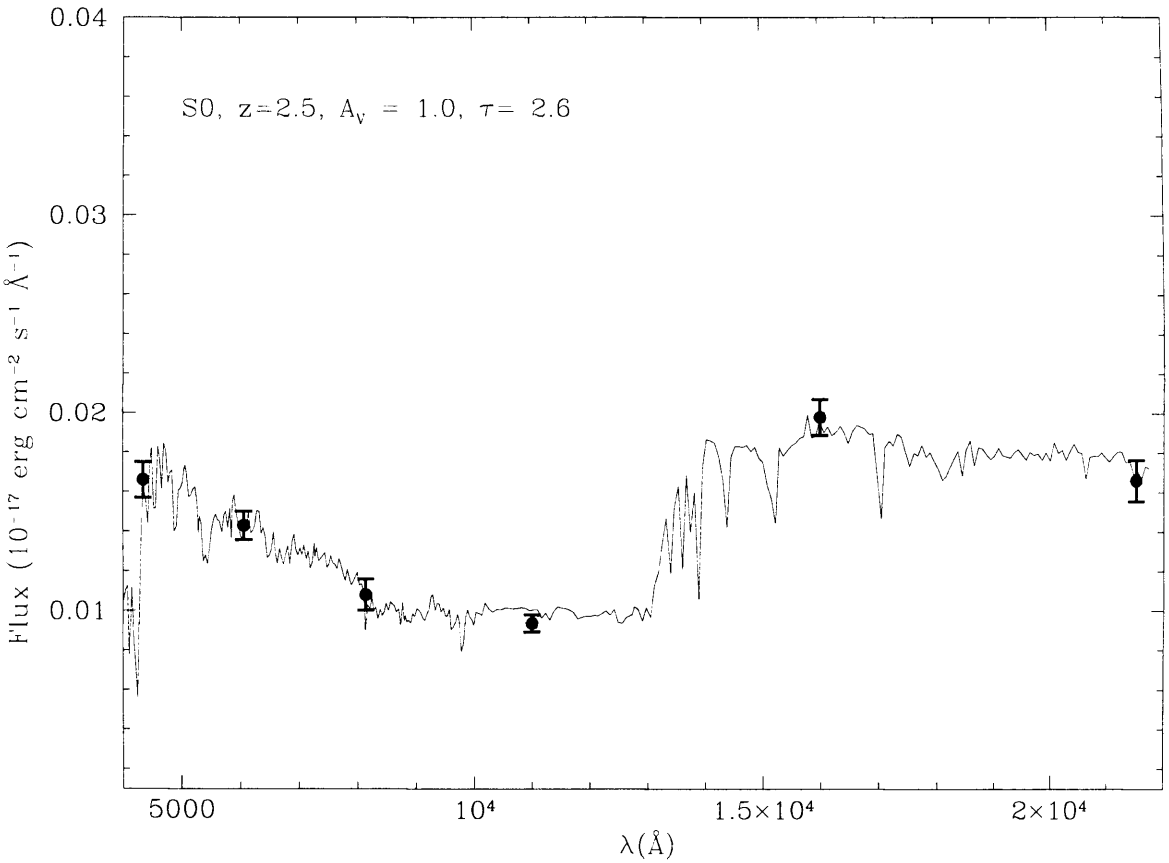

Figure 5.5: The best fitting spectral energy distribution for the host galaxy of GRB 030115, shown as an S0-galaxy at $z = 2.5$, as found by HYPERZ, overlayed are the photometric points from *HST*.

and lies at a redshift comparable to that of many sub-mm sources (which have a median redshift of $z \sim 2.4$; Chapman et al. 2003). Although early sub-mm afterglow observations have only provided an upper limit to the 850 μm flux (Hoge et al. 2003), the depth of these observations would not have been sufficient to detect any other GRB host to-date (Tanvir et al. 2004).

Figure 5.6 shows the R-K colour of the host galaxies of GRBs versus their redshift. K-band data is taken from Le Floc'h et al. (2003) and Chary et al. (2002) (and references therein). The host galaxy of GRB 030115 lies significantly above the curve that represents the majority of the GRB host galaxies. Indeed its spectral type was best fit as an Sc. However, it remains significantly under-luminous in the optical (rest-frame UV) (R* / 8). In contrast it is apparently over-luminous in the K-band (K* $\times$ 4). It is possible that this is due to extinction within the disk of the host galaxy which we may be viewing

edge on. The majority of the optical light produced at the centre of the galaxy could then not escape through the dusty disk of the galaxy, resulting in its red colour.

The absence of a single red sub-mm emitting galaxy from the list of GRB hosts is particularly puzzling given the widespread belief that most of the sub-mm emission from these objects is due to dust heating by massive stars (Le Floc'h et al. 2003; Fynbo et al. 2003). The presence of GRB 030115 within a very red host offers some evidence that a fraction of GRBs are extinguished and come from larger galaxies with red global colours. However, the proportion of bursts which may lie within this class is very poorly constrained so far (see also Klose et al. 2000, 2003). Unfortunately, the faintness of the afterglow GRB 030115 in the optical precluded high-resolution spectroscopic study of the ISM of the host.

5.4.1 Host Galaxy Star Formation Rate and Extinction

At $z \sim 2$ the broadband ACS images cover rest-frame wavelengths of approximately 1550, 2160 and 2900 Å for F435W, F606W and F814W, respectively. From this it was possible to obtain a measure of both the host galaxy extinction and star formation rate.

Star formation measures based purely on the rest-frame UV luminosity are prone to significant errors due to the effects of dust scattering and absorption of UV light. Therefore, measurements without an extinction correction provide only a lower limit on the star formation rate. Using the relation of Kennicutt (1998),

$$\mathrm{SFR}(M_{\odot}\mathrm{yr}^{-1}) = 1.4 \times 10^{-28} L_{\nu}(\mathrm{erg\ s^{-1}\ Hz^{-1}\ (1500\text{-}2800\ \text{Å})}), \tag{5.1}$$

A flux (uncorrected for dust extinction) is obtained of $F_{\nu} = 2.13 \times 10^{-30}$ erg s^{-1} cm^{-2} which, using the standard choice of cosmology, implies a value of $L_{\nu} = 4\pi d_l^2 F_{\nu}/(1+z) = 3.1 \times 10^{28}$ ergs s^{-1} Hz^{-1}. This gives a SFR of 4.4 M$_{\odot}$ yr^{-1}, in the F606W passband.

Given the red colour of the observed afterglow it may be expected that there is significant dust within the host galaxy and, therefore, substantial scattering and absorption of the restframe UV flux. This UV flux is then re-radiated in the far infrared. Meurer, Heckman & Calzetti (1999; hereafter M99) have calibrated this effect for local starburst galaxies and find a strong correlation between restframe ultraviolet spectral slope and the relative flux at 60 μm. Under the assumption that the relation found

for local starbursts holds at higher redshifts (which may be expected, see section 2, M99) it is possible to obtain a better measure of the star formation rate and the extinction within the host galaxy. The relation given in M99 for extinction is

$$A_{1600} = 4.43 + 1.99\beta. \tag{5.2}$$

The relation for spectral slope for $(F606W - F814W)_{AB}$ at redshift z is given by

$$\beta = 3.23(F606W - F814W)_{AB} - 5.22 + 2.66z - 0.545z^2. \tag{5.3}$$

This results in $\beta = 0.44$, corresponding to A_{1600} = 5.3. Correcting the star formation rate for this extinction implies a very large star formation rate of $\sim 500 M_{\odot}$ yr^{-1}.

While this result remains highly uncertain the extreme star formation rate and red colour of the GRB 030115 host galaxy make it the GRB host that is most similar to the sub-mm bright galaxies. Despite this, SCUBA observations have recently failed to find any evidence for sub-mm emission for this host galaxy despite deep 850 μm observations reaching an RMS of <1 mJy (Priddey et al. submitted).

5.5 A possible cluster at $z \sim 2.5$

In addition to obtaining the photometric redshift for GRB 030115, it has also been possible to extract photometric redshifts for other galaxies within the field. The histogram of photometric redshifts determined by HYPERZ is shown in Figure 5.7. All objects shown were detected by SExtractor with a 5σ limit of F160W(AB) =25.0. As can be seen, there exists a strong peak in the redshift distribution at $z = 2.5$, the favoured photometric redshift for the host galaxy using these selection criteria. The RMS of galaxies at redshift $2 < z < 3$ within this fit is ~ 0.12, indicating that there may be an association (such as an edge-on sheet of galaxies) or possibly a cluster at this redshift. The galaxies which form this association are all galaxies with luminosity at, or somewhat larger than, L* (in the H-band). As such only the brightest members are visible, while the more numerous, fainter galaxies are not detected.

In order to quantify the potential significance of this association, it is necessary to determine the level of overdensity which exists at this redshift. To achieve this it is necessary to examine the distribution of redshifts seen in other deep surveys. Few surveys reach the limits obtained here (although most cover a much wider area). The deep surveys used here were the GOODs survey (Giavalisco et al. 2004), the

GRB	R-K (afterglow)	R-K (host)	z	Mag 1 day	Refs
GRB 970228	4.17 ± 0.4*	2.00 ± 0.50	0.69	20.3	Fruchter et al. 1999
GRB 970508	1.96 ± 0.2	2.40 ± 0.60	0.83	21.0	Chary et al. 2002
GRB 970828	Dark	3.60 ± 0.60	0.96	-	Djorgovski et al. 1998
GRB 971214		3.20 ± 0.40	3.42	23.0	Chary et al. 2002
GRB 980613	4.01 ± 0.40	2.10 ± 0.30	1.10	23.1	Chary et al. 2002
GRB 980703	3.10 ± 0.30	2.80 ± 0.30	0.97	21.0	Chary et al. 2002
GRB 981226	Dark	3.40 ± 0.50	-	-	Le Floc'h et al. 2003
GRB 990123	3.01 ± 0.30	2.40 ± 0.80	1.60	20.40	Chary et al. 2002
GRB 990506	Dark	4.05 ± 0.35	1.31	-	Le Floc'h et al. 2003
GRB 990712	-	1.80 ± 0.30	0.43	21.25	Le Floc'h et al. 2003
GRB 991208	2.59 ± 0.3	2.60 ± 0.40	0.71	18.50	Chary et al. 2002
GRB 000210	Dark	2.50 ± 0.30	0.85	-	Le Floc'h et al. 2003
GRB 000418	-	2.50 ± 0.40	1.12	21.90	Bloom et al. 2002
GRB 010111	3.41 ± 0.10	3.75 ± 0.45	-	22.40	Le Floc'h et al. 2003
GRB 010222	2.99 ± 0.3	2.20 ± 0.30	1.48	20.15	Frail et al.
GRB 010921	-	2.40 ± 0.25	0.45	19.29	Price et al. 2002
GRB 030115	6.00 ± 0.4	5.35 ± 0.2	1.7	25.50	This work

Table 5.4: The colours and magnitudes of host galaxies and afterglows of a sample of GRB host galaxies. Also shown is the redshift of the host galaxy and the magnitude at one day (taken from Pian 2001).

Hubble Deep Field North (HDF-N) and South (HDF-S) and the Hubble Ultradeep Field (UDF). For the HDF-N and UDF there is deep NICMOS imaging in F110W and F160W, for the GOODs survey and the HDF-S the IR imaging comes from ground based observatories, mostly deep VLT/ISAAC imaging. The optical imaging in the HDF-N and HDF-S was performed by WFPC2 and in the case of GOODs and the UDF was taken with ACS. In order to confirm the accuracy of the photometric redshifts determined by HYPERZ, fits were performed on each of the photometric catalogues and compared the accuracy with known spectroscopic redshifts (in order that the catalogues are representative of an equally deep survey a magnitude cut was imposed so that the range of magnitude was restricted to F160W(AB) < 25, or H(AB) < 25 (for ground based observations)). The selection of objects in these samples is essentially

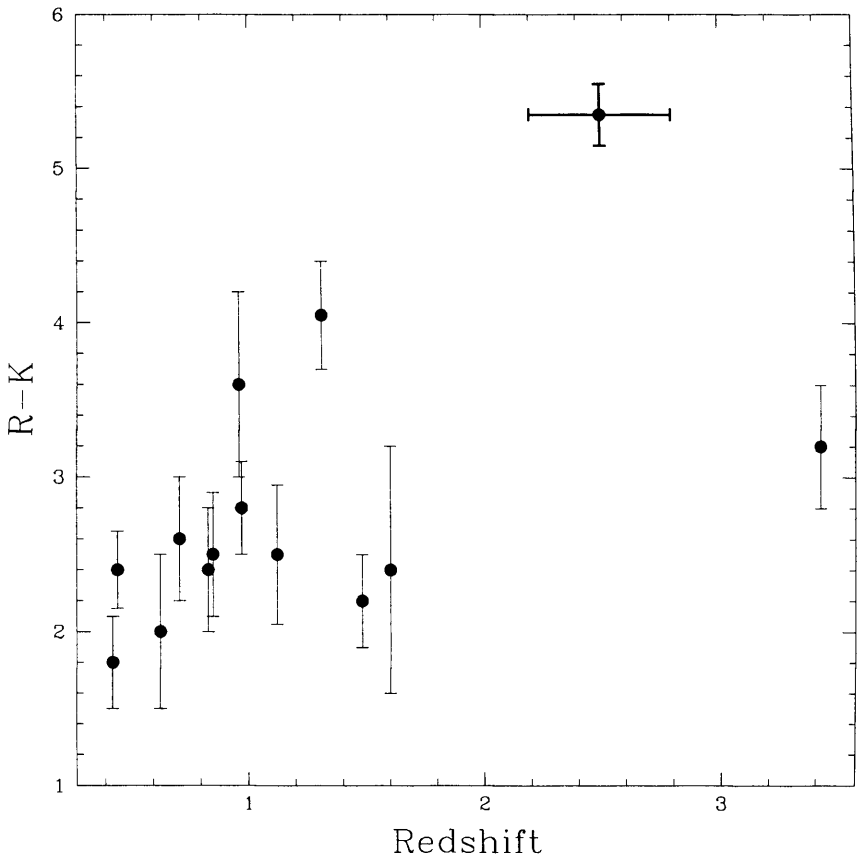

Figure 5.6: The (R-K) colours of GRB host galaxies as a function of redshift (data taken from Le Floc'h et al. 2003), the host of GRB 030115 is shown in bold (with the errorbar in z) it can be seen to lie significantly above the typical R-K colours of GRB hosts.

identical to the sensitivity of the observations of GRB 030115.

A potential problem with the determination of photometric redshifts via the template fitting *only* is that, at times, the redshift is poorly constrained (due often to a very low χ^2/dof ($<< 1$)). This commonly leads to low redshift systems being placed in higher redshift bins. Bayesian techniques can solve this problem by eliminating systems which would be overly luminous at a given redshift (for example an 18th magnitude object may fit well at $z = 0.1$ or $z = 2.5$, but would clearly be excessively luminous were it to genuinely lie at $z = 2.5$, making $z = 0.1$ the more likely redshift). Using BPZ on both the HDF and the GRB 030115 field can help to overcome this problem and does reduce the number of objects lying in the $2 < z < 3$ bin. However, the Bayesian priors used here are based on

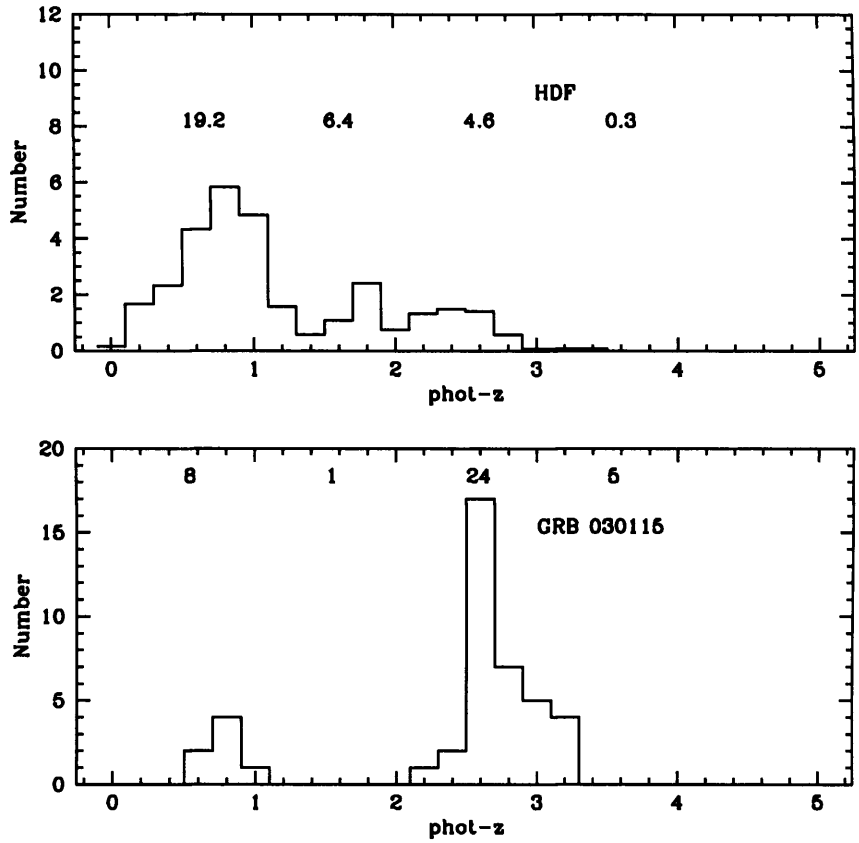

Figure 5.7: Histogram of photometric redshifts for the HDF (top) and the GRB 030115 field (bottom). The HDF photometric redshifts were determined from a catalogue with F160W(AB) < 25 and with the omission of the U-band data. They have been normalised to represent the expected numbers in the GRB 030115 field surveyed. The numbers above each histogram represent the number of objects found to lie in the redshift bins $0 < z < 1$,$1 < z < 2$,$2 < z < 3$ and $3 < z < \infty$ by HYPERZ. The possible biases within this determination are discussed in Section 5.5.

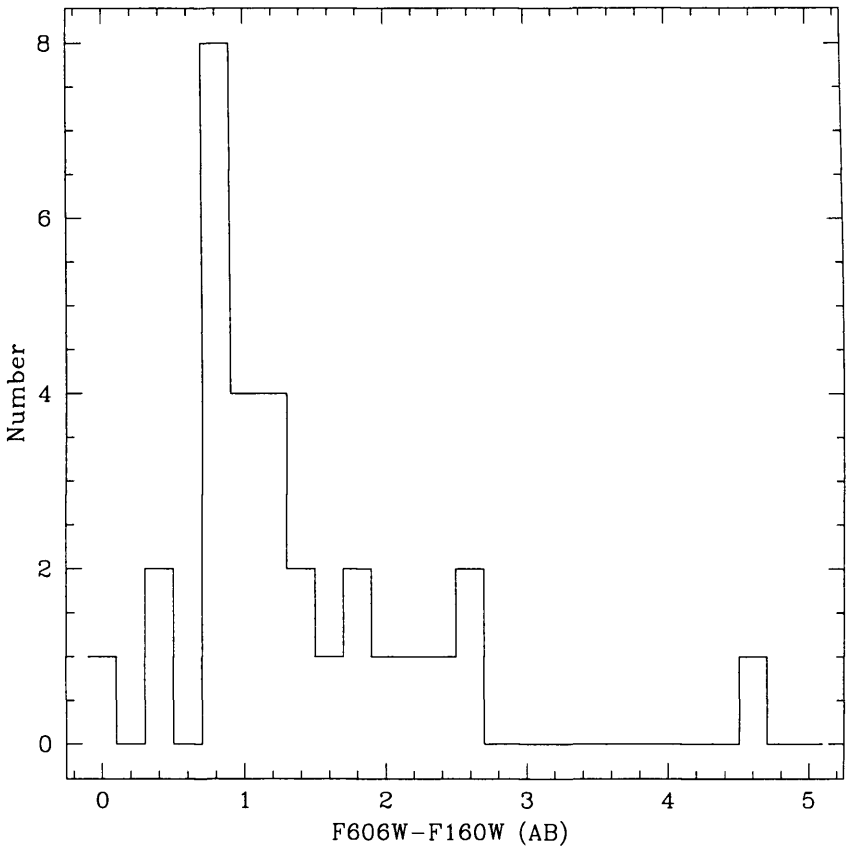

Figure 5.8: Histogram of the colours of possible cluster members for GRB 030115. Although some are very red objects, indicating an older stellar population, many exhibit blue colours (F606W-F160W(AB) = 1), which are typical of star forming systems.

observed luminosity functions of field galaxies, whereas galaxies within clusters may be expected to be more luminous. In practice, using BPZ on the GRB 030115 resulted in 5 objects being moved to a lower redshift bin and a slight broadening of the measured peak. Nonetheless, the apparent overdensity remains, favouring a cluster at the redshift of the GRB host galaxy. Also comparison of the photometric redshifts with the known spectroscopic redshifts in the HDF and the GOODs survey implies that with the choice of filters and limiting magnitudes $< 10\%$ of low redshift galaxies are placed at $z > 2$ by HYPERZ. Thus it is reasonable to conclude that, at most, ~ 20 % of the galaxies placed in the $2 < z < 3$ bin are falsely located. Even if these are removed, there remains a substantial overdensity in the expected number of galaxies at this redshift, and therefore most likely there is a true association at this redshift, possibly a cluster of which the host galaxy of GRB 030115 is a member.

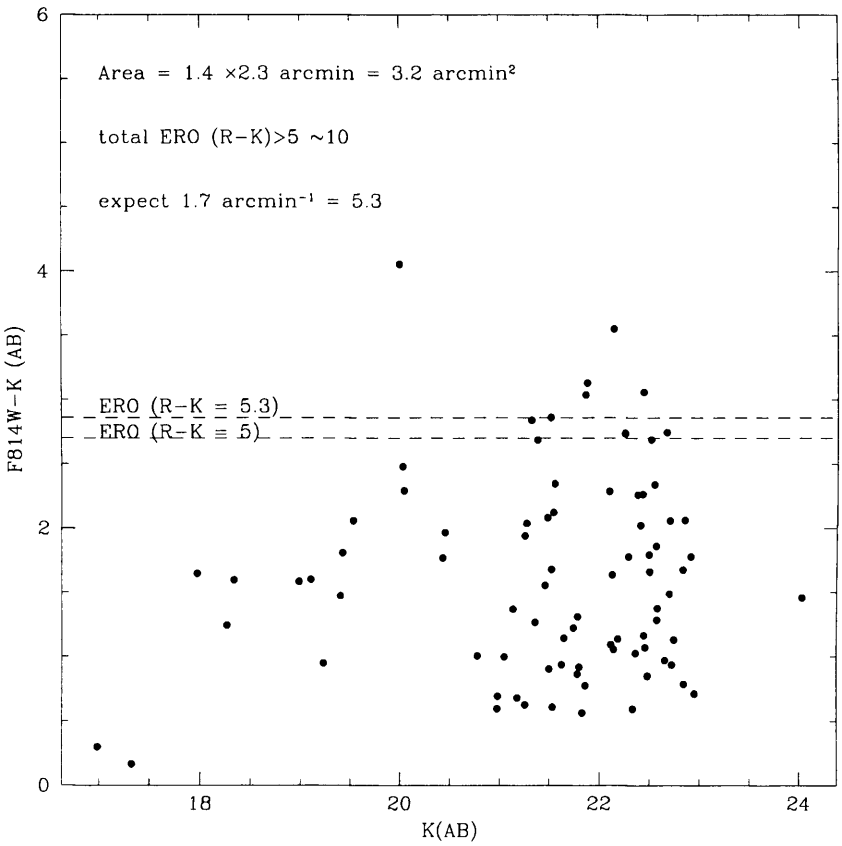

Figure 5.9: The colour magnitude plot for the GRB 030115 field, compiled with a combination of ACS and ISAAC data. The colour cuts which correspond to spectral slopes appropriate for R-K =5 and R-K = 5.35 are shown. Approximately 10 galaxies in this field are EROs to a limiting magnitude of K(AB) = 23, there are also a number of other galaxies with very red (but not extremely red) colours. This is a factor of $\sim$ 2 overdense with respect to EROs studied within the *GOODs* field.

Without spectroscopic redshifts for a number of members, the nature of the structure cannot be determined unambiguously; it is possible that it is a larger scale association with a broad velocity dispersion which is not gravitationally bound. However, should the depth of this overdensity be comparable to its observed width in the *HST* images, then the association would be a cluster which would have evolved by now to a cluster comparable in richness to that of Coma (Somerville 2004).

Figure 5.8 shows the histogram of colours for all galaxies found to lie in the redshift range $2 < z < 3$. While a few can be seen to have red colours comparable to the GRB host galaxy, the majority of the objects have much bluer colours, consistent with their being star-forming galaxies at this redshift. The host itself is typical of what would be expected of a galaxy in the center of a cluster at its redshift: a red and luminous galaxy still forming stars but in the process of evolving into a modern day elliptical.

5.5.1 The number of density of EROs about GRB 030115

EROs are generally defined by a colour limit at around R-K > 5, although various other more stringent cuts e.g. R-K>5.35, R-K>6, are also used[§]. The original definitions for EROs were based on the expected colours of primeval elliptical galaxies (Elston et al. 1988). In practice EROs consist both of old passive systems (Daddi et al. 2000) and dusty star forming galaxies.

The deepest IR image of GRB 030115 is taken in the F160W filter (approximately H-band), while the deepest optical image was obtained at F814W (approximately I-band). These are different from the standard colour cuts used to define EROs however it is possible to ascertain the colours between these two filters that would be expected for a ERO which had R-K>5. These equivalent colours are F814W-F160W > 1.85 (AB), which is an effectively identical spectral slope to R-K=5 in Vega magnitudes. In the approximately 0.5 arcmin^2 surveyed a total of 5 galaxies meeting this criterion are found. Three of these lie within the $z = 2.5$ overdensity with the other two having poor photometry (4 rather than 6 colours with non-detections at F110W and F222M) fitting better at z$\sim$ 0.7, but also having acceptable fits ($\chi^2/dof < 2$) at $z = 2.5$.

[§]The original ERO cuts were based on the observed magnitude of the galaxies when compared to Vega, it is now common (especially when using *HST*) to use AB magnitudes, which compare the magnitude of the galaxy to the magnitude of star which is essentially flat in F_ν. In the optical (V & R) the difference between AB and Vega magnitudes is very small but it is 1.92 magnitudes at K

A larger region surrounding GRB 030115 was also searched by using the ACS image in conjunction with the K-band image obtained with ISAAC. The GRB still contributes some flux in this image and therefore the photometry of the host galaxy is not reliable. Excluding this source, there are $\sim$ 10 EROs within this 3.2 arcmin^2 region to a limit of K<23 (AB). Comparing this with ERO number counts (e.g. Moustakas et al. 2004; Gilbank et al. 2003) indicates that EROs in this field are overdense by a factor $\sim$ 2. In practice using the "average" number of EROs is somewhat misleading since EROs are often highly clustered. Figure 5.9 shows the colour magnitude diagram for the GRB 030115 region.

5.6 Energetics

The observed fluence of GRB 030115 in the 4-40 keV band was 9×10^{-7} ergs cm^{-2}. Assuming a typical GRB spectrum this corresponds to an isotropic energy release of E_{iso} of $\sim 1 \times 10^{53}$ ergs. Fitting the K-band lightcurve with a broken power law reveals evidence for a break at Δt =9 hours from $\alpha_1 = 0.70$ to $\alpha_2 = 1.8$. If this were associated with a jet break then the inferred energy would be 8×10^{50} ergs, consistent with the "standard" GRB energy of 10^{51} ergs (Bloom et al. 2003). However, it should be noted that the inference of a jet break at Δt =9 hours is somewhat uncertain, since the colour changes within the afterglow make the identification of an achromatic break difficult.

The radio afterglow of GRB 030115 was observed at 8.4 GHz and 4.8 GHz (Frail & Berger 2003; Rol et al. 2003). The peak radio luminosity at $z = 2.5$ is $\sim 10^{31}$ ergs s^{-1} Hz^{-1}, typical of GRB afterglows in general (Frail et al. 2004). The decay of the afterglow at 8.46 GHz is broadly in accordance with what would be predicted for the post jet break decay at frequencies below the peak frequency (i.e., $F \propto t^{-1/3}$ between the self-absorption break and peak frequencies $\nu_{sa} < \nu < \nu_m$). ¶

¶The radio data used here can be found at http://www.aoc.nrao.edu/~dfrail/grb_public.shtml

5.7 The origin of the optical faintness of GRB 030115

5.7.1 Extinction

GRB 030115 exhibits an exceptionally red colour ($R - K \approx 6$) but was not at extreme redshift. This is very unusual for GRB afterglows which typically have spectra well described as ν^{-1}, corresponding to $R - K = 2.9$. Furthermore, the colour of the GRB 030115 afterglow is not well defined by a single power-law, but has significant curvature in the spectral energy distribution occurring at shorter wavelengths. The reddening of the afterglow due to extinction within the Milky Way is small, $E(B - V) = 0.024$ (Schlegel, Finkbeiner & Davies 1998), making extinction in the host galaxy the most likely explanation. In order to estimate the extinction along the line of sight to GRB 030115, the afterglow spectral energy distribution was fit with an extinction model of the form $F_\nu = \nu^\beta \times 10^{-0.4A_\nu}$. Thus it was possible to obtain the extinction at a given frequency A_ν based on the fitting models given by Pei (1993), relevant for differing dust to gas ratios and metallicities which are reflected in the MW, LMC and SMC. These fits resulted in unphysical parameters for the afterglow spectrum (namely $\beta > 0$, and $A_V = 4$, with MW-like extinction).

The above measurement could be compromised by several effects. The first is that while the afterglow is bright (and hence the errors small) a truly simultaneous SED is only obtained in three colours (J,H,K) while the R-band data were extrapolated over a factor 2 in time. If the afterglow decay does not behave as a pure power-law (which is quite possible since it now appears that many GRB afterglows exhibit "bumpy" behaviour), then this may be problematic. A further possibility is that of dust destruction local to the GRB. Under many schemes (e.g., Waxman & Draine 2000; Fruchter, Krolik & Rhoads 2001) dust can be destroyed by the prompt X-ray/EUV emission over a distance of several hundred parsecs about the burst site. This dust destruction removes the small grain sizes, leaving the larger ones unaffected and will change the extinction law to one dominated by larger grains (e.g., Maiolino *et al.* 2000). The true extinction along our sight line to the GRB is then the composite of the dust local to the GRB environment and that at larger distances in the host galaxy (which in this case shows evidence of being dusty). The true extinction law may be very different from those which describe sources in the local Universe and this is the likely reason for the poor fit of these laws to the data presented here. A final possibility is that the afterglow spectrum has some intrinsic curvature, most likely due to the cooling break lying in the IR-band at the time of the observation. However, the apparent colour changes

seen in the second epoch are not easily explained as the cooling break, especially since later data are not consistent with this steepened slope.

5.7.2 A dark burst caught?

It is instructive to compare the colours of the host galaxy of GRB 030115 with those of the host galaxies of other GRBs, which typically exhibit blue colours (e.g., Fruchter et al. 1999). Fig. 5.10 shows the R-magnitude of a selection of GRBs plotted against the R−K colour of their host galaxies. While this plot is limited by small number statistics, it can clearly be seen, that of the GRBs detected in the R-band at Δt =24 hours, GRB 030115 is the faintest. It also lies in the most reddened host galaxy. The least squares fit to the data is shown and this does show some correlation between R-K colour and the magnitude of the afterglow at 1 day. However, much power to this fit is provided by GRB 030115 and it is therefore not possible to conclusively demonstrate a real trend whereby dark (faint) GRBs lie in reddened host galaxies.

Fig. 5.11 shows the colours of GRB afterglows, plotted against the colours of their host galaxies. The effective power-law index β is plotted across the broadest range of wavelengths available for an individual burst. This plot shows little evidence for any correlation between host colour and afterglow colour. However, the extreme nature of GRB 030115 can be clearly seen since both afterglow and host galaxy are very red.

The magnitude of GRB 030115 at Δt =24 hours is the faintest GRB ever detected in the optical at this epoch. The magnitude is deeper than the limits placed on many other "dark" GRBs (see Figure. 5.10). This implies that GRB 030115 lies in a region of parameter space which would have been consistent with a dark GRB.

5.8 Conclusions

In this chapter the discovery of the afterglow of GRB 030115 has been reported. Originating from a (photometrically determined) redshift of $\sim$ 2.5, the afterglow was the faintest seen in the R-band after 24 hours. The decay rate was faster than the mean of most GRBs, with an average decay rate over

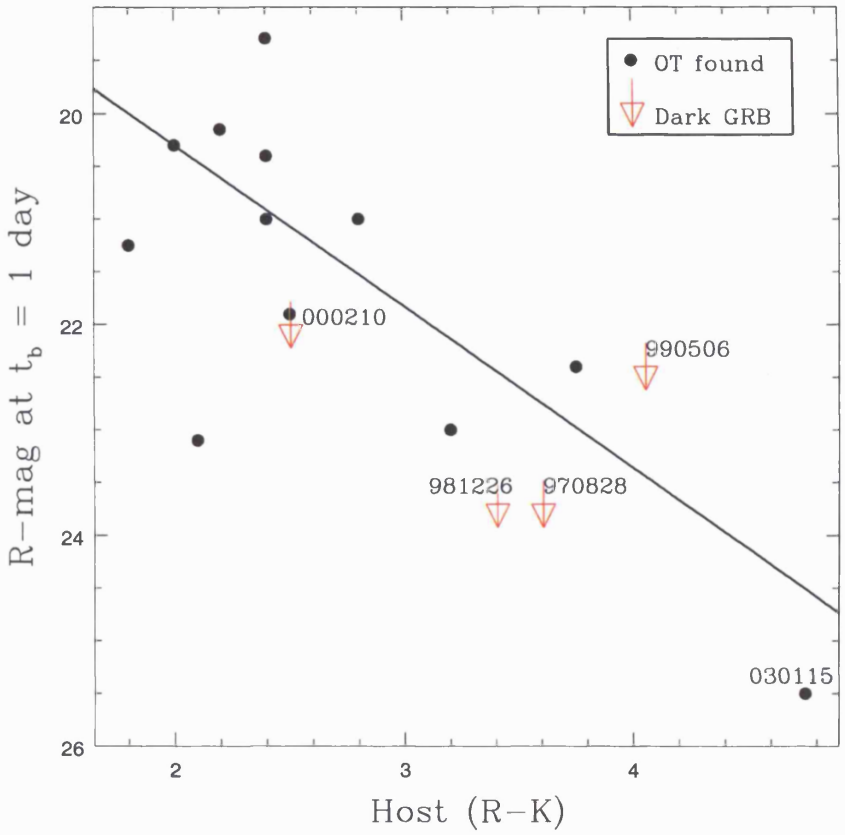

Figure 5.10: The broadband colours of GRB host galaxies (R-K) versus the R-magnitude of their afterglows at Δt =1 day. In cases where observations at 1 day are not available, the magnitude is calculated from an extrapolation of a point near one day, based on the published decay slope for each burst. The red arrows indicate the limits placed on the dark GRBs. The assumed decay law (for extrapolating the limits to Δt =1 day is $\alpha = 1$). The solid line indicates the least squares fit to the data. Only those bursts with solid detections have been used in the fit. The dark bursts are plotted for comparison.

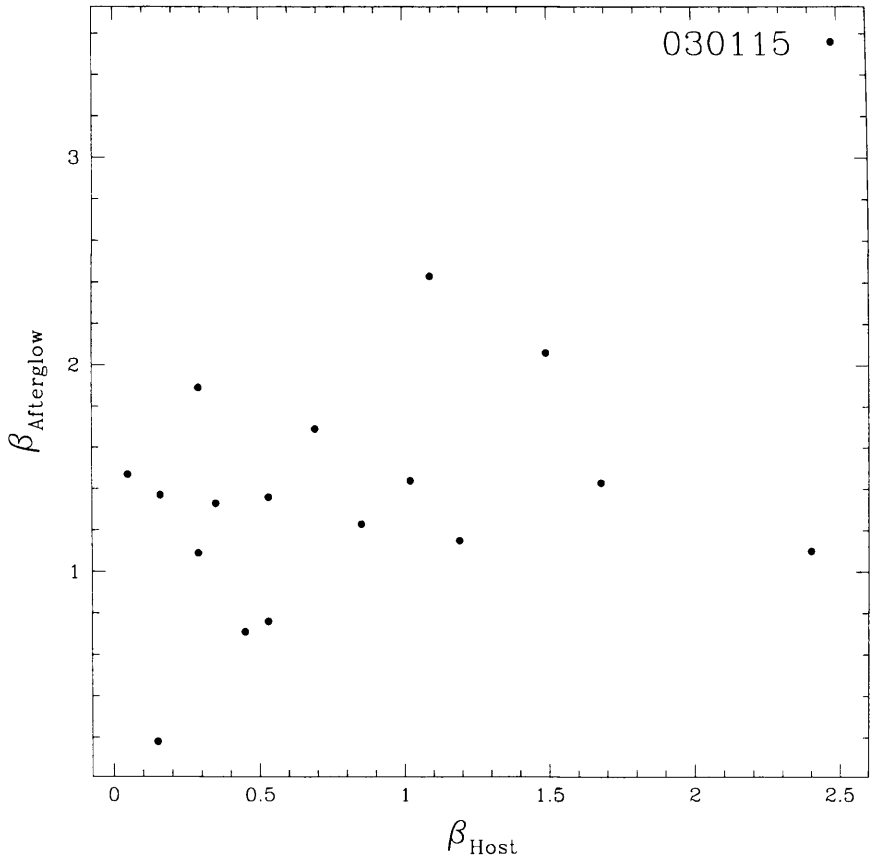

Figure 5.11: The colours of GRB afterglows and their host galaxies, plotted against one another. The determination of β is done on the widest wavelength range available for a given afterglow or host galaxy. In each case the range of wavelengths used for the determination of β is the largest available. In order to ascertain the colours the magnitudes have been normalised to a common epoch using the published values of α_1, α_2 and Δt (the pre and post-break decay slopes, and the time of the break, under the assumption that it is the jet break) and assuming an achromatic evolution. For low redshift afterglows colour information is taken from the early afterglow,where supernovae contamination should not affect the observed colour. For afterglows which are seen to change colour (e.g. GRB 970508 (Galama et al. 1997)), GRB 000301c (Rhoads & Fruchter, 2001) and GRB 030115 (this work) the values are approximate, and are where possible worked out from observations at close epochs.

the first 24 hours of $\alpha \sim 1.5$. The faintness of the afterglow in the optical is, therefore, likely to be a function of both this rapid decline and its extremely red spectrum.

Comparison of both the afterglow and host galaxy with those observed for other GRBs implies that the latter is the most reddened of any GRB host galaxy for which an afterglow has been seen. This is in contrast to some previous cases, where red afterglows have been observed to lie in blue galaxies (e.g. GRB 000418, Klose et al. 2001; Gorosabel et al. 2003). However, none of these afterglows is as extreme as that of GRB 030115, which has a flux density below the upper limits set for the large majority of dark GRBs at similar epochs. Therefore, it may be that some of the dark GRBs so far observed evolved in similar ways to GRB 030115 and were simply missed due to the lack of early IR observations. IR-robotic observations (e.g., REM, Liverpool Telescope) may be very successful at locating such afterglows in the future and will provide valuable statistics on the number of GRBs occurring in obscured galaxies. In turn, these GRB hosts offer a useful tool in characterising the nature of embedded star formation. Indeed, moderate resolution spectroscopy of these sources at early times may be one of the best means of providing a detailed study of the environments of such galaxies, which are too optically faint for normal absorption line studies.

GRB 030115 also lies in a potentially significant overdensity of galaxies at $z \sim 2.5$. This association consists of a high ERO density, consisting of either dust enshrouded star formation or old, passive systems as well as bluer systems with active unobscured star formation. This represents one of the richest associations found at $z > 2$.

Further observations are necessary to confirm the existence of this cluster. Thus far, low-redshift GRBs have been found in field galaxies. However, this may be as much star formation at the current epoch takes place in such systems. Massive elliptical galaxies underwent strong formation at around $z = 2$ (e.g Heavens et al. 2004; Chapman et al. 2004). As GRBs are studied in more detail in the high redshift universe it might be expected that they will be found in clusters, or much richer regions, representing the change in the locations of star formation throughout cosmic history.

Chapter 6

Cosmic Explosions and their Host Galaxies

6.1 Gamma-Ray Bursts and Star Formation

Massive stars burn through their fuel much more rapidly than lower mass systems, ending their lives as supernovae and GRBs while many of the stars around them are still very young. Because of this, supernovae and GRBs can act as beacons for regions of star formation throughout the universe. A crucial goal of modern cosmology has been the determination of the global star formation rate and its evolution with cosmic time (e.g. Madau et al. 1996; Bunker et al. 2004). GRBs have long been cited as a possible means of determining the star formation rate. If they are a truly unbiased tracer of star formation in general, then their rate as a function of redshift, can be used as a simple proxy for the star formation rate, while the galaxy type fractions and luminosity function can be used as a measure of "typical" star forming galaxies in each redshift bin. GRBs may have several crucial advantages as star formation rate indicators. In particular, the prompt γ-ray emission, X-ray and to a lesser extent IR afterglow are largely immune from the effects of host galaxy extinction, thus they can be used to probe star formation in highly obscured environments, where it is thought a significant fraction of star formation occurs at high redshift (e.g. Smail et al. 2002). Secondly the selection function for GRB host galaxies is independent of the host galaxy magnitude, unlike other galaxy samples which are, by necessity, flux limited. However the use of GRBs as star formation probes depends crucially on how well their relationship to star formation is understood.

The resulting question is, of course, are GRBs unbiased tracers of star formation? This question has been addressed by a variety of authors from both a theoretical and observational perspective. However, these studies suffer from significant uncertanties. In particular observational constraints which compare the properties of GRB host galaxies to other high redshift star forming populations such as Lyman-α emitting galaxies, Lyman break galaxies or sub-mm galaxies have to make assumptions about the extent to which these other galaxy populations trace star formation in general, biases which are not well understood. For example studies of Lyman break galaxies indicate that essentially all of the star formation is represented by ultraviolet emission from these objects (e.g. Adelberger & Steidel, 2000), while studies at sub-mm wavelengths imply that the vast majority of high redshift star formation is highly dust obscured (e.g. Blain et al. 1999; Smail et al. 2002). GRBs could potentially remove this uncertainty, since they represent the actual process of stellar collapse and have prompt emission which is immune to dust, but they must be calibrated. So the question is then what sample of galaxies provide a good measure of massive star formation? The host galaxies of core collapse supernovae are this natural comparison. Since it is expected that *all* stars over some mass of around 8 $M_{\odot}$ undergo a supernova explosion, these objects should be ideal tracers of star formation in general. By using all types of core collapse events the sample is clearly including all of these stars, while GRB hosts only probe a subset of them.

This work presented in this chapter investigates the comparative properties of the hosts of core collapse supernovae and GRBs. As well as studying the properties of the galaxies themselves, the distribution of the supernovae and GRBs on their hosts is also investigated. The remarkable result is that GRBs and core collapse supernovae are very different. Supernovae trace the blue light of their host galaxies which are typically grand design spirals, in contrast GRBs are highly concentrated on their host galaxy light and are found preferably in small and sub-luminous systems. This result is best understood in terms of GRBs being restricted to a reduced range of chemical compositions and being favoured in low metallicity environments.

6.2 The sample

A total of forty two GRB host galaxies have been observed with *HST* at various times after outburst. Most of the cameras on the spacecraft have been used to make these observations including STIS,

ACS, WFPC2 and NICMOS (see chapter 2 for further details). *HST* observations are vital to detailed study the host galaxies, since they are typically compact and unresolved by ground based observations and thus only *HST* can easily resolve all of the host galaxies, and therefore allow examination of their morphology and the locations of the GRBs on them. For this work, optical observations were used, corresponding to rest frame blue or ultraviolet light for these high redshift galaxies. This light is primarily produced by young massive stars and so is ideal for investigating ongoing star formation with the host galaxies.

STIS observations contain little colour information, but have a central wavelength comparable to the F606W filter (a broad V-R filter in the Johnson system). Where possible, this filter has been used for observations with WFPC2 or ACS. However, the GRB host galaxies have been imaged by a number of different programmes using different observational setups. Not all of these have used the F606W filter. In these cases images taken in F555W or F775W are used, these correspond roughly to Johnson V and SDSS-I band filters. All of the *HST* data presented here have been reduced via the drizzle algorithm (see chapter 2). The precise values of the `pixfrac` and `scale` parameters were determined by the instrumental response and the number of dither positions available. In general, STIS data are reduced using a `pixfrac` of 0.7 and `scale` 0.5 while ACS and WFPC2 data are reduced using `pixfrac` = 1 and `scale` = 0.66 and 0.71 respectively.

The work presented here is based both on the locations of GRBs on their host galaxies but also on the host galaxies themselves. Studies of the locations require accurate positions (typically smaller than the resolution of the telescope), while studies of the host galaxies only require positions that are accurate enough to locate the host galaxy without ambiguity. Therefore, two sample cuts have been performed. All 42 objects are used for studies of the properties of the host galaxies themselves, while *only* those for which the positional error is < 0.15 arcseconds are used for studies of the position. Astrometry to determine the positions of the GRBs on their host galaxy was performed differentially between the late time images and images taken earlier, when the afterglow was still bright and dominated the host galaxy light (astrometry was performed using the IRAF tasks `geomp` and `geotran`). Where possible, earlier *HST* observations were used, since they allowed the most accurate positions to be determined via direct subtraction of co-aligned images. Measurements of the position of the residual emission in the subtracted images allow the afterglow to be placed on the image with an accuracy of a fraction of a pixel. In other cases ground based images were used, although these normally resulted in larger error boxes. In cases where the projected position of the GRBs on their host galaxies was less accurate that

the PSF of the telescope (i.e. a position error larger than 0.1 arcseconds), the images were convolved with a gaussian mask equal to the difference in resolution between the PSF and error box. This mimics observing the host galaxies at a resolution consistent with the error box size.

A mosaic of the host galaxies of GRBs imaged with HST along with the positions of the GRBs on these hosts is shown in Figure 6.1.

6.3 Supernova host galaxies

Supernovae have not received as much attention as GRBs as possible probes of the star formation rate since they are much fainter, and can typically only be seen out to redshifts of ~ 1. This means that they cannot contribute any information at around $z \sim 2$, where star formation is thought to peak, and certainly cannot be used to pin down the very uncertain star formation rate beyond $z \sim 4$ *. However they can be found in large numbers by deep searches out to $z \sim 1$. Therefore, a comparative study of the properties of low redshift GRBs and supernovae is one of best ways to relate GRBs to star formation.

6.3.1 The GOODS Survey

The Great Observatories Origins Deep Survey (GOODS) was designed to be a deep survey conducted in the Hubble Deep Field North and Chandra Deep Field South. It was a large multi-observatory programme utilising all of the currently flying NASA "great observatories" (*HST, Chandra, Spitzer*). The aims and initial results of the survey are described in Giavalisco et al. (2004, and references therein). By design, each of the *HST* fields was imaged multiple times over the course of a year, resulting in five individual epochs, each separated by ~ 45 days. This strategy was designed to locate type Ia supernovae at $z > 1$, an epoch where cosmic deceleration should be observable (Riess et al. 2004). The discovery of these supernovae and the constraints they put on high redshift supernovae rates and cosmology have been reported by Riess et al. (2004), Strolger et al. (2004) and Dahlen et al. (2004). The selection criteria are described in detail by Strolger et al. (2004). However, as well as discovering a large number of SN Ia the survey also uncovered core collapse supernovae (SN CC)

*Although this is currently the case the detection of high redshift supernovae is one of the primary science goals of the next generation of extremely large ground based telescopes

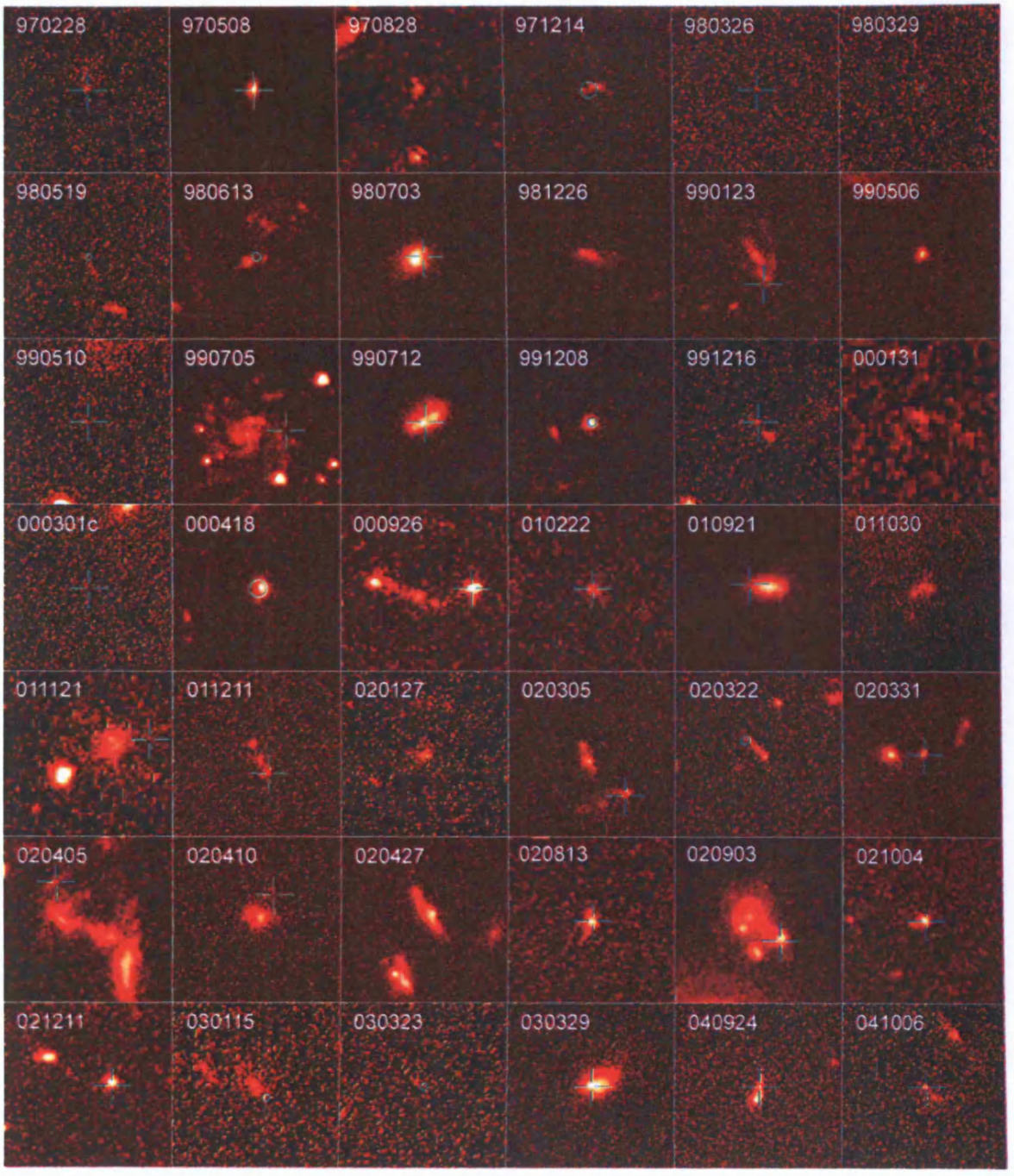

Figure 6.1: A mosiac of all the host galaxies of GRBs which have been observed with HST. Crosses represent bursts which the position of the GRB is know to better than the resolution of the telescope. Circles show the 1σ error in the position in the case that the error is larger than the instrumental resolution but smaller than 0.15". Images without marking are those for which the error in position is small enough to identify a unique host galaxy, but too large to perform studies of the location of the burst within its host.

in approximately equal numbers. Core collapse supernovae were not targeted for intensive followup as was the case for SN Ia's and as such their lightcurves were not, in general, sufficiently well sampled to obtain accurate sub-typing of the supernovae (i.e. into the Ib/c, IIP, IIn subtypes). However, it was possible to accurately distinguish these events as being due to core collapse, since core collapse supernovae exhibit differing colours and lightcurve shapes from SN Ia.

An important aspect of the supernovae selected in this survey is that their selection function is uniform. Local supernova surveys typically target specific galaxy catalogues, thereby biasing the hosts to bright objects. Surveys at higher redshift generally obtain insufficient depth to see core collapse events (which are normally >2 magnitudes fainter than SN Ia) and are also difficult to see against brighter host galaxies. In contrast, *HST* can perform both a deep search at moderate redshift and a search which is not biased by host galaxy luminosity. The invariant PSF of *HST* makes it possible to locate transient objects via the direct subtraction of two or more epochs of imaging and is not significantly affected by the underlying host galaxy light which is accurately subtracted out.

For each of the supernovae observed a redshift estimate is also available and is determined either spectroscopically or by a photometric redshift based on the B(V-R)IZJHK imaging obtained of the field by both *HST* and the ISAAC instrument on the VLT. Photometric redshifts were obtained using the BPZ code, which was described in the previous chapter. Details relating to the redshift determination for these galaxies can be found in Strolger et al. (2004). Figure 6.2 is a mosaic showing the hosts of the core collapse supernovae.

6.4 The positions of GRBs and supernovae on their host galaxies

If GRBs do trace massive star formation then it would be expected that they would trace the blue light within their host galaxies, as has long been expected, though never conclusively demonstrated, for supernovae. However, determining if this is the case can be complex, especially for high redshift galaxies which often have irregular morphologies and are made up of several components. For these galaxies the common astronomical procedure of defining a centroid and then measuring the radial light profile from this location is an imperfect method, since it fails to take into account the irregular morphology of the host galaxies and the "bumpy" distribution of star forming regions.

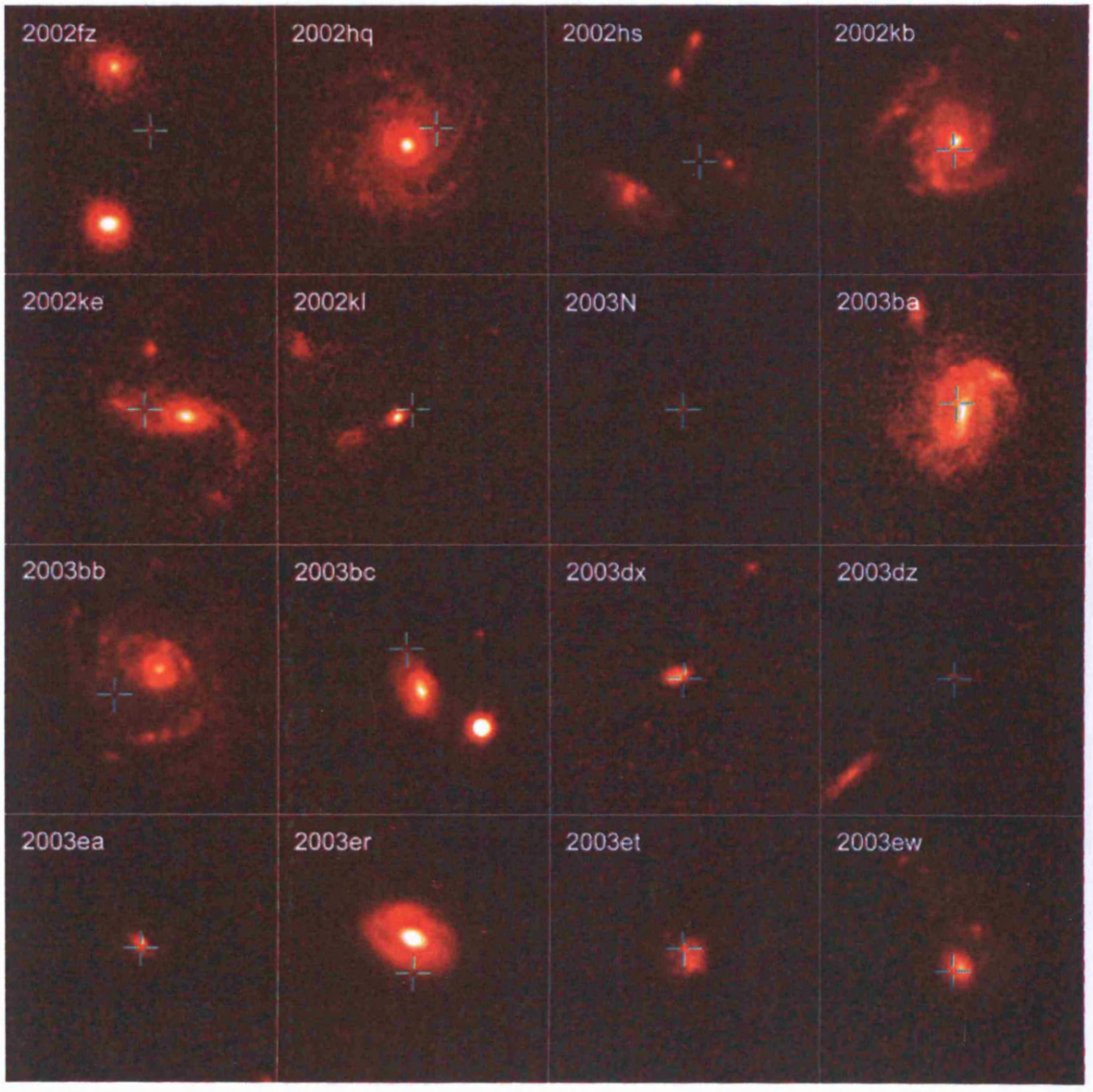

Figure 6.2: The host galaxies of the core collapse supernovae found during the GOODS survey, the supernova name is shown and the location of the SN on its host galaxy is marked with a green cross, in each case the error of the SN position is known to better than a pixel.

To take into account these effects, it was necessary to determine a new method to address this problem. Here, this was done by initially defining the extent of the host galaxy via SExtractor (Bertin & Arnouts 1998). To do this, the galaxy was defined as being a connected set of pixels where the signal to noise within the pixel was > 1. In practice, this is a somewhat conservative approach since it underestimates the true size of the host galaxy. However, since the area not included within the SExtractor masks contains very little light it has a negligible affect on the results presented here. Once the galaxy has been defined, its individual pixels are sorted into ascending order and the fraction of light which lies in pixels of higher and lower surface brightness is measured. This is repeated for each supernova or GRB host galaxy so that the distribution of the positions on the light of the host galaxies is found. This is then tested against the expectation that the probability of finding a GRB or SN in a given pixel is proportional to the light within that pixel (i.e. if the explosions track the distribution of light then the fraction determined by this method should be uniformly distributed between zero and one)

The distribution of both GRBs and SN on the light of their host galaxies is shown in Figure 6.3. As can be seen, the distribution of supernovae essentially tracks the light within their host galaxies while GRBs appear to be more concentrated on the brightest regions of the host galaxies. Formally, the result of a Komoglorov-Smirnov test find that the SN are indistinguishable from the distribution of the underlying light ($P_{KS} = 0.6$) while for GRBs this hypothesis is rejected at high significance ($P_{KS} = 0.001$). Indeed testing the two distributions directly against each other rejects the possibility that they are drawn from the same underlying distribution at a probability of $> 99\%$. This result is robust and shows no dependence of the size or magnitudes of the host galaxies which are used. This implies that the locations of the GRBs within their host galaxies are indeed different to those of core collapse supernovae. This may indicate that GRBs are being caused by the most massive, youngest stars within the galaxy. Young stars are typically located in bright OB associations which can dominate the light of the galaxy, especially if the galaxy is irregular and low luminosity as is common for GRB hosts (an example of this is the Tarantula Nebula in the Large Magellanic Cloud, the birthplace of SN 1987A).

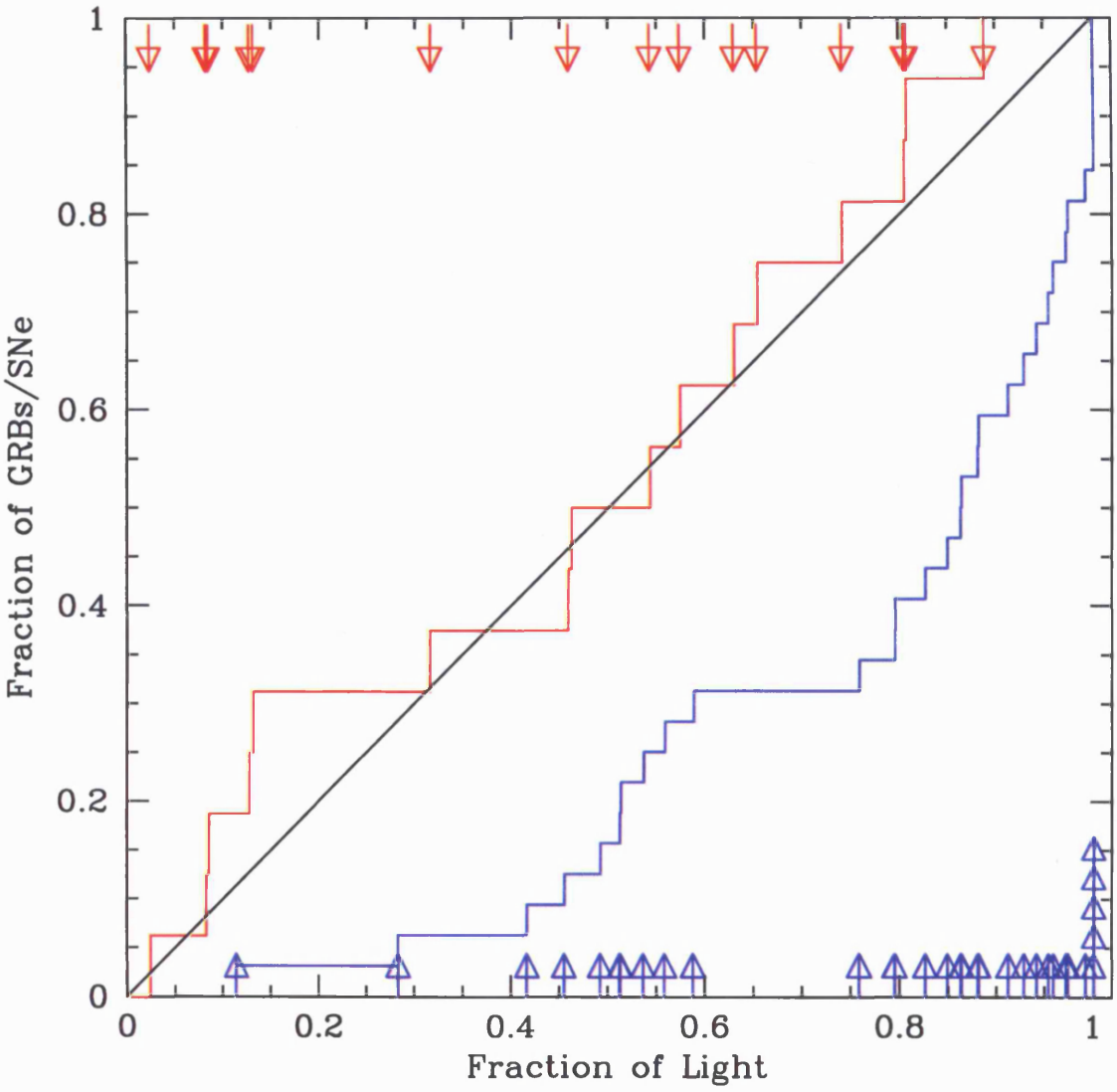

Figure 6.3: The locations of explosions in relation to host light. This figure shows the location of core collapse supernovae (red) and GRBs (blue) with respect to the light of their host galaxies. For each object an arrow indicates the fraction of total host light in pixels fainter than or equal to the light in the pixel at the location of the transient. The cumulative fraction of GRBs or SN found at a given fraction of the total light is shown as a histogram. Were the GRBs and supernovae to track the light identically, their histograms would follow the diagonal line.

6.5 Comparative properties of the hosts of GRBs and supernovae

In addition to comparing the locations of the GRBs and supernovae, it is also instructive to compare the properties of the host galaxies themselves. It is not reasonable to compare the entire population of GRB host galaxies with those of the supernovae since they occupy a much larger range of redshift, where the evolution of the luminosity function may be significant. Therefore, the comparison was performed only with GRB hosts at $z < 1.20$, which produces a mean redshift and standard deviation which is similar for both GRBs and supernovae.

A comparison of the respective galaxy morphologies reveals an immediate difference. The spiral fraction of the supernovae host galaxies is $\sim$ 50%, while for the GRBs only one of 19 host galaxies is a grand design spiral. Although this morphological difference is only marginally significant statistically, it hints at differences in the populations. These can be seen more clearly by investigating the magnitude and size distributions of each of the populations.

Figure 6.4 shows the absolute magnitudes and sizes of both GRB and supernovae host galaxies, including a total of 20 GRB host galaxies and 16 SN hosts, all with known photometric or spectroscopic redshifts. For the magnitude distribution, four GRB hosts have been added that have not been observed with HST but have reliable detections via ground based observations. The absolute magnitudes have been derived from the observed photometry using a standard ΛCDM cosmology with $\Omega_m = 0.27, \Omega_\Lambda = 0.73$ and $H_0 = 71$ km s^{-1} Mpc^{-1}. The magnitudes have also been corrected for foreground extinction, but no K-correction has been assumed. Hence, the observed magnitude is simply corrected for the effects of luminosity distance and band stretching with increasing redshift but has not been corrected for the expected spectrum of the host galaxies (in essence this is assuming a flat spectrum in F_ν).

The figure clearly shows that the host galaxies are different both in their absolute magnitude and size distributions. GRB hosts are both smaller and less luminous that the SN hosts (although size and magnitude are somewhat correlated). Formally a KS test rejects the hypothesis that the two distributions are drawn from the same underlying distribution at levels of $\sim$ 97.5 % and 99.5% for luminosity and size respectively.

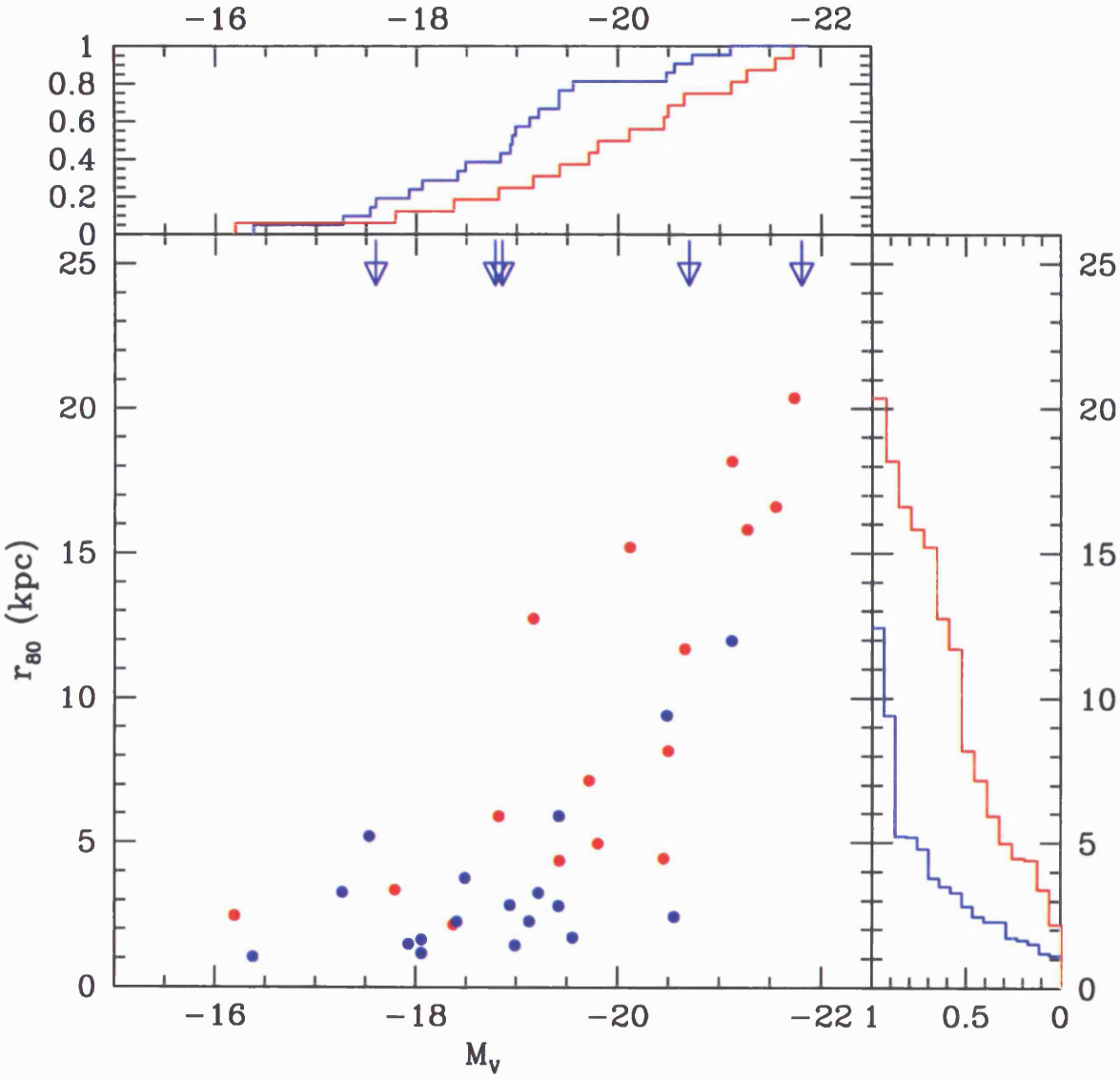

Figure 6.4: Absolute magnitudes and size distributions for the hosts of GRBs and SN: The hosts of GRBs (blue) and supernovae (red) are represented as points in the main panel with absolute magnitudes on the x-axis and the 80% light radii on the y-axis. The plot is then projected onto the two side panels where one dimensional plots of the histograms of the two populations are shown in each of the two dimensions, absolute magnitude and 80% light radius.

6.6 Discussion: Why are GRBs and supernovae different?

Although evidence is now conclusive that GRBs are caused in the catastrophic collapse of massive stars, it is clear from the results presented here that they are not indicative of core collapse in general and, therefore, are not totally unbiased star formation tracers. The host galaxies are both smaller and less luminous than supernovae hosts. However, this alone does not obviously suggest why GRBs should be found in such systems since this is a difference which occurs on an individual stellar scale. The most likely explanation is in fact not related directly to their size or luminosity, but is most likely due to their metallicity or chemical evolution. There exists a well known correlation between the mass of galaxies and their metallicity (e.g. Tremonti et al. 2004), which is perhaps best demonstrated by the decreasing metallicity seen between the Milky Way, the Large Magellanic Cloud and the Small Magellanic Cloud. Therefore, the metallicity of GRB host galaxies is probably much lower than in the supernova hosts and implies that GRBs are preferentially produced in low metallicity environments.

Some other evidence for a low metallicity preference already exists. The hosts of five GRBs (GRB 980325, 990712, 020903, 030329 and 031203) have metallicity measures, and in all cases the metallicity is less than one-third solar. Additionally Lyman-α imaging of GRB host galaxies reveals that they are almost always Lyman-α emitters, whereas Lyman break galaxies at similar redshifts have a Lyman-α emission fraction of only 25% (Fynbo et al. 2003). These photons are easily obscured by any dust which forms in higher metallicity environments and the high rate of Lyman-α emission from GRB host galaxies favours a low metallicity environment.

The production of a GRB is thought to be reliant on three major factors, these are:

1. The formation of a nascent black hole at the core of a massive star
2. Sufficient angular momentum that the envelope of the star cannot collapse directly onto the nascent black hole
3. A baryon free environment that can be penetrated by the relativistic jet. In practice this is represented by the formation of a type Ib/c supernova once the hydrogen envelope has been lost.

The production of GRBs as a function of metallicity can thus be explored, keeping these criteria in mind. Mass loss from massive stars via stellar winds increases with increasing metallicity due to the

photon pressure on their metal rich atmospheres. Massive stars at high metallicity can lose much of their mass prior to their collapse as supernovae. This can inhibit the production of a GRB in two crucial ways. First is that the final mass of the star is often insufficient to form a black hole and a neutron star is formed instead. Secondly, the mass loss extracts not only mass but also angular momentum from the star. The matter, coupled to magnetic field from the star acts as a magnetic break which significantly slows the stars rotation so that upon collapse to a black hole (if one forms) the matter falls directly into the black hole and does not create the torus which is thought to be vital for GRB production.

However, while this explains why GRBs cannot be produced by single massive stars at high metallicity lower metallicity objects can fall foul of the final criterion. At very low metallicity, the star loses none of its outer envelope and, therefore, at the time of core collapse retains its hydrogen envelope, which inhibits the launching of the jet. Hence, single stars at very low metallicity may not create GRBs either. Therefore, it may be the case that GRBs can be formed only over a narrow range of metallicity where the envelope can be lost, but where angular momentum and mass loss do not preclude GRB formation.

It has been suggested that the most probable mechanism for obtaining GRBs is via close binary interactions which both spin up the GRB progenitor and remove its envelope (Izzard, Ramirez-Ruiz & Tout; Podsiadlowski et al. 2004). Under this mechanism, it is possible to remove the outer hydrogen atmosphere of the star via mass transfer or common envelope evolution, while retaining significant angular momentum (since the stars remain tidally locked). It is not entirely obvious why lower metallicity should be especially favoured in this scenario, since full population synthesis calculations of the binary pathways to GRB production remain to be performed.

The low metallicity hypothesis may also explain one of the most puzzling results from studies of GRB hosts. None of the GRB hosts is a red, sub-millimeter bright galaxy. These highly dust enshrouded galaxies at redshifts of $\sim$ 1 -3 are believed to be the site of a large fraction of star formation in the distant universe. While some GRB hosts do show sub-mm emission, this is typically faint and their optical colours are very blue. In contrast, most strong submm galaxies have very red optical colours and are distinct from GRB host galaxies (Berger et al. 2003; Smail et al. 2004). However, these systems typically have higher metallicities since they are both massive and commonly merging which results in greater mixing and a higher metallicity. If GRBs do favour low metallicity environments then it would be expected that they would select against bright sub-mm galaxies, as seems to be observed.

GRB	CAMERA	ABMAG	ERROR	A_{606}	$ABMAG_{corr}$	ARCSEC	KPC	z	SCALE	M_V	F_{light}	ERROR(")
970228	STIS	25.88	0.072	0.62	25.26	0.461	3.26	0.685	7.080	-17.26	-	0.025
970508	STIS	25.19	0.009	0.14	25.05	0.194	1.48	0.84	7.645	-17.92	100	0.007
970828	WFPC2	24.43	0.095	0.10	24.33	0.355	2.82	0.958	7.952	-18.93	-	-
971214	STIS	26.35	0.047	0.05	25.30	0.315	2.36	3.42	7.512	-20.49	53.52	0.150
980326	STIS	29.73	0.199	0.24	29.49	0.078	-	1	8.04	-13.85	100	0.033
980329	STIS	27.25	0.106	0.21	27.04	0.334	-	-	-	-	79.40	0.038
980425	GROUND	15.19	-	0.17	-	-	-	0.0085	0.172	-17.59	-	-
980519	STIS	28.09	0.111	0.77	27.32	0.173	-	-	-	-	84.83	0.052
980613	STIS	25.33	0.029	0.25	25.08	0.456	3.75	1.10	8.216	-18.48	41.56	0.075
980703	STIS	22.91	0.004	0.17	22.74	0.304	2.42	0.97	7.979	-20.55	55.74	0.035
981226	STIS	25.04	0.021	0.06	24.98	0.488	-	-	-	-	-	-
990123	STIS	24.41	0.019	0.14	24.27	0.586	5.01	1.60	8.556	-20.07	11.29	0.005
990506	STIS	25.53	0.015	0.18	25.35	0.182	1.53	1.30	8.439	-18.56	-	-
990510	STIS	28.20	0.129	0.58	27.62	0.205	1.75	1.62	8.557	-16.75	79.36	0.006
990705	STIS	22.78	0.007	0.23	22.55	1.218	9.38	0.86	7.703	-20.47	-	0.028
990712	STIS	22.45	0.003	0.10	22.35	0.404	2.25	0.43	5.582	-19.12	97.14	0.012
991208	STIS	24.60	0.007	0.05	24.55	0.161	1.16	0.71	7.186	-18.05	94.05	0.073
991216	STIS	26.79	0.098	1.80	24.99	0.278	2.25	1.02	8.080	-18.40	82.51	0.030

Table 6.1: Fundamental properties of GRB host galaxies as observed by HST. The table shows the GRB ID (column 1), the camera on HST used to perform the observation (column 2), the magnitude of the host galaxy in the AB-magnitude system, taken at the filter closest to the F606W passband and the associated error (columns 3& 4). Additionally the magnitude corrected for foreground extinction is also shown (columns 5&6). The parameters describing the physical extent of the host galaxy are also shown, including the 80% light radius (column 7) the physical extent this corresponds to (column 8) at the given redshift (column 9) and the scale of the image at the redshift (column 10, in kpc/"). Columns 11 and 12 show the absolute V band magnitude of the host galaxy and the fraction of light which lies in pixels with a lower surface brightness than the pixel containing the GRB.

GRB	CAMERA	ABMAG	ERROR	A_{606}	$ABMAG_{corr}$	ARCSEC	KPC	z	SCALE	M_V	F_{light}	ERROR(")
000131	WFPC2	24.86	0.119	0.10	24.76	0.882	5.93	4.50	6.734	-21.50	49.12	0.100
000210	GROUND	24.22	0.1*	0.05	24.17	-	-	0.85	7.764	-18.83	-	-
000301	STIS	28.90	0.121	0.15	28.75	0.118	1.00	2.03	8.462	-16.07	51.22	0.006
000418	STIS	24.15	0.006	0.10	24.05	0.207	1.70	1.12	8.245	-19.55	45.38	0.150
000911	GROUND	-	-	0.32	-	-	-	1.06	8.183	-18.95	-	-
000926	WFPC2	24.18	0.030	0.08	24.10	1.212	10.25	2.04	8.462	-20.73	100	0.013
010222	WFPC2	25.61	0.089	0.06	25.55	0.337	2.87	1.47	8.531	-18.62	92.72	0.013
010921	WFPC2	22.58	0.012	0.42	22.16	0.482	2.76	0.45	5.733	-19.41	87.94	-
011030	STIS	25.75	0.032	1.18	24.57	0.466	-	-	-	-	-	-
011121	WFPC2	23.23	0.052	1.58	21.65	1.18	5.89	0.36	4.998	-19.41	51.11	0.016
011211	STIS	25.97	0.045	0.12	25.85	0.32	2.69	2.12	8.420	-19.05	95.30	0.006
020124	STIS	-	-	-	-	-	-	3.24	7.649	-	-	-
020305	STIS	25.23	0.032	0.15	25.08	0.030	-	-	-	-	91.10	0.006
020322	STIS	26.50	0.032	0.22	26.28	0.353	-	-	-	-	28.22	0.090
020331	STIS	25.86	0.035	0.24	25.62	0.191	-	-	-	-	100	0.007

Table 6.2: Continuation of the previous table for bursts from Jan 2000 - March 2002)

GRB	CAMERA	ABMAG	ERROR	A_{606}	$ABMAG_{corr}$	ARCSEC	KPC	z	SCALE	M_V	F_{light}	ERROR(")
020405	WFPC2	21.59	0.109	0.17	21.42	1.685	11.96	0.69	7.102	-21.11	58.67	0.010
020410	STIS	27.26	0.067	0.62	26.64	0.237	-	-	-	-	97.30	0.006
020427	STIS	24.61	0.009	0.08	24.53	0.486	-	-	-	-	-	-
020813	ACS	24.46	0.015	0.32	24.14	0.254	2.13	1.25	8.397	-19.69	88.04	0.008
020819	GROUND	19.48	-	-	-	-	-	0.41	5.425	-21.88	-	-
020903	ACS	21.63	-	0.37	21.26	0.372	1.43	0.25	3.876	-18.98	95.77	0.006
021004	ACS	24.63	0.014	0.17	24.46	0.218	1.81	2.33	8.301	-20.63	100	0.006
021211	ACS	25.43	0.018	0.08	25.35	0.202	1.63	1.02	8.080	-18.05	75.76	0.007
030115	ACS	25.58	0.030	0.05	25.53	0.638	-	2.5	-	-	86.30	0.060
030323	ACS	27.28	0.151	0.05	27.23	0.246	1.86	3.37	7.550	-18.53	86.20	0.060
030329	ACS	23.07	0.005	0.07	23.00	0.361	1.03	0.17	2.868	-16.37	99.13	0.006
031203	GROUND	-	-	-	-	-	-	0.105	1.903	-20.73	-	-
040924	ACS	23.93	0.027	0.12	23.81	0.420	3.234	0.859	7.700	-19.21	-	0.013
041006	ACS	25.15	0.061	0.06	25.09	0.720	5.19	0.716	7.210	-17.53	-	0.008

Table 6.3: Continuation of the previous table for bursts from April 2002 - October 2004

SN	ABMAG	ERR	ARCSEC	z	KPC	SCALE	M_V	F_{light}
2002fz	22.34	0.0107	1.531	0.84	11.70	7.645	-20.64	80.6
2002hq	20.93	0.0042	2.368	0.67	16.60	7.014	-21.54	2.2
2002hs	23.25	0.0171	1.632	0.90	12.75	7.812	-19.87	12.9
2002kb	20.54	0.0023	2.4104	0.58	15.82	6.565	-21.61	45.7
2002ke	21.05	0.0068	2.769	0.58	18.17	6.565	-21.10	54.1
2002kl	22.54	0.0056	1.09	0.41	5.91	5.425	-18.82	12.5
2003N	24.61	0.0219	0.66885	0.43	3.73	5.582	-17.09	62.8
2003ba	19.92	0.0008	1.8995	0.29	8.181	4.317	-20.65	88.7
2003bb	21.53	0.0059	2.568	0.95	20.37	7.934	-21.72	8.0
2003bc	21.77	0.0030	0.73865	0.51	4.450	6.147	-20.09	21.4
2003dx	23.26	0.0072	0.3733	0.46	2.167	5.806	-18.36	57.2
2003dz	25.67	0.0489	0.415	0.48	2.47	5.947	-16.18	46.0
2003ea	24.01	0.0104	0.56355	0.89	4.38	7.786	-19.42	65.2
2003er	21.24	0.0024	1.04305	0.63	7.16	6.826	-19.70	8.3
2003et	22.98	0.0086	0.653	0.83	4.97	7.614	-19.79	80.3
2003ew	21.97	0.0139	2.182	0.66	15.21	6.969	-20.10	74.0

Table 6.4: Properties of the host galaxies of core collapse supernovae found in the GOODS search. The SN name (column 1), AB-magnitude and error in the F606W (columns 2&3), 80% light radius (column 4), redshift (column 5) physical scale (column 6) and relative scale at that redshift (column 7) are also shown. Columns 8&9 show the V-band absolute magnitude and the fraction of light which lies in pixels with a lower surface brightness than the pixel containing the SN.

6.7 Conclusions

This chapter has presented the first results from a detailed analysis of the host galaxies of core collapse supernovae and long duration GRBs. Surprisingly, they are found to be very different, both in terms of the locations of the GRBs and supernovae on their host galaxies and in the intrinsic properties of the host galaxies themselves. This result implies that GRBs are imperfect star formation indicators and that they trace, at best, only a fraction of massive stars in the universe. The most likely explanation for the observed differences between these two populations is that GRBs are caused only by the collapse of the most massive and low metallicity stars. The most massive stars are likely to be most strongly clustered on the light of their host galaxies and go hand in hand with very young stellar populations. Furthermore, the low luminosity of the GRB host galaxies implies that they probably have a low mass and, therefore, lie at the low end of the known relationship between galaxy mass and metallicity. This low metallicity apparently increases the GRB rate.

It should be noted that there should be some overlap between the two samples that are used. Since GRBs are caused by some form of core collapse supernovae, it is clear that the two categories cannot be mutually exclusive. As it was not possible to further divide the core collapse supernova used here then it is likely that some of these SN are of type Ib/c, possibly even the high velocity variety . However as type Ib/c supernovae form less than 25% of observed core collapse supernovae, this overlap is most likely not significant. It is further likely that even when the beaming of GRBs is considered that not every type Ib/c supernova creates a GRB (something which the results reported here provide evidence for). Ultimately, the comparison of the locations of different subtypes of core collapse supernovae with the light of their host galaxies and the host galaxies themselves will enable the study of each type of supernova and its relationship to massive star formation.

Although these results imply that GRBs are imperfect star formation rate indicators they should not be ignored as probes of high redshift star formation. Firstly, they clearly do relate to star formation in some form. But while they may require moderately low metallicity it is not exceptionally low (i.e. it is $\sim Z_{\odot}/3$ or so). At higher redshifts the typical metallicity, even for more massive systems decreases. Therefore, at the highest redshifts GRBs may once again become unbiased tracers of star formation.

Chapter 7

Conclusions and Future Prospects

7.1 The current status of GRB astronomy

GRB astronomy is, at least from a multiwavelength perspective, a very new science. It is not yet 10 years since the first afterglow was discovered and the pace of progress has been phenomenal, with significant changes in the state of knowledge taking place over the timeframe on which this thesis has been completed. It has now been well established that GRBs lie in star forming galaxies at cosmological distances and that the long duration bursts are associated with the collapse of massive stars in a hydrogen deficient type Ic supernova. It has become clear that during this collapse the rapidly rotating massive star launches highly relativistic jets, which are the source of the GRB but illuminate only a small fraction of the sky. The shock created when this jet interacts with the medium around the star sets up a synchrotron spectrum which is the observed afterglow to the burst. The luminosity of this afterglow is exceptionally large and can be seen at very high redshifts, while the imprinted signature of the host galaxy and intergalactic medium can be used to probe the chemical composition of high redshift galaxies in unprecedented detail.

Throughout this thesis the connection between GRBs, supernovae and star formation has been investigated. This has been attempted via a multi-faceted approach making use of many of the techniques which allow constraints on the GRB environment to be made. This includes studying the properties of the associated supernovae; looking at the signature of the burst environment imprinted upon the after-

glow, studying the locations of bursts within their host galaxies and the galaxies themselves. The key results from each aspect of this work are summarised here.

7.2 Gamma-Ray Bursts, X-ray Flashes and Supernovae

Studies of the supernovae associated with GRBs have been presented in chapters 3 and 4. This work demonstrates that a variety of supernova properties can be seen in GRBs. A "standard" to which all GRB SN are compared is SN 1998bw, which was the first supernova to be associated with a GRB. It was a type Ic supernova, a subtype of core collapse supernovae which show no discernible hydrogen, helium or silicon lines in their spectra. This supernova subtype are most likely caused by the final collapse of a Wolf-Rayet star and this has now become the favoured progenitor for long duration GRBs. However, SN 1998bw was far from normal, even amongst this extreme brand of supernovae. It was exceptionally bright (about 10 times as bright as the typical SN Ic) and also had very high velocity ejecta, making it one of the most unusual supernovae seen. Indeed, its energy release was an order of magnitude larger than is typical for a supernova and has led to the suggestion of the name "hypernovae" to describe such highly energetic events. However, the work presented in chapter 3 demonstrates that not all supernovae associated with GRBs are so extreme.

The supernova associated with GRB 020410 had $z \sim 0.5$ and $M_V \sim -17$, approximately a factor of 10 fainter than SN 1998bw and comparable to the mean magnitudes of type Ic supernovae. This result was amongst the first to demonstrate that supernovae associated with GRBs are far from standard candles and showed significant breadth is possible in the luminosity function. Indeed, results published subsequent to this analysis have confirmed this result and demonstrate that the supernovae associated with GRBs span at least a factor 10 in absolute magnitude and are largely consistent with being drawn from the general luminosity function of SN Ic's (Soderberg et al. 2005a).

Furthermore GRB 020410 was the first optical GRB signature to be discovered by an orbiting observatory (although this has now become more routine with the launch of *Swift*). After initial ground based searches had failed to find any afterglow, the *HST* observations instead located the peak of the supernova emission, making GRB 020410 one of very few bursts that have been discovered purely by the contribution of supernova light. That the faint supernova could be seen, and easily distinguished from the afterglow component, relied on the fact that for this burst the afterglow was faint. For brighter

GRBs the contrast between afterglow and supernova would be significantly lower, making accurate identification difficult. It is possible that similar faint supernovae could be hidden in the afterglows of many bright GRBs.

The origin of the X-ray Flashes, and their relationship to GRBs has been one of the key questions of GRB astronomy over the last few years. The strongest link between GRBs and XRFs would naturally be made if they could also be associated with core collapse supernovae, and thus directly linked with the same class of progenitor. Indeed, if XRFs do typically lie at lower redshifts as is suggested by their prompt emission properties, then it should be relatively straightforward to locate the associated supernovae since all supernovae have spectral shapes which peak at around 6000 Å . Therefore they are best studied at low redshift. A search for such supernovae is presented in chapter 4, where deep *HST* imaging taken in two epochs is used to search for variability associated with the supernova. Intriguingly no signatures are found to very deep limits (R> 28th magnitude). Supernovae such as SN 1998bw would have been visible out to z$\sim$ 1.5 in searches to this depth, while even faint SN should be visible to z$\sim$1. There are various possible explanations for the absence of signatures to these XRFs without recourse to a scenario in which the SN are truly not present (the old adage that "absence of evidence is not evidence of absence"). Briefly summarised these explanations are:

That the bursts lie at higher redshift than is suggested by the properties of their prompt X-ray and γ-ray emission, implying that the empirical relationship whereby the total energy release E_{iso} scales with the square of the peak energy of the νF_ν spectrum is incorrect.

The bursts may lie behind significant dust columns, effectively blocking all optical light. This is possible although it is interesting to note that very few GRB afterglows show such high columns. However it is possible that GRBs effectively destroy dust for many parsecs around their birth sight (e.g. Draine 2000; Fruchter, Krolik & Rhoads 2001). XRFs are significantly less luminous and therefore may not be such effective destroyers of dust, thus increasing the obscured fraction compared to GRBs.

These bursts may not be associated with supernovae, or at least with supernovae which occur close in time to the burst. Under some models for the production of GRBs there can be a significant delay (of several months) between the supernova and the GRB, if this were the case then, while still associated with core collapse no supernova signatures would be seen in XRFs.

Following the search presented in chapter 4, Soderberg et al. (2005b) have presented a similar search for

supernovae in the afterglows of four further XRFs. They find evidence for a supernova signature in only one case (XRF 020903 at $z = 0.25$). Although the limits to which they search are marginally shallower than those reported in chapter 4, the most constraining non-detection is achieved for XRF 040701 which has a known redshift of $z = 0.22$. The low redshift of this system implies that supernova signatures should be readily visible. However, none was seen to deep limits, implying that (in the absence of extinction) the supernova associated with this XRF is fainter than any known SN Ic. Further observations of XRFs, especially those with known redshift will help explain this result. As well as searching for supernova signatures in these high redshift events it is also important that more nearby supernovae are also studied. There is an inherent bias against finding faint supernovae, since they may fall below the detection limit of the instrument, or be invisible due to the small contrast between SN and host galaxy. Therefore, the faint end of the luminosity function is poorly constrained. Ongoing, deep, unbiased supernova searches (i.e. those which scan a large area of the sky and do not target specific galaxies) are perhaps the best means of addressing this issue.

7.3 Dust and decay: Gamma-Rays bursts from dusty host galaxies

Chapter 5 presents an in depth study of the afterglow of GRB 030115. The properties of this burst are in sharp contrast to those of most GRBs observed to date. The burst is one of very few which show significant evidence for extinction in their afterglow spectrum and was highly reddened, exhibiting and $R - K$ colour of 6 while most afterglows have $R - K < 3$. Followup of the afterglow at late times showed that it also originated from a very red host galaxy, the first GRB host galaxy to be categorised as an Extremely Red Object (ERO).

The identification of the very red afterglow has important implications for the nature of dark bursts. These bursts, undetected at optical wavelengths may be representations of a large number of physical processes, including dust obstruction, high redshift or an intrinsically broad luminosity function. GRB 030115 is a clear demonstration that at least a subset of these dark bursts are due to dust extinction in host galaxies at moderate redshift. Locating these afterglows is important if an unbiased sample of GRBs is to be collected, and the host galaxy of the burst provides an important demonstration of this.

The host, like the afterglow which originated from it is very red, most unlike GRB hosts in general. Indeed its optical/IR properties are similar to those of the sub-mm bright galaxies, which are thought to

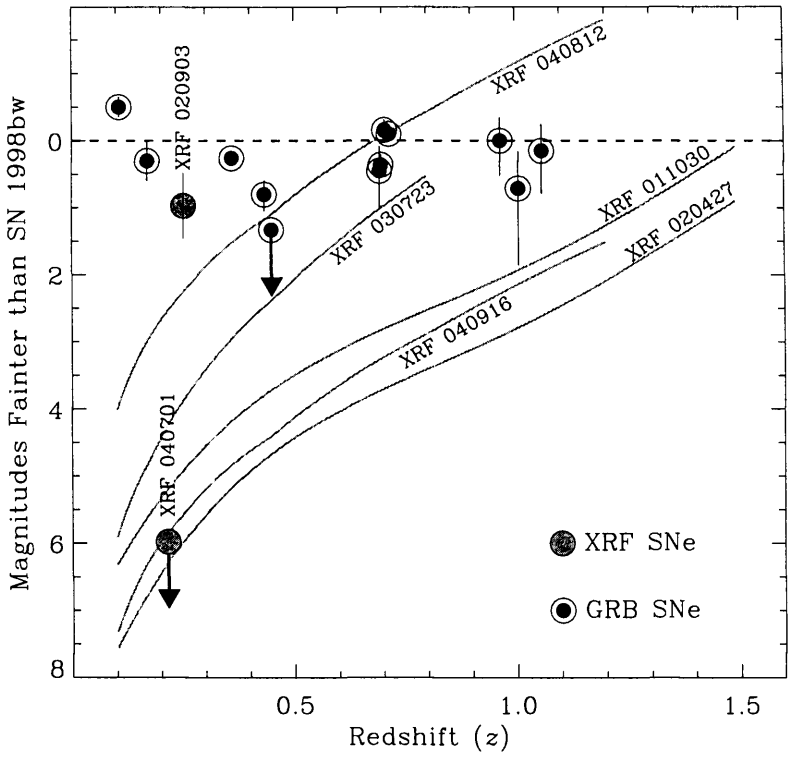

Figure 7.1: The luminosity function of XRF supernovae, taken from Soderberg et al. 2005. The plot shows the relative peak magnitude of supernovae in GRBs and XRF relative to the prototype SN 1998bw. The limits on XRF 011030 and 020427 which were derived in chapter 2 are shown.

be dusty, high redshift starbursts that host a significant fraction of high redshift star formation. These galaxies are typically much redder than GRB hosts, only a few of which show sub-mm emission and none of which is a bright sub-mm galaxy. Therefore it is natural to ask whether GRBs naturally select against these galaxies or if observational biases bar their detection since their optical afterglows may be heavily extinguished. A single object such as GRB 030115 cannot answer this question directly (especially since the host galaxies of several bursts which were invisible at optical wavelengths show very blue colours). However, it does imply that the range of host galaxy properties may be wider than had previously been thought.

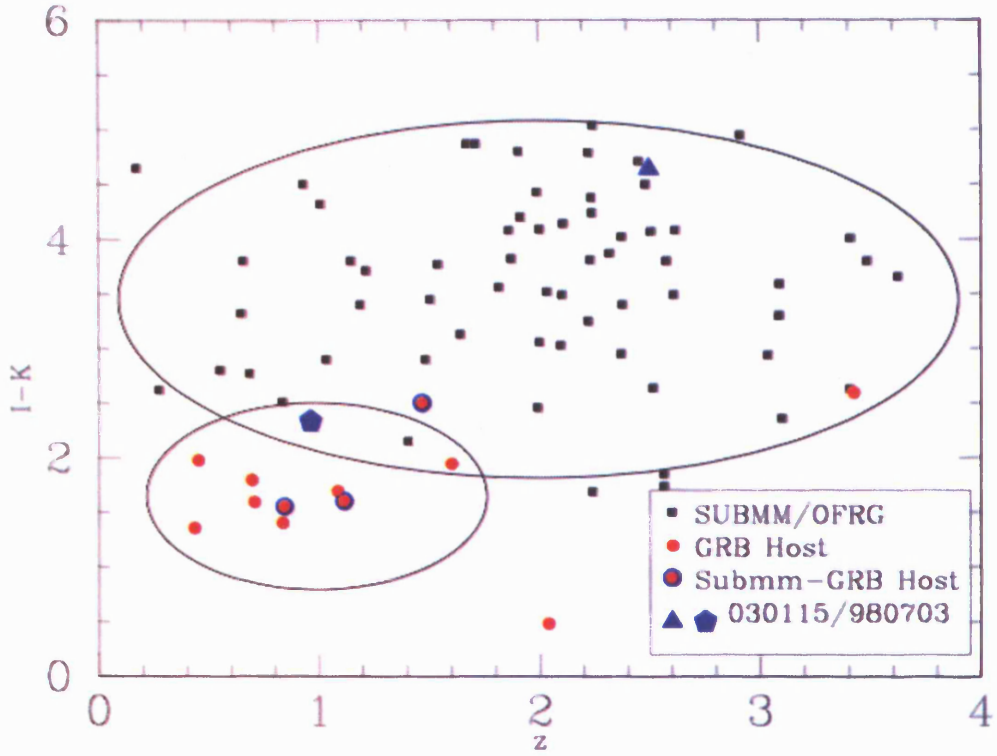

Figure 7.2: Compartive redshifts and colours for GRB host galaxies sub-mm emitters and optically faint radio galaxies (galaxies whose star formation is seen at radio wavelengths). Although the GRBs to date have a slightly lower mean redshift than the sub-mm emitters it can clearly be seen that they are, in general significantly bluer. The red dots indicate the GRB host galaxies while those which are ringed in blue are also detected (albeit faintly) at sub-mm wavelengths. The host of GRB 980703 is undetected at submm wavelengths but its star formation signature is seen in the radio. In contrast the host of GRB 030115 is the only host galaxy to show strong red colours, but is undetected in the sub-mm to deep limits (Priddey et al. in prep).

7.4 How do GRBs relate to massive star formation?

Finally a detailed study and comparison of the host galaxies of core collapse supernovae (SN II and SNIb/c) and GRBs is presented, with the aim of understanding the connection of GRBs to star formation in general. Since core collapse supernovae are formed via the final collapse of all stars with initial main sequences masses of $> 8\ M_{\odot}$ their host galaxies should be indicative of all of star formation. GRBs on the other hand form only hydrogen deficient supernovae, and their dependence on the local environment is not understood.

The comparison between the host galaxies is two-faceted. The first aspect is to investigate the distribution of the GRBs and supernovae on the light of their hosts while the second is to study the relative properties of the hosts themselves. These analyses show clearly that GRBs are occurring in different environments. Firstly, GRBs are very concentrated on the brightest regions of the host galaxies, while supernovae essentially trace the blue light within their hosts. Furthermore the host galaxies of GRBs are more compact and less luminous than those of supernovae. These two results imply strongly that GRBs only trace a small fraction of massive star formation and can be understood in terms of two effects.

The first is that GRBs are most likely caused by the collapse of the most massive O and B stars. These stars naturally clump together to form massive, luminous associations which are the likely birth-sights for GRBs. These OB associations are strong UV emitters and can frequently be the most luminous UV objects seen in galaxies.

The second result is more puzzling, since it is not immediately obvious why GRB hosts should be significantly different to those of supernovae, since their production depends on the evolution of a single star and not of a galactic population. However, more luminous high mass galaxies are known to have higher metallicities than lower mass systems and therefore it is most likely the differences observed are indicative of the differing chemical evolution of the two galaxy populations. Low metallicity has previously been suggested as being important to the production of GRBs, although many of the studies which have found this have been largely theoretical. Hence, the direct demonstration that GRBs require lower metallicities than supernovae provides an important observational constraint and implies that GRBs may be common in the high redshift universe, where the global metallicity is lower.

7.5 The Future

Until now GRB science has been largely opportunistic. The number of GRBs discovered has been small, and each burst has been studied as being interesting in its own right. It has so far been impossible to isolate specific sub-samples of bursts and obtain large, statistically uniform datasets. So while it has been possible to make great progress in our understanding of GRBs there remains much work to do.

7.5.1 Swift

The launch of *Swift* in November 2004 was pivotal to this endeavour. It carries γ-ray, X-ray and optical instruments which allow it to detect not only the prompt emission from the GRB itself but also the X-ray, and in some cases optical afterglow. *Swift's* Burst Alert Telescope (BAT) is the most sensitive wide field γ-ray detector yet flown (marginally more sensitive than BATSE) and so can detect many more bursts than *HETE-2* or *BeppoSAX*. This has already enabled an order of magnitude increase in the number of bursts discovered. However the crucial advantage of *Swift* is not simply its ability to deliver a larger sample of bursts but also that it is capable of delivering more accurate positions for the bursts. Positions from the BAT (or indeed the most accurate positions available from *INTEGRAL, HETE-2* and *BeppoSAX*) normally have an associated error radius of a few (3-5) arcminutes. However *Swift's* X-ray Telescope (XRT) can deliver positions accurate to 5 arcseconds*. This is not based on the prompt emission but rather the bright early emission from the afterglow. *Swift* can slew across the sky to point at the location of bursts detected by the BAT on a timescale of <100s enabling positions for the GRBs to be precisely defined so that large aperture ground based telescopes can easily search for the afterglow (a decrease from a 5 arcminute error box to a 5 arcsecond error box is a decrease in the area of sky that much be searched of 3600!). This enables deep searches for the afterglow to be carried out much more rapidly, increasing the probability that the afterglow will be found and a redshift established for the burst. This combination will enable statistical studies of a uniformly selected sample of bursts to be made for the first time, as well as answering some critical questions. The most pressing current questions are discussed below although, as the mission evolves it is possible, or even likely, that these will evolve.

**Swift* also contains a UV and Optical Camera (UVOT) which can deliver arcsecond positions for bright afterglows, however since many *Swift* bursts are faint it has not yet detected a large number of bursts

7.5.2 How does the GRB rate relate to metallicity?

Although the work presented here has, along with other recent work clearly demonstrated that GRBs are not perfect tracers of star formation it is still not clear precisely how their rate depends on metallicity, or if the properties of the bursts themselves can somehow be related to the burst environment. The simple problem here is that GRB host galaxies are very faint, and therefore difficult to study in detail. Although they are strong emission line objects the emission lines which are commonly used as metallicity measures for low redshift galaxies (H-alpha, [NII]) are often in the IR and not readily studied. It is crucial that accurate metallicity measures be secured for as many GRB hosts as possible, either via the hosts directly or via absorption line measurements in afterglow spectra. Additionally similar measures need to be made on an unbiased sample of supernova host galaxies (such as those found in GOODS) so that a meaningful comparison can be made.

Furthermore, although the evidence to date indicates that GRBs strongly prefer low metallicity environments, the selection function remains complex. As demonstrated by GRB 030115 not all GRB host galaxies are sub-luminous and blue and whether or not GRB 030115 is genuinely an outlier or represents a previously unrecognised population of hosts must be understood. Rapid IR observations of *Swift* bursts that will be undertaken at a number of observatories (e.g. the Liverpool Telescope and UKIRT) will be highly important in this respect.

7.5.3 What is the nature of the GRB host galaxies?

Although much progress has been made towards understanding GRB hosts via observations from the optical to sub-mm (and even in some cases, radio), they remain relatively poorly understood. While comparisons have been made between GRB hosts and other samples of galaxy, such as the comparison with supernova hosts presented in chapter 6, or the comparison with the sub-mm galaxies performed by Berger et al. (2003), it is not yet clear how GRB hosts fit into the "zoo" of high redshift star forming galaxies, and the reasons why the differences may appear (although it is clear that metallicity is an important factor). For example, it is not yet understood why the few GRB host galaxies that do exhibit sub-mm emission have very blue optical colours which cannot be remedied with a large dust content (e.g. Tanvir et al. 2004; Gorosabel et al. 2003a,b). Is there some, small, blue stellar envelope which surrounds these galaxies? Is there a somewhat lower mass of dust with a high temperature,

moving the black-body peak to shorter wavelengths and reducing the flux in the sub-mm? Or is there another source of energy to power the sub-mm emission, such as QSO activity? Observations of GRB hosts with *Spitzer* and *Chandra* will construct broad base-line SEDs of the hosts to measure the dust temperature, and search for any X-ray emission that may be indicative of an active nucleus.

In the future, millimetre observatories will further this endeavour. SCUBA-2 and APEX will be the first instruments on-line and will increase the sensitivity of observations of GRB hosts, enabling a larger fraction to be detected, and also allowing sub-mm spectral slopes to be measured by providing detection at more than a single wavelength. They will also allow a greater degree of "mapping" than is currently possible, enabling the galactic environments of the GRB hosts to be probed. In the longer term ALMA will be the workhorse observatory for these observations, providing continuum sensitivity better than 0.1 mJy (more than a factor of 10 improvement on what is currently possible). This increase in sensitivity will be important in answering the question; where does most star formation occur? Is it in massive systems (akin to the bright sub-mm galaxies) or in much fainter, but more numerous systems, akin to the GRB hosts? In essence its design will enable it to resolve in far-infrared background into individual galaxies, and measure their properties.

7.5.4 What is the GRB rate with redshift?

It is only recently that the first GRBs from very high redshifts have been found (GRB 050814 at $z = 5.3$ and GRB 050904 at $z = 6.3$, Jakobsson et al. 2005; Haislip et al. 2005). Locating such high redshift bursts is difficult, since despite their brightness, the luminosity distance to the bursts makes them too faint to be detected in great numbers and also because the star formation rate at $z > 6$ may be falling quite rapidly. However, ultimately it may be possible to use GRBs to pinpoint the first generation or essentially zero metal stars, and to use their afterglows to study the composition of the intergalactic medium at the time of the first epoch of star formation.

The redshift distribution, even at lower redshifts can be used as a proxy for star formation, or at the very least a subset of star formation. The star formation rate derived by the distribution of GRBs with redshift can then be compared with the star formation rate derived from other indicators such as Lyman-break or sub-mm galaxies. Even if GRBs only represent low metallicity star formation, it remains interesting to study the rate of star formation associated with GRBs, how this evolved with

cosmic time, and how it may differ from higher metallicity star formation, or the global rate.

7.5.5 What is the true GRB energy release and are they standard candles?

Assuming that the energy release from GRBs is isotropic then the range of energies associated with the bursts is very large, spanning 6 orders of magnitude from $10^{48} - 10^{54}$ ergs. However, when this energy is corrected for the effects of beaming the "true" energy release demonstrates a much lower spread of approximately one order of magnitude about a mean value of 10^{51} ergs. This is already a tight correlation, but, remarkably, the residuals about this relationship correlate very tightly with the peak energy of the νF_ν spectrum, reducing the scatter to only $\sim$ 30%. This is sufficiently narrow that it may be possible to use GRBs as standard candles. GRBs are visible at much higher redshifts than SN Ia or X-ray bright clusters, and can therefore be used to probe the equation of state at early cosmic epochs. Although the scatter in the GRB energies is currently larger than the $\sim$ 7 % attainable for SN Ia (Riess et al. 1998) differing cosmologies can be more readily distinguished at higher redshifts. Hence GRBs may yet be a highly useful tool for cosmography. Unfortunately, *Swift* is not optimised for this study since the energy range of the Burst Alert Telescope is only 15-150 keV and does not allow the peak energy to be well constrained. Consequently the use of GRBs as standard candles may not attain its maximum potential until the launch of the Gamma-Ray Large Area Telescope (*GLAST*). *GLAST* will contain a GRB monitor sensitive of a wide spectral range of 5 keV to 25 MeV and a Large Area Telescope (LAT) sensitive at the very high energy windows of 20 MeV to 300 GeV. The combination of the two will allow approximately 100 bursts per year to be localised to better than 10 arcminute accuracy, while simultaneously recording the spectrum of the burst over a wide energy window. Although the locations of the bursts will be known much less accurately than is now possible with *Swift* (i.e. 10 arcminutes rather than 10 arcseconds) the spectral information may allow GRBs to be used much more precisely as cosmographic tools.

7.5.6 What is the precise nature of the stars which produce GRBs?

Although evidence is now overwhelming that GRBs are produced by the collapse of massive stars, the precise nature of these stars, and the evolutionary pathway that they have followed to collapse remains a mystery. It is generally thought that a type Ic supernova is caused by the collapse of a Wolf Rayet

star. These massive stars have lost their hydrogen envelopes and naturally explain the lack of hydrogen lines in the optical spectra of SN Ic. However, this remains to be demonstrated conclusively. It is also not known what effect binarity plays on the creation of GRBs (or indeed on SN Ic).

This question can (and will) be addressed both by studies of the GRBs and of local supernovae. The strongest constraints on the nature of the progenitors can be obtained by directly imaging the progenitor prior to its collapse, as has now been done for several nearby supernovae (e.g. Smartt et al. 2004). However this is taxing observationally and is especially difficult for SN Ic since they are much rarer than type II events and the Wolf-Rayet stars are also less luminous that the blue supergiants which produce SN II. Furthermore this method selects against small, low metallicity galaxies since, by necessity, these searches target massive systems where the probability of observing a SN is high. Nonetheless, some constraints have been placed on the production of high velocity SN Ic's via pre-imaging observations of SN 2002ap (Smartt et al. 2002).

An alternative approach is to study the structure of the ISM close to the progenitor star, since the afterglow shines through this matter and illuminates the structure in the stellar wind. The velocity structure seen in the wind can then be used as a proxy for the mass loss history of the star and can be compared to the mass loss seen in galactic massive stars. With a larger number of afterglows being discovered at early times by *Swift*, more detailed spectroscopic observations will be possible while the afterglow remains bright, enabling this method to make more substantial contributions than has been possible thus far.

Finally, theoretical modeling of the progenitor systems has an important role to play, especially as binarity may well play a significant role in the production of long GRBs. The production of a GRB is thought to be strongly dependent on the production of a black hole accretion disk (BHAD) system. However, creating these systems is far from straightforward, since any material which forms within the disk must possess sufficient angular momentum to remain in the disk, rather than fall directly onto the nascent black hole. Simulations of single stars indicate that they fall short of this angular momentum by an order or magnitude or more and thus cannot easily produce GRBs. Binary evolution can remove this problem, since stars in a tight binary become tidally locked with a rotation period equal to the period of the binary orbit. Sufficiently tight binaries, therefore, naturally create rapidly rotating stellar cores and can produce BHAD systems upon collapse. However, systems which create GRBs in this way may pass through a number of evolutionary states and occupy a relatively small region of parameter space.

For example, they must be close enough to form a BHAD but also sufficiently wide that they do not merge due to frictional loses while in the common envelope phase. Thus, identifying these production channels is a important step in the pinpointing of GRB progenitors.

7.5.7 What are the short duration GRBs?

Essentially all of the work presented in this thesis deals directly with the longer duration, soft spectrum GRBs. A clear second class exists. With durations < 2s and a harder spectra they have been difficult to study in detail, due to the technical difficulties in localising them via hard, rather than soft X-ray instruments, and because it is apparent that their afterglows are fainter than for the longer duration bursts. At the time this thesis started, there had been only one moderately deeply followed short GRB, GRB 020531 (Hurley et al. 2002) and in period from May 2002 until May 2005 only one further object was studied (GRB 021201). Neither of these events gave significant advances in our knowledge, since they were never localised to better than a few arcminutes. However, since the launch of *Swift* further progress has been made rapidly. Ironically not all of this progress is related directly to the observations *Swift* was expected to perform. Soon after its launch it was one of numerous X-ray and γ-ray observatories to observe a giant flare from SGR 1806-20 (Palmer et al. 2005). SGRs (Soft Gamma-Repeaters) are thought to be highly magnetised galactic neutron stars which undergo frequent outbursts due to the realignment of the stellar crust. Occasionally much large changes in the magnetic field occur which can result it the release of a significant fraction of the total magnetic energy. Such an event happened on the 27th December 2004 and was sufficiently bright that it saturated almost all detectors. Bright flares such as this would be easily visible in galaxies out to 70 Mpc. The temporal and spectral properties of this flare, while poorly constrained due to its extreme brightness and saturation of detectors do appear similar to those of short GRBs, implying that at least some short duration GRBs may be related to extragalactic soft-gamma repeaters.

The interesting implication of this is that it implies that many short GRBs may occur in relatively nearby galaxies and it might be expected that such galaxies would be identified by their brightness even in relatively large error boxes. Searches of the few error boxes only arcminutes in diameter failed to find any such bright galaxies, implying that these SGR flares could not account for the majority of short GRBs. However when cross-correlating the positions of BATSE short GRBs against those of IR bright galaxies found by IRAS, a significant correlation is seen (Tanvir et al. 2005). This correlation implies

that around 10 % of short bursts originate from within 100 Mpc, although they do not preferentially cluster in star forming galaxies as might be expected from the properties of known SGRs. While it is clear this result demonstrates that at least some subset of short GRBs lie much closer than longer duration bursts it does not conclusively demonstrate their origin.

Finally *Swift* did locate and slew to a genuine short GRB. GRB 050509b had a duration of only 40ms, making it amongst the shortest bursts seen, even by BATSE. It was also very faint with a total burst fluence of only $9.5 \pm 2.5 \times 10^{-9}$ ergs cm^{-2} (Gehrels et al. 2005). Nonetheless, the rapid *Swift* response found a faint, and fading X-ray source, allowing a position of a few arcseconds to be measured for the first time for a short GRB. The position of the burst fell on a merging galaxy cluster at $z = 0.225$ and was offset approximately 10" from the centre of the central dominant (cD) galaxy in one of the merging components. Although not conclusively associated with this galaxy, the probability of a chance alignment is small (around 10^{-4}) and indicates that the burst is likely to be related to the cluster. The galaxy is (as expected of cluster cD galaxies) a massive early type galaxy, with little or no ongoing star formation. Stellar core collapse would not be expected to occur in such a galaxy and indeed deep limits imply that there is no supernova associated with this burst (Hjorth et al. 2005). Furthermore, the large offset of about 35kpc for the X-ray source from the galaxy is consistent with what would be expected for a tight binary consisting of compact objects, since the supernova which led to the formation of each compact object would impart a large natal kick on the system. GRBs formed via NS-NS mergers would be expected at large projected distances from their host galaxies. Thus while only one event, GRB 050509b implies that the progenitors of short GRBs may, as has long been suspected, be caused by the coalescence of a compact binary.

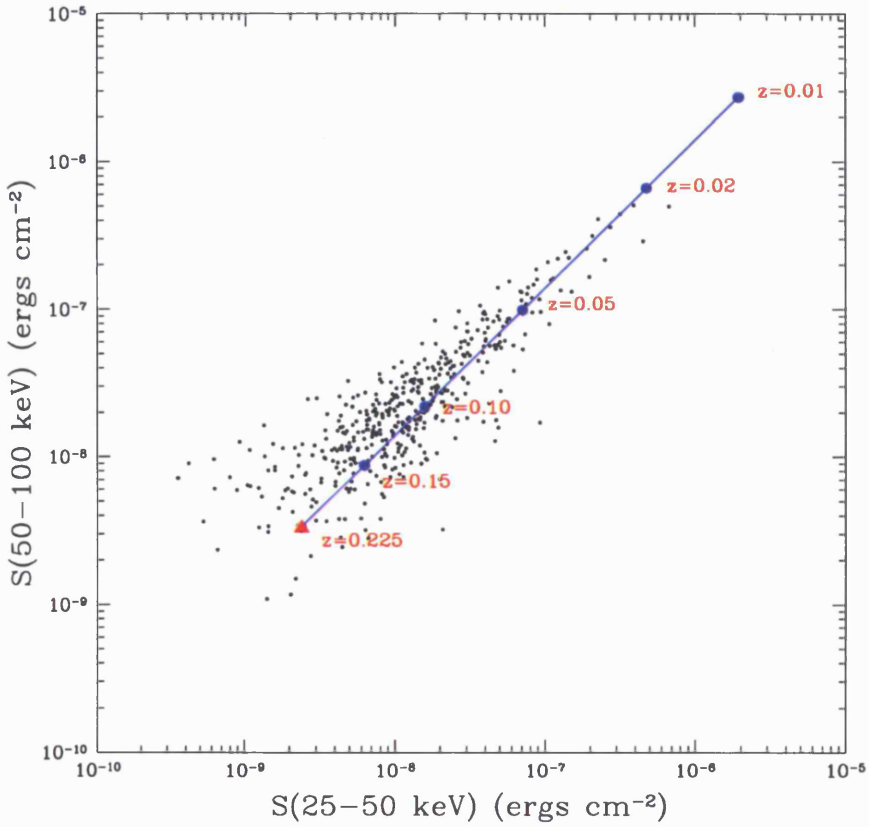

Figure 7.3: The location of GRB 050509b in the BATSE catalogue as it would appear at a number of redshifts (assuming that its true redshift is $z = 0.225$). At $z = 0.225$ the burst is amongst the faintest BATSE bursts while if it were found within 100 Mpc it would be in the brightest 1%. It would be brighter than any short GRB if it were to be found at <30 Mpc where a strong correlation with large scale structure is measured. This implies either than the progenitor for GRB 050509b and those for the nearby bursts are different or that there exists significant breadth in the luminosity function.

7.6 Epilogue: Lighting up the Universe with GRBs

GRB astronomy is a field only now moving out of its infancy. For much of the past 30 years the fascination with GRBs have been their mystery and the enduring question simply "what are Gamma-ray Bursts?" It is only now, nearly 40 years since the VELA satellites captured that first cosmic flash, that GRBs are beginning to give up their secrets. Does this make GRBs more or less interesting? Is this a simple case of solving a problem and moving on? The answer to this is a resounding no. It is simply the case that the focus of research must change. From the discovery of GRBs to the present day much of the research effort has been made to cast light on GRBs, now it is possible to step away from this, and let GRBs cast their light across the universe. Their huge luminosity may shed light on many of the crucial questions in contemporary astrophysics, including the location of the first stars, the chemical evolution of the universe and the origin of gravitational waves. As such GRBs promise to be powerful astrophysical tools well beyond the lifetime of *Swift*. As objects which will be studied by almost all of the major future missions (*Con-X, JWST, LIGO-II, ALMA* and *GLAST*), they will be at the forefront of astrophysical research for many years to come.

BIBLIOGRAPHY

[1] Adelberger, K. L., & Steidel, C. C. 2000, *ApJ* , 544, 218

[2] Akerlof, C., et al. 1999, Nature, 398, 400

[3] Alard, C., Lupton, R., 2000, ApJ, 503, 325

[4] Amati, L., et al. 2002, *A&A* , 390, 81

[5] Amati, L., et al. 2004, ArXiv Astrophysics e-prints, astro-ph/0407166

[6] Anderson, M.I., et al. 2000, A&A 364, L54

[7] Atteia, J.-L. 2003, *A&A* , 407, L1

[8] Band, D., et al. 1993, *ApJ* , 413, 281

[9] Barnard, V. E., et al. 2003, *MNRAS* , 338, 1

[10] Barraud, C. et al. 2003, A&A, 400, 1021

[11] Benítez, N. 2000, *ApJ* , 536, 571

[12] Berger, E. et al. 2002, *ApJ* , 581, 981

[13] Berger, E., Frail, D.A., 2003, GCN circ.1817

[14] Berger, E., Cowie, L. L., Kulkarni, S. R., Frail, D. A., Aussel, H., & Barger, A. J. 2003, *ApJ* , 588, 99

[15] Berger, E., et al. 2002, *ApJ* , 581, 981

[16] Berger, E., et al. 2003, Nature, 426, 154

[17] Berger, E. et al. 2004, GRB Circular Network, 2631

[18] Bersier, D., et al. , 2003, ApJ, 584, 43

[19] Bersier, D., et al. 2004, GRB Circular Network, 2544

[20] Bertin, G., Arnouts, S., 1996, A&AS, 117, 393B

[21] Bertoldi, F., Frail, D. A., Berger, E., Menten, K. M., Kulkarni, S. 2003, GCN circ. 1835

[22] Blain, A. W., Smail, I., Ivison, R. J., & Kneib, J.-P. 1999, *MNRAS* , 302, 632

[23] Blake, C., Lamb, D. Q., Barentine, J., Dembicky, J., McCall, B., York, D. G., & McMillan, R. 2003, GRB Circular Network, 1808, 1

[24] Bloom, J. S. et al. 1999, Nature, 401, 453

[25] Bloom, J. S., Frail, D. A., & Sari, R. 2001, *AJ* , 121, 2879

[26] Bloom, J. S. et al. 2002, *ApJL* , 572, L45

[27] Bloom, J. S., Kulkarni, S. R., & Djorgovski, S. G. 2002, *AJ* , 123, 1111

[28] Bloom, J. S., Frail, D. A., & Kulkarni, S. R. 2003, *ApJ* , 594, 674

[29] Bloom, J. S., Fox, D., van Dokkum, P. G., Kulkarni, S. R., Berger, E., Djorgovski, S. G., & Frail, D. A. 2003, *ApJ* , 599, 957

[30] Bloom, J. S., van Dokkum, P. G., Bailyn, C. D., Buxton, M. M., Kulkarni, S. R., & Schmidt, B. P. 2004, *AJ* , 127, 252

[31] Bohlin, R. C., Savage, B. D., & Drake, J. F. 1978, *ApJ* , 224, 132

[32] Bolzonella, M., Miralles, J.-M., & Pelló, R. 2000, *A&A* , 363, 476

[33] Branch, D., Falk, S. W., Uomoto, A. K., Wills, B. J., McCall, M. L., & Rybski, P. 1981, *ApJ* , 244, 780

[34] Briggs, M. S., et al. 1996, *ApJ* , 459, 40

[35] Bunker, A. J., Stanway, E. R., Ellis, R. S., & McMahon, R. G. 2004, *MNRAS* , 355, 374

[36] Butler, N. R., et al. 2004, ArXiv Astrophysics e-prints, astro-ph/0408453

[37] Calzetti, D., Armus, L., Bohlin, R. C., Kinney, A. L., Koornneef, J., & Storchi-Bergmann, T. 2000, *ApJ* , 533, 682

[38] Cappellaro, E., Mazzali, P. A., Benetti, S., Danziger, I. J., Turatto, M., della Valle, M., & Patat, F. 1997, *A&A* , 328, 203

[39] Cash, W., Charles, P., Bowyer, S., Walter, F., Ayres, T. R., & Linsky, J. L. 1979, *ApJL* , 231, L137

[40] Castro, S., et al. 2003, ApJ, 586, 128

[41] Castro-Tirado, A. J. & Gorosabel, J. 1999, *A&AS* , 138, 449

[42] Castro-Tirado, A. J. et al. 2001, *A&A* , 370, 398

[43] Castro-Tirado, A. J., Gorosabel, J., Castro Cerón, J. M., Nelson, B., & Tristram, P. 2002, GRB Circular Network, 1355

[44] Castro-Tirado, A., Gorosabel, J., Sanchez-Fernandez, C., Lund, N., Brandt, S., & Castro Ceron, J. M. 2002, GRB Circular Network, 1439

[45] Castro-Tirado, A. J. et al. 2003, *A&A* , 411, L315

[46] Castro-Tirado A.J., Gorosabel, J., Casabova, V., 2003, GCN circ. 1807

[47] Cavallo, G., & Rees, M. J. 1978, *MNRAS* , 183, 359

[48] Cavanagh, B., Hirst, P., Jenness, T., Economou, F., Currie, M. J., Todd, S., & Ryder, S. D. 2003, ASP Conf. Ser. 295: Astronomical Data Analysis Software and Systems XII, 12, 237

[49] Chapman, S. C., Blain, A. W., Ivison, R. J., & Smail, I. R. 2003, Nature 422, 695

[50] Chary, R., Becklin, E.E., Armus, L., 2003, ApJ, 566, 229

[51] Christensen, L., Hjorth, J., Gorosabel, J., 2004a, A&A, 425, 913

[52] Cobb, B. E., Bailyn, C. D., van Dokkum, P. G., Buxton, M. M., & Bloom, J. S. 2004, *ApJL* , 608, L93

[53] Costa, E. et al. 1997, Nature, 387, 783

[54] Dado, S., Dar, A. & De Rujula, A. 2004, A&A, 422, 381

[55] Dahlen, T., et al. 2004, *ApJ* , 613, 189

[56] Diercks, A., et al. , 1998, ApJ, 503, L105

[57] Della Valle, M. et al. 2003, *A&A* , 406, L33

[58] Dermer, C. D., Chiang, J., & Bottcher, M. 1999, ApJ, 513, 656

[59] de Vaucouleurs, G., de Vaucouleurs, A., Buta, R., Ables, H. D., & Hewitt, A. V. 1981, PASP, 93, 36

[60] Dickey, J. M. & Lockman, F. J. 1990, *ARA&A* , 28, 215

[61] Djorgovski, S. G., Frail, D. A., Kulkarni, S. R., Bloom, J. S., Odewahn, S. C., & Diercks, A. 2001, *ApJ* , 562, 654

[62] Draine, B. T. 2000, *ApJ* , 532, 273

[63] Eichler, D., Livio, M., Piran, T., & Schramm, D. N. 1989, Nature, 340, 126

[64] Esin, A. A. & Blandford, R. 2000, *ApJL* , 534, L151

[65] Flaccomio, E., Garnavich, P., & Stanek, K. 2003, GCN circ. 1806

[66] Foley, R. J., et al. 2003, PASP, 115, 1220

[67] Fox, D. W. 2002a, GRB Circular Network, 1392

[68] Fox, D. W. 2002b, GRB Circular Network, 1387

[69] Fox, D. W. 2002, GCN circ. 1564

[70] Fox, D. W., et al. 2003, *ApJL* , 586, L5

[71] Fox, D. W., et al. 2003, Nature, 422, 284

[72] Fox, D.B., 2004, GRB Circular Network, 2630

[73] Frail, D. A., Kulkarni, S. R., Nicastro, S. R., Feroci, M., & Taylor, G. B. 1997, Nature, 389, 261

[74] Frail, D. A., et al. 2001, *ApJL* , 562, L55

[75] Frail, D. A., Wieringa, M. H., Berger, E., & Wark, R. 2002, GRB Circular Network, 1380

[76] Frail, D. A. et al. 2002, *ApJ* , 565, 829

[77] Frail, D.A., Berger, E., 2003, GCN circ. 1827

[78] Fruchter, A. S. et al. 1999, *ApJL* , 519, L13

[79] Fruchter, A., Krolik, J. H., & Rhoads, J. E. 2001, *ApJ* , 563, 597

[80] Fruchter, A. S., Levan, A. J., Burud, I., & Nugent, P. E. 2002, GRB Circular Network, 1453

[81] Fruchter, A. S. & Hook, R. N. 2002, PASP, 114, 144

[82] Fruchter, A., Patel, S., Kouveliotou, C., Rhoads, J., Holland, S., Burud, I., & Wijers, R. 2002a, GRB Circular Network, 1268

[83] Fruchter, A., Rhoads, J., Burud, I., Levan, A., Patel, S., Kouveliotou, C., Gorosabel, J., & Hjorth, J. 2002b, GRB Circular Network, 1440

[84] Fryer, C. L., Woosley, S. E., & Hartmann, D. H. 1999, *ApJ* , 526, 152

[85] Fynbo, J. P U., et al. 2001, *A&A* , 369, 373

[86] Fynbo, J. P. U., et al. 2003, *A&A* , 406, L63

[87] Fynbo, J. P. U., et al. 2004, *ApJ* , 609, 962

[88] Galama, T. J., et al. 1998, Nature, 395, 670

[89] Galama, T. J. et al. 2000, *ApJ* , 536, 185

[90] Galama, T. J. et al. 2003, *ApJ* , 587, 135

[91] Gal-Yam, A., Ofek, E. O., & Shemmer, O. 2002, *MNRAS* , 332, L73

[92] Gal-Yam, A., et al. 2004, *ApJL* , 609, L59

[93] Gandolfi, G. 2001, GRB Circular Network, 1119

[94] Gandolfi, G. 2002a, GRB Circular Network, 1366

[95] Gandolfi, G. 2002b, GRB Circular Network, 1358

[96] Gandolfi, G. 2002c, GRB Circular Network, 1349

[97] Garnavich, P. et al. 2003, IAU Circular, 8108, 2

[98] Garnavich, P.M., et al., 2003, ApJ, 582, 924

[99] Gehrels, N. et al. 2005, Nature, 437, 851

[100] Ghirlanda, G., Ghisellini, G., & Lazzati, D. 2004, *ApJ* , 616, 331

[101] Giavalisco, M., et al. 2004, *ApJL* , 600, L93

[102] Gilliland, R. L., Nugent, P. E., & Phillips, M. M. 1999, *ApJ* , 521, 30

[103] Gladders, M., Hall, P., GCN circ. 1495

[104] Greiner, J. et al. 2003, ApJ, 599, 1223

[105] Gorosabel, J., Castro-Tirado, A. J., Pedrosa, A., Zapatero-Osorio, M. R., Fernandes, A. J. L., Feroci, M., Costa, E., & Frontera, F. 1999, *A&A* , 347, L31

[106] Gorosabel, J., et al. 2002, *A&A* , 384, 11

[107] Gorosabel, J. et al. 2003b, *A&A* , 400, 127

[108] Gorosabel, J. et al. 2003a, *A&A* , 409, 123

[109] Gorosabel, J. et al. 2005, *A&A* , 437, 411

[110] Granot, J., Nakar, E., & Piran, T. 2003, Nature, 426, 138

[111] Groot, P. J., et al 1998, *ApJL* , 493, L27

[113] Haislip, J.B. et al. 2005, Nature, submitted, astro-ph/0509660

[113] Harrison, F. A., et al. 1999, *ApJL* , 523, L121

[114] Harrison, F. A., Yost, S., Fox, D., Heise, J., Kulkarni, S. R., Price, P. A., & Berger, E. 2001, GRB Circular Network, 1143

[115] Heavens, A., Panter, B., Jimenez, R., & Dunlop, J. 2004, Nature, 428, 625

[116] Heise, J., in't Zand, J., Kippen, R. M., & Woods, P. M. 2001a, Gamma-ray Bursts in the Afterglow Era, 16

[117] Heise, J., in't Zand, J. J. M., Kulkarni, S. R., & Costa, E. 2001b, GRB Circular Network, 1138, 1

[118] Hjorth, J., et al. 2002, *ApJ* , 576, 113

[119] Hjorth, J., et al. 2003a, Nature, 423, 847

[120] Hjorth, J., et al. 2003b, *ApJ* , 597, 699

[121] Hjorth, J., et al. 2005, ArXiv Astrophysics e-prints, arXiv:astro-ph/0506123

[122] Hoge, J. C., Stevens, J. A., Moriarty-Schieven, G., & Tilanus, R. P. J. 2003, GCN circ. 1832

[123] Hogg, D. W. & Fruchter, A. S. 1999, *ApJ* , 520, 54

[124] Holland, S. T., et al. 2003, *AJ* , 125, 2291

[125] Huang, Y. F., Dai, Z. G., & Lu, T. 2002, *MNRAS* , 332, 735

[126] Hurley, K., et al. 2002, *ApJ* , 567, 447

[127] in't Zand, J., Reali, F., Granata, S., Lowes, P., & Piro, L. 2002, GRB Circular Network, 1383

[128] Iwamoto, K., et al. 2000, *ApJ* , 534, 660

[129] Izzard, R. G., Ramirez-Ruiz, E., & Tout, C. A. 2004, *MNRAS* , 348, 1215

[130] Jakobsson, P., Hjorth, J., Fynbo, J. P. U., Watson, D., Pedersen, K., Björnsson, G., & Gorosabel, J. 2004, *ApJL* , 617, L21

[132] Jakobsson, P., et al. 2004, *A&A* , 427, 785

[132] Jakobsson, P., et al. 2005, A&A, submitted, astro-ph/0509888

[133] Katz, J. I., Piran, T. 1998, ApJ, 501, 425

[134] Kawai N., *et al* 2003, GCN circ. 1816

[135] Kilmartin, P. & Gilmore, A. 2002, GRB Circular Network, 1350, 1

[136] Kennicutt, R. C. 1998, *ARA&A* , 36, 189

[137] Klose, S. et al. 2003, *ApJ* , 592, 1025

[138] Klose, S. et al. 2000, *ApJ* , 545, 271

[139] Kouveliotou, C., Meegan, C. A., Fishman, G. J., Bhat, N. P., Briggs, M. S., Koshut, T. M., Paciesas, W. S., & Pendleton, G. N. 1993, *ApJL* , 413, L101

[140] Kouveliotou, C., et al. 2004, *ApJ* , 608, 872

[141] Lamb, D. Q., et al. 2004, New Astronomy Review, 48, 423

[142] Lamb, D. Q., Donaghy, T. Q., & Graziani, C. 2003, ArXiv Astrophysics e-prints, astro-ph/0312634

[143] Le Floc'h, E., et al. 2003, *A&A* , 400, 499

[144] Levan, A.J., Merrill, M., Rol, E., Dell'Antonio, I., Rhoads, J., Fruchter, A.S., 2003, GCN circ. 1818

[145] Lipkin, Y. M., et al. 2004, *ApJ* , 606, 381

[146] Lloyd-Ronning, N., & Ramirez-Ruiz, E. 2002, ApJ, 576, 101

[147] MacFadyen, A. I., Woosley, S. E., & Heger, A. 2001, *ApJ* , 550, 410

[148] Madau, P., Ferguson, H. C., Dickinson, M. E., Giavalisco, M., Steidel, C. C., & Fruchter, A. 1996, *MNRAS* , 283, 1388

[149] Maiolino, R., Marconi, A., Salvati, M., Risaliti, G., Severgnini, P., Oliva, E., La Franca, F., & Vanzi, L. 2001, *A&A* , 365, 28

[150] Malesani, D., et al. 2004, *ApJL* , 609, L5

[151] Masetti N., Palazzi, E., Pian, E., 2003b, GCN circ. 1823

[152] Masetti, N. et al. 2003, *A&A* , 404, 465

[153] Matheson, T., et al. 2003, ApJ, 582, 5

[154] Matheson, T., et al. 2003, *ApJ* , 599, 394

[155] McKenzie, E. H. & Schaefer, B. E. 1999, PASP, 111, 964

[156] Mészáros, P., & Rees, M. J. 1992, *MNRAS* , 257, 29P

[157] Mészáros, P. 2002, *ARA&A* , 40, 137

[158] Mészáros, P., Ramirez-Ruiz, E., Rees, M. J., Zhang, B. 2002, ApJ, 578, 812

[159] Metzger, M. R., Djorgovski, S. G., Kulkarni, S. R., Steidel, C. C., Adelberger, K. L., Frail, D. A., Costa, E., & Frontera, F. 1997, Nature, 387, 879

[160] Meurer, G. R., Heckman, T. M., & Calzetti, D. 1999, *ApJ* , 521, 64

[161] Millard, J., et al. 1999, *ApJ* , 527, 746

[162] Miller, G. E. & Scalo, J. M. 1979, *ApJS* , 41, 513

[163] Mirabal, N., et al. 2003, *ApJ* , 595, 935

[164] Moustakas, L. A., et al. 2004, *ApJL* , 600, L131

[165] Nicastro, L., Piro, L., Gandolfi, G., Feroci, M., Capalbi, M., Perri, M., Heise, J., & in't Zand, J. 2002, GRB Circular Network, 1374

[166] Nicastro, L et al, 2004, A&A, in prep

[167] Nugent, P., Kim, A., & Perlmutter, S. 2002, PASP, 114, 803

[168] Paczynski, B., & Rhoads, J. E. 1993, *ApJL* , 418, L5

[169] Palmer, D. M., et al. 2005, Nature, 434, 1107

[170] Panaitescu, A., & Kumar, P. 2001, *ApJL* , 560, L49

[171] Pandey, S. B., Anupama, G. C., Sagar, R., Bhattacharya, D., Sahu, D. K., & Pandey, J. C. 2003, *MNRAS* , 340, 375

[172] Patat, F., et al. 2001, *ApJ* , 555, 900

[173] Pei., Y.C. 1992, *ApJ* , 395, 130

[174] Pian, E. 2003, LNP Vol. 598: Supernovae and Gamma-Ray Bursters, 598, 343

[175] Pian, E. et al. 2004, GRB Circular Network, 2638

[176] Piro, L. et al. 2002, *ApJ* , 577, 680

[177] Podsiadlowski, P., Mazzali, P. A., Nomoto, K., Lazzati, D., & Cappellaro, E. 2004, *ApJL* , 607, L17

[178] Preece, R. D., Briggs, M. S., Mallozzi, R. S., Pendleton, G. N., Paciesas, W. S., & Band, D. L. 2000, *ApJS* , 126, 19

[179] Price, P. et al. 2003, ApJ, 584, 931

[180] Price, P. A. et al. 2003a, *ApJ* , 589, 838

[181] Priddey, R. et al. 2005, MNRAS, submitted

[182] Ramirez-Ruiz, E., Lloyd-Ronning, N. M. 2002, New Astron., 7, 197

[183] Ramirez-Ruiz, E., Celotti, A., & Rees, M. J. 2002, MNRAS, 337, 1349

[184] Ramirez-Ruiz, E., & Madau, P. 2004, ApJ, 608, L89

[185] Rees, M. J., & Meszaros, P. 1998, *ApJL* , 496, L1

[186] Reichart, D. E., et al. 1999, *ApJ* , 517, 692

[187] Reichart, D. E. 2001, *ApJ* , 554, 643

[188] Riess, A. G., et al. 2004, *ApJ* , 607, 665

[189] Rhoads, J. E. & Fruchter, A. S. 2001, *ApJ* , 546, 117

[190] Rhoads, J. E. 1999, *ApJ* , 525, 737

[191] Rhoads, J. E., Burud, I., Fruchter, A., Kouveliotou, C., & Wood-Vasey, W. M. 2001, GRB Circular Network, 1140

[192] Rhoads, J. E. 2001, *ApJ* , 557, 943

[193] Rhoads, J. E. 2003, *ApJ* , 591, 1097

[194] Richardson, D. Branch, D., Casebeer, D., Millard, J., Thomas, R.C., Baron, E., 2002 *ApJ* 123, 745

[195] Richmond, M. W. et al. 1996, *AJ* , 111, 327

[196] Rol, E. & Wijers, R. 2003, GCN circ. 1864

[197] Rol, E. et al. 2004, ApJ, in prep.

[198] Sakamoto, T., et al. 2004, ArXiv Astrophysics e-prints, astro-ph/0409128

[199] Savaglio, S., Fall, S. M., & Fiore, F. 2003, *ApJ* , 585, 638

[200] Sari, R., Piran, T., & Narayan, R. 1998, *ApJL* , 497, L17

[201] Sazonov, S., Lutovinov, A., & Sunyaev, R. 2004, Nature, 430, 646

[202] Schlegel, D. J., Finkbeiner, D. P., & Davis, M. 1998, *ApJ* , 500, 525

[203] Smail, I., Ivison, R. J., Blain, A. W., & Kneib, J.-P. 2002, *MNRAS* , 331, 495

[204] Smail, I., Chapman, S. C., Blain, A. W., & Ivison, R. J. 2004, *ApJ* , 616, 71

[205] Smartt, S. J., Vreeswijk, P. M., Ramirez-Ruiz, E., Gilmore, G. F., Meikle, W. P. S., Ferguson, A. M. N., & Knapen, J. H. 2002, *ApJL* , 572, L147

[206] Smartt, S. J., Maund, J. R., Hendry, M. A., Tout, C. A., Gilmore, G. F., Mattila, S., & Benn, C. R. 2004, Science, 303, 499

[207] Soderberg, A. M., et al. 2004, *ApJ* , 606, 994

[208] Soderberg, A. M., et al. 2005a, ArXiv Astrophysics e-prints, arXiv:astro-ph/0504359

[209] Soderberg, A. M., et al. 2005b, *ApJ* , 627, 877

[210] Stanek, K. Z., Garnavich, P. M., Kaluzny, J., Pych, W., & Thompson, I. 1999, *ApJL* , 522, L39

[211] Stanek, K. Z., et al. 2003, *ApJL* , 591, L17

[212] Strolger, L., et al. 2004, *ApJ* , 613, 200

[214] Tanvir, N. R., et al. 2004, *MNRAS* , 352, 1073

[214] Tanvir, N. R., Chapman, R., Levan, A., Priddey, R., Nature, in press

[215] Taylor, G. B., Bloom, J. S., Frail, D. A., Kulkarni, S. R., Djorgovski, S. G., & Jacoby, B. A. 2000, *ApJL* , 537, L17

[216] Taylor, G. B., Frail, D. A., & Kulkarni, S. R. 2001, GRB Circular Network, 1136

[217] Thomsen, B., et al. 2004, *A&A* , 419, L21

[218] Tremonti, C. A., et al. 2004, *ApJ* , 613, 898

[219] Trentham, N., Ramirez-Ruiz, E., & Blain, A. W., 2002, MNRAS, 334, 983

[220] van Dokkum, P. G. & Bloom, J. S. 2003, GRB Circular Network, 2380

[221] van Paradijs, J. et al. 1997, Nature, 386, 686

[222] van Paradijs, J., Kouveliotou, C., & Wijers, R. A. M. J. 2000, *ARA&A* , 38, 379

[223] Vaughan, S., et al. 2004, *ApJL* , 603, L5

[224] Vietri, M. & Stella, L. 1998, *ApJL* , 507, L45

[225] Vrba F., et al. 2000, ApJ, 528, 254

[226] Vrba F., Luginbuhl, C., Henden, A., 2003, GCN circ. 1822

[227] Vreeswijk, P.M., et al. 1999, ApJ, 523, 171

[228] Vreeswijk, P. M. et al. 2001, *ApJ* , 546, 672

[229] Vreeswijk, P. M., et al. 2004, *A&A* , 419, 927

[230] Wang, X., & Loeb, A. 2000, *ApJ* , 535, 788

[231] Watson, D., et al. 2004, *ApJL* , 605, L101

[232] Waxman, E. & Draine, B. T. 2000, *ApJ* , 537, 796

[233] Woosley, S. E. 1993, *ApJ* , 405, 273

[234] Woosley, S. E. & MacFadyen, A. I. 1999, *A&AS* , 138, 499

[235] Wieringa, M. H., Berger, E., Fox, D. W., & Frail, D. A. 2002, GRB Circular Network, 1390

[236] Willingale, R., Osborne, J. P., O'Brien, P. T., Ward, M. J., Levan, A., & Page, K. L. 2004, MNRAS, 349, 31

[237] Yamazaki, R., Ioka, K., & Nakamura, T. 2002, *ApJL* , 571, L31

[238] Yost et al. 2002, ApJ, 577, 155

[239] Yost, S. A., Harrison, F. A., Sari, R., & Frail, D. A. 2003, *ApJ* , 597, 459

[240] Zeh, A., Klose, S., & Hartmann, D. H. 2004, *ApJ* , 609, 952

[241] Zhang, B. & Mészáros, P. 2002, ApJ, 581, 1236

[242] Zhang, W., Woosley, S. E., & MacFadyen, A. I. 2003, ApJ, 586, 356